UNIVERSIDADE FEDERAL DO RIO GRANDE DO SUL

INSTITUTO DE QUÍMICA

PROGRAMA DE PÓS-GRADUAÇÃO EM QUÍMICA

TESE DE DOUTORADO

APROVEITAMENTO DE BIOMASSA RESIDUAL VEGETAL E HÍBRIDOS ORGÂNICOS E INORGÂNICOS PARA A REMOÇÃO DE POLUENTES ORGÂNICOS

ANDERSON JOSÉ BARCELLOS LEITE

Porto Alegre, outubro de 2018.

UNIVERSIDADE FEDERAL DO RIO GRANDE DO SUL

INSTITUTO DE QUÍMICA

PROGRAMA DE PÓS-GRADUAÇÃO EM QUÍMICA

ANDERSON JOSÉ BARCELLOS LEITE

APROVEITAMENTO DE BIOMASSA RESIDUAL VEGETAL E HÍBRIDOS ORGÂNICOS E INORGÂNICOS PARA A REMOÇÃO DE POLUENTES ORGÂNICOS

Tese apresentada como requisito parcial para a

obtenção do grau de Doutor em Química

Orientador:

Prof. Dr. Silvio Luis Pereira Dias

Co-Orientador:

Prof. Dr. Éder Cláudio Lima

Porto Alegre, outubro de 2018.

A presente tese foi realizada inteiramente pelo autor, exceto as colaborações, as quais foram devidamente citadas nos agradecimentos, no período entre agosto de 2014 e setembro de 2018, no Instituto de Química da Universidade Federal do Rio Grande do Sul, sob Orientação do Professor Doutor Silvio Luis Pereira Dias e Co-orientação do Professor Doutor Éder Cláudio Lima. A tese foi julgada adequada para a obtenção do título de Doutor em Química pela seguinte banca examinadora:

Profa. Dra. Leliz Ticona Arenas

Profa. Dra. Rosângela Assis Jacques

Prof. Dr. Vitor Paulo Pereira

Prof. Dr. Caciano Pelayo Zapata Norena

Prof. Dr. Silvio Luis Pereira Dias
(Orientador)

Prof. Dr. Éder Cláudio Lima
(Co-orientador)

Anderson José Barcellos Leite
(Doutorando)

Dedico esta tese à minha família, que sempre me apoiou e sem a qual, com certeza, não iria concluir essa etapa tão importante em minha vida. A meu pai, José, um pai exemplar, meu grande amigo, meu ídolo e inspirador em meus estudos. À memória de minha mãe, Leda, que tenho a certeza de que no Plano Superior está muito feliz por essa conquista da qual ela é muito importante. A meu irmão e melhor amigo, Jorge, que sempre acreditou em meu potencial e me incentivou muito. A meu sobrinho, Gabriel, grande amigo e que considero meu irmão mais novo, pelos momentos de descontração e alegria. À minha esposa, Laritza, pelo amor, dedicação, carinho, companheirismo e por seu apoio.

AGRADECIMENTOS

Primeiramente a Deus, por dar-me forças nos momentos de dificuldade e fazer com que seja possível realizar essa etapa tão importante em minha vida.

Aos meus orientadores, professor Dr. Silvio Luis Pereira Dias e ao professor Dr. Éder Cláudio Lima, pela orientação, amizade, dedicação, ensinamentos transmitidos e confiança em meu trabalho.

Aos professores que fizeram parte da banca de minha defesa, professora Dra. Leliz Ticona Arenas, professora Dra. Rosângela Assis Jacques, professor Dr. Vitor Paulo Pereira e ao professor Dr. Caciano Pelayo Zapata Norena pela contribuição dada a este trabalho, de forma a qualificá-lo mais.

Aos amigos e colegas de laboratório Caroline Saucier, Cibele Umpierres, Diana Caicedo, Glaydson dos Reis, Janaina Costa, Liziê Prola e Pascal Thue, pelo apoio técnico, debates científicos, e agradáveis momentos de descontração.

Aos alunos de Iniciação Científica Robert Pilger, Viviana Schmidt, Beatris Mello e Carine Correa, pela valiosa colaboração na execução deste trabalho, pela amizade e agradáveis momentos de descontração.

Ao Dr. Júlio Vaghetti e aos bolsistas premmium do LAMAT, pelo auxílio na realização das análises de FTIR e TGA/DTG.

Aos demais professores e funcionários do Instituto de Química da UFRGS, peloapoio técnico e ao ensino de qualidade.

À minha família, pelo amor, apoio, carinho e incentivo.

A todos que de torceram para que a conclusão dessa etapa fosse realizada com êxito e que contribuíram para a realização deste trabalho.

À Coordenação de Aperfeiçoamento de Pessoal de Nível Superior (CAPES) e ao Conselho Nacional de Desenvolvimento Científico e Tecnológico (CNPq), pelo apoio financeiro.

PRODUÇÃO BIBLIOGRÁFICA

ARTIGOS PUBLICADOS A PARTIR DESTA TESE

Leite, A. J. B.; Sophia A, C.; Thue, P. S.; Dos Reis, G. S.; Dias, S. L. P.; Lima E. C.; Vaghetti, J. C. P.; Pavan, F. A.; Alencar, W. S. Activated carbon from avocado seeds for the removal of phenolic compounds from aqueous solutions. *Desal. Wat. Treat.***2017**, 71, 168 - 181.

Leite, A.B.; Saucier, C.; Lima, E. C.; Dos Reis, G. S.; Umpierres, C.S.; Mello, B. L.; Shirmardi, M.; Dias, S. L. P.; Sampaio, C. H. Activated carbons from avocado seed: optimisation and application for removal of several emerging organic compounds. *Environ Sci Pollut Res***2018**, 25, 7647–7661.

Leite, A. J. B.; Lima, E. C. ; Dos Reis, G. S.; Thue, P. S.; Saucier, C.; Rodembusch, F. S.; Dias, S. L. P.; Umpierres, C. S. Hybrid adsorbents of tannin and APTES (3-aminopropyltriethoxysilane) and their application for the highly efficient removal of Acid Red 1 dye from aqueous solutions. *J. Environ. Chem. Eng.***2017**, 5, 4307-4318.

OUTROS ARTIGOS PUBLICADOS

Bazzo, A.; Adebayo, M. A.; Dias, S. L. P.; Lima, E. C.; Vaghetti, J. C. P.; De Oliveira, E. R.; Leite, A. J.B.; Pavan, F. Avocado seed powder: characterization and its application for crystal violet dye removal from aqueous solutions. *Desal. Wat. Treat.***2017**, 57, 15873–15888.

PATENTES

Lima, Eder C.; Thue, Pascal S.; Dias, Silvio L. P.; Umpierres, Cibele S.; Costa, Janaina B.; Leite, Anderson J. B.; Vanni, Gabriel. CARVÃO ATIVADO ADSORVENTE E DE ALTA MAGNETIZAÇÃO, PROCESSO DE OBTENÇÃO E USO DO CARVÃO ATIVADO ADSORVENTE E DE ALTA MAGNETIZAÇÃO. Categoria: Processo. Instituição onde foi depositada: INPI - Instituto Nacional da Propriedade Industrial. País: Brasil. Natureza: Patente de Invenção. Número do registro: BR 1020180681303. Número do Depósito PCT: 870180127855.

SUMÁRIO

LISTA DE FIGURAS

LISTA DE TABELAS

LISTA DE ABREVIATURAS E SÍMBOLOS

q_e	Quantidade de adsorvato adsorvida no equilíbrio (mg g^{-1})
C_e	Concentração de adsorvato restante no equilíbrio (mg L^{-1})
K_L	Constante de equilíbrio de Langmuir (L mg^{-1})
Q_{max}	Capacidade máxima de adsorção (mg g^{-1})
K_F	Constante de equilíbrio de Freundlich [mg g^{-1}(mg L^{-1})$^{-1/nF}$]
n_F	Expoente de Freundlich (adimensional)
K_g	Constante de equilíbrio de Liu (L mg^{-1})
n_L	Expoente de Liu (adimensional)
θ_t	Número de sítios ativos disponíveis na superfície do adsorvente
SEM	Microscopia eletrônica de varredura (do inglês *scanning electron microscopy*)
FTIR	Espectroscopia vibracional na região do infravermelho com transformada de Fourier (do inglês *Fourier transform infrared spectroscopy*)
BET	Brunauer, Emmett e Teller
AS	Caroço de abacate (do ingles *avocado seed*)
ASAC	Carvão ativado de caroço de abacate (do ingles *avocado seed activated carbon*)
RES	Resorcinol
AMP	3-aminofenol
HI	Razão hidrofobicidade- hidrofilicidade (do ingles *hydrophobicity-hydrophilicity ratio*)
APTES	3-aminopropiltrietoxisilanno (do ingles *3-aminopropyltriethoxysilane*)
AR 1	Corante vermelho ácido 1(do ingles *acid red 1 dye*)
EPA	Agência de proteção Ambiental Norte Americana (EPA, do inglês *Environmental Protection Agency*)
Q	Quantidade de adsorvato adsorvida (mg g^{-1})
C_o	Concentração inicial de RES ou AMP em contato com o adsorvente (mg L^{-1})
C_f	Concentração de compostos fenólicos após o processo de adsorção (mg L^{-1})
R^2	Coeficiente de determinação

R^2_{adj}	Coeficiente de determinação ajustado
SD	Desvio padrão (do inglês *standard deviation)*
$q_{i,model}$	Valor de q teórico individual predito por um dado modelo
$q_{i,exp}$	Valor de q experimental individual
$\bar{q}_{exp}$	Média dos valores experimentais de q

RESUMO

Esta tese consiste em três artigos científicos, sendo os dois primeiros anexos sobre o preparo, caracterização e aplicação de carvões ativos no tratamento de soluções aquosas com contaminantes orgânicos e o terceiro anexo sobre a aplicação de um adsorvente híbrido de tanino e APTES a remoção de corante vermelho ácido 1. No primeiro artigo (**anexo 1**), foi produzido um carvão ativo de caroço de abacate (ASAC) sintetizado através do processo de aquecimento por micro-ondas usando $ZnCl_2$como agente ativante. O carvão ASAC foi caracterizado utilizando-se as técnicas analíticas, isotermas de N_2, espectroscopia de infravermelho por transformada de Fourier (FTIR) e microscopia eletrônica de varredura (MEV). A área superficial do carvão ASAC foi de 1.432 m^2 g^{-1}. O ASAC preparado foi utilizado para adsorção de resorcinol e 3-aminofenol a partir de soluções aquosas. Modelos cinéticos são pseudo-primeira ordem, pseudo-segundo ordem, e ordem fraccionária Avrami e isotermas (Freundlich, Langmuir, e Liu) foram aplicadas aos dados experimentais de adsorção. Os resultados demonstram capacidade máxima de adsorção para resorcinol (406,9 mg g^{-1}) e 3-aminofenol (454,5 mg g^{-1}) a 50 ° C. No segundo artigo (**anexo 2**), foram preparados carvões ativos de caroço de abacate por pirólise convencional. Com a finalidade de determinar a melhor condição para a produção desses carvões, foi empregado um experimento fatorial completo (DOE) com três pontos centrais variando a temperatura e o tempo de pirólise. Os dois fatores avaliados (temperatura e tempo de pirólise) influenciaram fortemente os valores de S_{BET}, volume de poros, razão hidrofobicidade – hidrofilicidade (HI) e grupos funcionais. O carvão ativado produzido apresentou alta área superficial na faixa de 1122-1584 m^2 g^{-1}. A caracterização da superfície revelou que os carbonos ativados por sementes de abacate (ASACs) possuem superfícies hidrofílicas e possuem grupos predominantemente ácidos em suas superfícies. Os ASACs preparados foram empregados na adsorção de 25 compostos orgânicos emergentes, como 10 fármacos e 15 compostos fenólicos que apresentaram altos valores de captação para todos os poluentes emergentes. No terceiro artigo (**anexo 3**), foram preparados adsorventes híbridos pela reação de tanino com diferentes quantidades de 3-aminopropiltrietoxissilano (APTES). Os materiais foram caracterizados por MEV, TEM, FTIR, CHN, isotermas de adsorção / dessorção de N_2 e sorção de vapor (adsorção de água e n-heptano - para determinação da razão hidrofobicidade - hidrofilicidade). Os

materiais modificados foram utilizados como adsorventes para a remoção do corante ácido vermelho 1 (AR-1) das soluções. Para os experimentos de adsorção, as melhores condições experimentais foram alcançadas em pH 2,0, tempo de contato de 8 h e a 50 ° C. Os dados de adsorção cinética e de equilíbrio foram bem representados pela isoterma de Liu e Modelos cinéticos de ordem geral, respectivamente. A capacidade máxima de adsorção de 418,3 mg g^{-1} foi obtida em 50 ^{0} C para um material tanino-APTES com proporção de 1: 1 (Tan-Ap-1.0). Com base em dados experimentais, verificou-se que interações eletrostáticas e ligações de hidrogênio entre o adsorvente e o corante AR-1 desempenharam o papel mais importante no processo de adsorção.

ABSTRACT

This thesis consists of three scientific articles, the first two annexes on the preparation, characterization and application of active coals in the treatment of aqueous solutions with organic contaminants and the third appendix on the application of a hybrid tannin adsorbent and APTES the dye removal. In the first article, an active avocado char (ASAC) synthesized through the microwave heating process was produced using $ZnCl_2$ as the activating agent. The ASAC coal was characterized using analytical techniques, N_2 isotherms, Fourier transform infrared spectroscopy (FTIR) and scanning electron microscopy (SEM). The surface area of the ASAC coal was 1,432 m^2 g^{-1}.The prepared ASAC was used for adsorption of resorcinol and 3-aminophenol from aqueous solutions. Kinetic models are pseudo-first order, pseudo-second order, and fractional order Avrami and isotherms (Freundlich, Langmuir, and Liu) were applied to experimental adsorption data. The results showed maximum adsorption capacity for resorcinol (406.9 mg g^{-1}) and 3 - aminophenol (454.5 mg g^{-1}) at 50 ° C. In the second article, active carbons of avocado seed were prepared by conventional pyrolysis. In order to determine the best condition for the production of these coals, a complete factorial experiment (DOE) with three central points was used, varying the temperature and the pyrolysis time. The two factors evaluated (temperature and pyrolysis time) strongly influenced S_{BET}, pore volume, hydrophobicity - hydrophilicity (HI) ratio and functional groups. The activated carbon produced high specific surface areas in the range of 1122-1584 m^2 g^{-1}. Surface characterization revealed that the activated carbon by avocado seeds (ASACs) have hydrophilic surfaces and have predominantly acidic groups on their surfaces. The ASACs prepared were used in the adsorption of 25 emerging organic compounds, such as 10 drugs and 15 phenolic compounds that showed high uptake values for all emerging pollutants. In the third article, hybrid adsorbents were prepared by the reaction of tannin with different amounts of 3-aminopropyltriethoxysilane (APTES). The materials were characterized by MEV, TEM, FTIR, CHN, adsorption / desorption isotherms of N_2 and vapor sorption (water adsorption and n-heptane - to determine hydrophobicity - hydrophilicity ratio).The modified materials were used as adsorbents for the removal of the red acid dye 1 (AR-1) from the solutions. For the adsorption experiments, the best experimental conditions were reached at pH 2.0, contact time 8 H and 50 ° C. The kinetic and equilibrium

adsorption data were well represented by the Liu isotherm and kinetic models of general order, respectively. The maximum adsorption capacity of 418.3 mg g - 1 was obtained at 50 ° C for 1: 1 tannin - APTES material (Tan - Ap - 1.0). Based on experimental data, it was verified that electrostatic interactions and hydrogen bonds between the adsorbent and the AR-1 dye played the most important role in the adsorption process.

1. INTRODUÇÃO

A poluição da água devido a poluentes orgânicos causou preocupações ambientais crescentes nas últimas décadas[1,2]. Numerosas indústrias geram resíduos fenólicos, tais como as de: resinas de plantas de gás, papel e celulose, madeira compensada, tintas, produtos farmacêuticos, petróleo, têxteis, plástico, etc., águas residuais de descarga contendo diferentes tipos de contaminantes fenólicos[1,2]. As águas residuais fenólicas são conhecidas como tóxicas e cancerígenas. Por isso, há uma crescente conscientização sobre o impacto desses contaminantes nos recursos hídricos.

Os compostos fenólicos rapidamente se fototransformam e formam subprodutos que podem representar sérios riscos para os organismos aquáticos e aos seres humanos[1,2]. A ingestão de água contaminada com fenóis pode causar sérios danos gastrointestinais, tremores musculares, dificuldade em andar e morte nos seres vivos [1,2]. Devido aos altos riscos ambientais envolvidos e à toxicidade dos efluentes, é importante remover fenol e compostos fenólicos de fluxos aquosos industriais contaminados antes de serem descartados em quaisquer corpos hídricos[1,2].

Fármacos e seus metabólitos podem ser, de forma imprópria, eliminados e/ ou excretados por pacientes, sendo destinados aos efluentes aquosos municipais, gerando assim problemas ambientais[3]. Podem ser citados como fonte desses contaminantes os hospitais e as indústrias farmacêuticas[4]. Devido à sua elevada solubilidade em água, muitos fármacos não são completamente removidos nas estações de tratamento de efluentes[5-7]. Esses medicamentos, mesmo que presentes em baixas concentrações (ng L^{-1} até µg L^{-1}), podem oferecer riscos à saúde humana[3,4].

Adsorventes híbridos (produzidos a partir de biomassa e material inorgânico) têm sido empregados para elevar a capacidade de adsorção dos materiais orgânicos, através da modificação da superfície dos mesmos[8]. Taninos são um tipo de biopolímero natural que possuem alta hidrofilicidade, entretanto é necessário realizar imobilização antes de ser empregados como adsorventes[8].

Vários processos de tratamento utilizados para a remoção de contaminantes emergentes a partir de água e / ou águas residuais são a separação por membrana[9], processos avançados de oxidação[10,11], oxidação eletroquímica[12], processos biológicos[13,14], microfiltração e nanofiltração[15,16] e adsorção[17-19]. Estes processos de tratamento químicos, biológicos e físicos têm suas próprias vantagens e desvantagens.

Os métodos encontraram aplicação limitada, pois são complexos e / ou não econômicos. No entanto, a adsorção foi considerada o método mais atraente para a remoção de poluentes orgânicos. O processo de adsorção apresenta algumas vantagens:

(i) o método é simples;

(ii) os adsorventes são reutilizáveis;

(iii) trata-se um processo de baixo custo[17-20].

Recentemente, vários materiais foram utilizados como adsorventes ou como precursores para a preparação de adsorventes. Tais materiais incluem nanotubos de carbono[21], sílica[22], polissiloxanos[23], zeólitas[24], lodo de esgoto[23,25], lodo de curtume[26] e resíduos agroindustriais como casca de romã[27], serragem de madeira[28,29], casca pinhão[30], casca de carvalho[31], casca de cacau[32], etc. No entanto, é importante a prospecção de novos materiais que possam conter maior capacidade de adsorção, de modo a remover uma alta gama de poluentes altamente tóxicos de sistemas aquosos.

Devido às propriedades texturais, especialmente o volume de poros e a área de superficial específica, os carvões ativados são amplamente utilizados para a adsorção de poluentes orgânicos a partir de soluções aquosas[25,26, 28-32]. Os carvões ativados podem ser preparados através do processo de pirólise usando-se a pirólise térmica convencional ou o processo assistido por microondas[28,30]. A principal diferença entre os métodos é a forma como o calor é gerado. As micro-ondas fornecem energia diretamente no leito de carvão[26,28,29] enquanto o aquecimento convencional usa a condução e / ou a convecção[30]. O aquecimento por micro-ondas é vantajoso em relação à pirólise convencional, razão pela qual a carbonização ocorre com um tempo menor de pirólise (menos de 10 min)[26,32]. Como resultado, há um aumento rápido da temperatura[26,32], e uma diminuição notável no consumo de energia[26].

A principal vantagem e novidade do presente estudo é que os carbonos ativados induzidos por micro-ondas foram preparados por um único estágio de pirólise. A biomassa impregnada com inorgânicos só pode ser carbonizada em forno de microondas[29]. Esta é a principal razão pela qual os pesquisadores carbonizam os precursores orgânicos em um forno convencional para produzir material carbonizado (isto é, condutor de micro-ondas) e, posteriormente, a ativação do mesmo através da indução de microondas[33-35]. Por outro lado, no presente estudo, a impregnação do material de carbonoso com inorgânicos é realizada antes da pirólise assistida por micro-ondas. Esse procedimento pode ser realizado em uma única etapa[26,28,29,35]. Este processo de uma única etapa reduz o tempo total para a produção de carvões ativados. Outra

novidade e vantagem deste trabalho é que o tempo total de pirólise, incluindo o tempo para o resfriamento do reator de quartzo, em nosso estudo foi inferior a 11 min.

2. OBJETIVOS

2.1. OBJETIVO GERAL

O presente estudo tem como objetivo principal verificar a eficiência de remoção de poluentes orgânicos através do processo de adsorção, empregando-se o caroço de abacate como material precursor para a obtenção de carvão ativo (remoção de fármacos e compostos fenólicos), bem como o emprego de materiais híbridos orgânicos e inorgânicos (remoção de corante).

2.2. OBJETIVOS ESPECÍFICOS

- Preparação e caracterização do carvão ativo a partir do caroço de abacate por meio de processo de micro-ondas.
- Preparação e caracterização do carvão ativo a partir do caroço de abacate por meio de processo de forno térmico
- Preparação e caraterização de adsorvente híbrido orgânico e inorgânico a partir de taninos e de diferentes proporções de APTES (3-aminopropiltrietoxisilano).
- Avaliar os efeitos dos parâmetros de pH e dosagem nos processos de adsorção e cinéticos no uso dos adsorventes produzidos.
- Avaliar as isotermas de equilíbrio para a remoção dos contaminantes estudados.
- Verificar as capacidades de adsorção dos adsorventes produzidos na remoção dos poluentes orgânicos

3. REVISÃO BIBLIOGRÁFICA

3.1. CONTAMINANTES EMERGENTES

Contaminantes emergentes são compostos químicos que estão sendo detectados em águas, em níveis diferentes do esperado, de acordo com a Agência de proteção Ambiental Norte Americana (EPA, do inglês *Environmental Protection Agency*)[36]. Pertencem a essa classe de compostos: produtos de higiene pessoal, fármacos, drogas ilícitas, pesticidas, aditivos alimentares.

Ao se empregar o termo "emergente" não significa que esses compostos estejam sendo liberados no meio ambiente recentemente mas que o interesse da comunidade científica nesses materiais é recente devido aos danos que podem causar quando apresentados em pequenas quantidades[37].

3.2. COMPOSTOS FENÓLICOS

O fenol e seus compostos derivados são considerados como poluentes ambientais e agentes cancerígenos[38,39] e estão muito presentes em efluentes industriais, pois apresentam grande emprego em diversas áreas como: na produção de inseticidas, drogas, herbicidas, resinas artificiais[38] indústrias farmacêuticas e siderúrgicas, unidades petroquímicas, indústrias de gaseificação de carvão[40-42],fabricação de papel, madeira, borracha, tintas e indústrias de pesticidas[43].

Compostos fenólicos apresentam alta toxicidade, baixa degradabilidade e alta demanda de oxigênio e podem ser absorvidos por nosso corpo através do contato com a pele, do canal alimentar e de vias respiratórias[39]. Tais compostos mesmo em baixas concentrações ($0{,}1 \mu g\ L^{-1}$)[44] podem apresentar toxicidade para a vida humana e aquática.

A intoxicação causada pelos compostos fenólicos pode apresentar graves riscos à saúde humana, tais como: náuseas, vômitos, dores de garganta, de estômago, entre outras, ocorrendo posteriormente queda de pressão arterial, coma e convulsão[45-48].Esses compostos apresentam alta toxicidade para algumas formas de vida aquática em concentrações acima de 50 $\mu g\ L^{-1}$. Compostos fenólicos possuem a capacidade de se

combinar com o cloro existente na água potável, originando clorofenóis, compostos com maior toxicidade[49,50].

Neste trabalho, foram utilizados como adsorvatos os fenóis Resorcinol e 3-Aminofenol, por estarem presentes em diversos efluentes industriais, sendo compostos de alta toxicidade e devido ao processo de adsorção apresentar grande capacidade de remoção dos mesmos.

3.2.1.Resorcinol

Resorcinol é um composto fenólico fatal se ingerido, causando danos à pele e ao pulmão, causa irritabilidade e pode causar metahemoglobinemia, afetando o sistema cardiovascular, sistema nervoso central, sangue, fígado e rins.

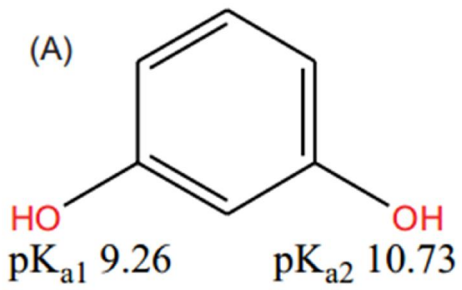

Figura 1(A). Fórmula estrutural da resorcina, valores de pKa estão apresentados na molécula.

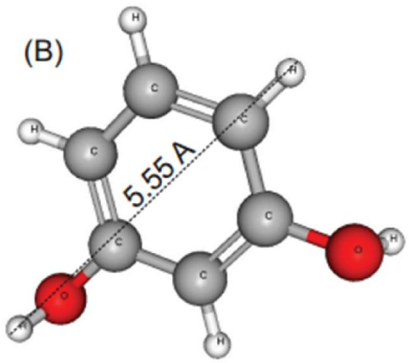

Figura 1(B). Fórmula estrutural tridimensional otimizada da resorcina. Área superficial de Van der Waals = 158,58 A^2 (pH 4,4 – 9,9). Área superficial polar = 40,46 A^2 (pH 0,0 – 9,1). Momento dipolar = 0,33 Debye, log P = 1,37. Balanço hidrofílico-lipofílico de Davies (HLB) = 7,95. As dimensões da molécula foram calculadas usando o *software* Marvin Sketch versão 16.6.6.0.

3.2.2. 3-Aminofenol

Compostos aromáticos que possuem nitrogênio também são uma grande preocupação, não só porque causam graves problemas de saúde, mas, ao mesmo tempo, são venenos importantes para os catalisadores[18]. Muitos dos compostos aromáticos são conhecidos por serem convertidos em CO_2, H_2O e pequenas moléculas, dependendo dos tipos de substituintes e os seus desaparecimentos fotocatalíticos foram medido[51-57].

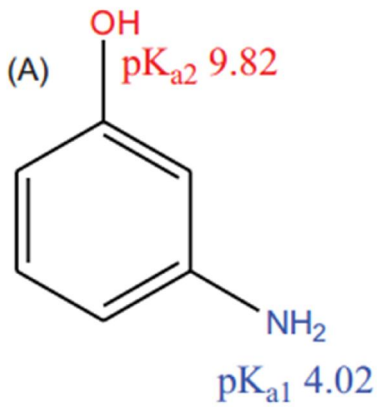

Figura 2 (A). Fórmula estrutural do 3-aminofenol, valores de pKa estão apresentados na molécula.

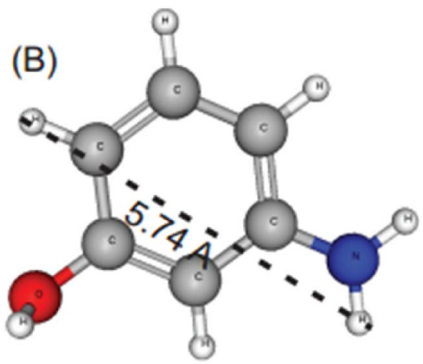

Figura 2(B). Fómula estrutural tridimensional otimizada do 3-aminofenol.Área superficial de Van der Waals = 161,92 A^2 (pH 4,4 – 9,9). Área superficial polar = 46,25 A^2 (pH 4,4 – 9,9). Momento dipolar = 4,09 Debye, log P = 0,84. Balanço hidrofílico-lipofílico de Davies (HLB) = 7,95. As dimensões da molécula foram calculadas usando o *software* Marvin Sketch versão 16.6.6.0.

3.3. FÁRMACOS

Os fármacos, devido ao fato de serem moléculas biologicamente ativas, são considerados contaminantes ambientais. A grande maioria desses compostos possui características lipofílicas e são, geralmente, pouco degradáveis no meio ambiente[58]. Essas características fazem com que os fármacos sejam bioacumulados no ambiente. Cerca de 3.000 compostos, atualmente, são empregados como fármacos de diversos tipos como: antibióticos, antidepressivos, analgésicos, entre outros[59].

Como os fármacos são produzidos para seguir rotas metabólicas específicas, podem também apresentar efeitos colaterais[60]. Dentre os principais danos causados pelos fármacos, podem ser citados: disfunção endócrina[61], absorção pelas plantas[62] e bioacúmulo na cadeia alimentar[63]. Associam-se a esses riscos o surgimento de superbactérias[64], câncer[65] e infertilidade humana[66].

Devido ao rápido desenvolvimento de técnicas analíticas, é possível realizar-se um estudo sobre a ocorrência de fármacos no ambiente, sendo possível a quantificação de concentrações muito baixas (μg L^{-1} e ng L^{-1}) em efluentes aquosos, água superficial e subterrânea[67]. O surgimento desses compostos em meios aquosos pode ocorrer por diversas formas sendo a principal fonte os efluentes de ETEs[68] .

Os fármacos apresentam importantes características que os distinguem de outros contaminantes, como[69,70]:

- Apresentam diversas formas, grupos funcionais e estruturas, sendo formados por uma ampla diversidade de moléculas.
- São moléculas polares com mais de um grupo ionizável, lipofílicos e alguns apresentam solubilidade em água.

- Podem permanecer no ambiente por longos períodos, como alguns anos.
- Após a administração, podem modificar sua estrutura química, através de rotas metabólicas.

A remoção, de forma efetiva, dos fármacos de efluentes aquosos é uma questão de saúde pública, pois não se obtém muitas informações sobre o efeito que podem causar, quando ingeridos traços de fármacos em águas potáveis[71,72]. Dentre os grupos de fármacos mais encontrados em águas estão os antibióticos, anti-inflamatórios e analgésicos[73,74,75].

A amoxicilina é um antibiótico, pertencente à classe das penicilinas, sendo utilizada no tratamento de diversos tipos de infecções bacterianas, tanto em seres humanos quanto em animais. Devido à sua facilidade de absorção oral, a amoxicilina possui um maior consumo quando comparada a outros tipos de antibióticos. Por não ser biodegradável, é capaz de inibir a fotossíntese de algas[76].

A nimesulida é um anti-inflamatório pertencente à classe das sulfonamidas. È consumida mundialmente sendo, no Brasil, um dos anti-inflamatórios mais utilizados. Segundo alguns estudos, a nimesulida pode causar danos aos rins e fígado[77].

O paracetamol é um analgésico e antipirético, empregado no alívio de dores e febre. É um dos fármacos mais encontrados mundialmente em águas superficiais e efluentes. Altas doses desse medicamento podem causar danos ao fígado e aos rins[78,79].

3.4. Corantes

Os primeiros relatos sobre a utilização de corantes conhecida foi há aproximadamente 4.000 anos atrás, sendo encontrado o corante azul índigo em envoltórios de múmias em no Egito. Os corantes naturais eram empregados até quase o final do século XIX, obtidos através de plantas e pequenos animais como moluscos e insetos. O primeiro corante orgânico sintético, a mauveína, foi descoberto por Perkin, em 1856[80].

Os corantes, naturais ou sintéticos, podem ser definidos como compostos que possuem coloração intensa e conferem cor a um material quando foram aplicadas ao

mesmo. A presença de corantes em corpos hídricos pode causar a mortalidade da vida aquática, diminuição da demanda química de oxigênio e de processos fotossintéticos, assim como podem ser tóxicos ou carcinogênicos[81]. A molécula de corante é constituída por duas partes em sua composição: o grupo cromóforo, que apresenta ligações duplas conjugadas contendo elétrons deslocalizados, que são os responsáveis pela cor, e os auxocromos que são grupos ionizáveis, responsáveis pela solubilidade em água e aumentam sua afinidade com a fibra[81,82].

3.4.1. Fixação do corante

O corante normalmente é fixado à fibra têxtil em solução aquosa e basicamente são quatro tipos de interações responsáveis por esse processo, sendo elas:

- Interações de Van der Waals: baseiam-se na interação máxima entre os orbitais π do corante e da molécula da fibra, de modo que as moléculas do corante sejam "ancoradas" fixamente sobre a fibra através de afinidade, sem a formação de ligação química propriamente dita. Pode-se encontrar esse tipo de interação nas tinturas de lã e poliéster com corantes que possuam alta afinidade com celulose[83].
- Interações iônicas: baseiam-se na mútua interação entre o centro positivo (grupos amino e carboxilatos da fibra) com a carga da molécula de corante. Exemplos mais comumente observados para esse tipo de interação são: tintura de lã, seda e poliamida[83].
- Interações de hidrogênio: ligações realizadas entre os átomos de hidrogênio covalentemente ligados no corante com elementos que possuam pares de elétrons livres de átomos doadores. Exemplos: tinturas de lã, seda e fibras sintéticas[83].
- Interações covalentes: baseiam-se na ligação covalente entre a molécula de corante, contendo grupo eletrofílico e resíduos nucleofílicos da fibra. Exemplos: tinturas de fibra de algodão[83].

3.4.2. Classificação dos corantes

Os corantes podem ser classificados de acordo com sua estrutura química ou devido à maneira pela qual é fixado na fibra têxtil.

- Corantes ácidos: também chamados de corantes aniônicos, apresentam grupos sulfônicos em sua estrutura. São solúveis em água[83].
- Corantes básicos: também chamados de corantes catiônicos, realizam ligações iônicas com grupos que apresentam cargas opostas presentes nas fibras[83].
- Corantes reativos: apresentam grupo eletrofílico com a capacidade de formar ligações covalentes com grupos que constituintes das fibras celulósicas, como hidroxila, amino e tióis. Dentre os diversos tipos de corantes reativos, podem ser citados como os mais importantes os que possuem a função azo e antraquinonas como grupos cromóforos. Este tipo de corantes apresenta alta solubilidade em água[83].
- Corantes dispersos: corantes insolúveis em água, empregados em fibras hidrofóbicas e em celulose[83].
- Corantes diretos: corantes aniônicos solúveis em água. O tingimento ocorre devido às interações de Van der Waals. Esses corantes apresentam grupo azo em sua estrutura[83].

3.5. Origem e produção de abacate

Segundo relatos, o abacate existia desde o descobrimento das Américas. Por volta de 1520, o abacate já era conhecido na Colômbia e entre os anos de 1532 a 1550 surgiu no México[84], que é o maior produtor mundial, tendo como um dos pratos mais conhecidos a *Guacamole*.

No Brasil, os primeiros relatos oficiais sobre o abacate são de 1893, quando os abacateiros das espécies Antilhana, forneceram as primeiras sementes da espécie para o Brasil. A safra anual do abacate é de cerca de 150 toneladas, porém no ano de 2008, chegou a 173 mil toneladas[85].

O abacate comercial é representado por três grupos, que são:

- Mexicana (Persea americana variedade *drymfolia*): encontrada nas regiões com elevadas altitudes na América Central (México) e Cordilheira dos Andes, é a espécie mais resistente ao frio, conseguindo suportar até – 6^0 C.
- Guatemalense (Persea americana variedade *guatemalensis*): tem origem nas regiões com elevadas altitudes na América Central (Guatemala, Belize e El Salvador) e apresenta como principal característica a casca mais espessa e rugosa, além do fato de o caroço ser preso à polpa.
- Antilhana (Persea americana variedade americana): são os abacates conhecidos como "comuns". São oriundos das regiões tropicais da América do Sul e regiões baixas da América Central (Panamá e Costa Rica).

No Brasil são comercializados diversos tipos de abacate, cada um com um período específico para a colheita, formato e peso, sendo os principais tipos: Fucks, Geada, Margarida, Ouro Verde, Breda, Fortuna, Quintal e Hass.

Na Figura 3 estão representados os principais tipos de abacate comercializados no Brasil:

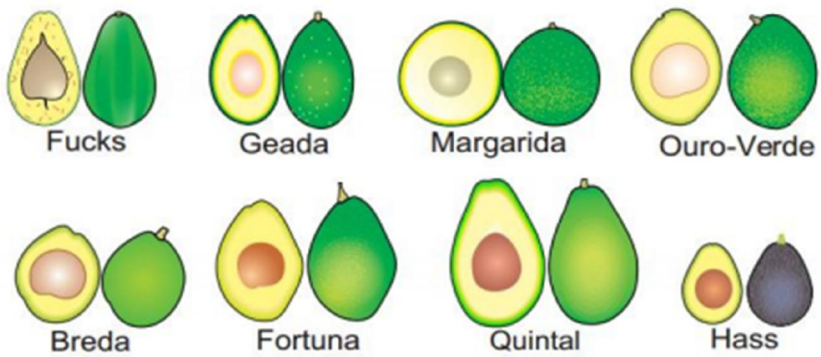

Figura 3: Tipos de abacate comercializados no Brasil[80].

O caroço de abacate apresenta em sua composição majoritariamente compostos fenólicos como: flavonoides, ácidos fenólicos, antocianinas, catequinas e as

proantocianidinas. O caroço pode representar cerca de 10 a 25% do peso do abacate, podendo variar de acordo com a espécie em questão.

4. ADSORÇÃO

A remoção de contaminantes do meio aquático ou de efluentes aquosos é um tema que preocupa a comunidade científica, e devido a isso existem muitas pesquisas para uma melhor efetividade nesse processo. Dentre os métodos empregados para a remoção de contaminantes, a adsorção é um dos métodos mais eficazes[87,88]. O processo de adsorção consiste na separação de substâncias, onde existe a transferência de um ou mais analitos de um meio para uma superfície. Adsorvato é denominada a espécie a qual está sendo transferida para uma superfície, é denominado adsorvente onde será retido o adsorvato[89].

De acordo com a magnitude das forças existentes neste processo, a adsorção pode ser de dois tipos: fisissorção (adsorção física) ou quimissorção (adsorção química). Na fisissorção, existe uma interação entre os grupos funcionais presentes na superfície do adsorvente com o adsorvato.

A quimissorção é um processo caracterizado pela formação de ligações químicas que ocorrem entre os adsorventes e adsorvatos e possuem energia de ligação superiores quando comparadas às forças de ligação da fisissorção. No processo de quimissorção, as moléculas de adsorvato são atraídas para sítios ativos específicos do adsorvente. Nesse tipo de adsorção, o processo ocorre em uma única camada, sendo possivelmente mais camadas através do processo de fisissorção[89,90,91].

Existem muitas diferenças entre os dois processos de adsorção, porém a principal diferença está na diferença de valores de entalpia de ligação. Na fisissorção, a interação ocorre através de forças de Van der Waals, com um valor de entalpia de ligação de até 20 kJ mol^{-1} [89]. Na quimissorção, os valores de entalpia variam geralmente de 80 a 400 kJ mol^{-1} [90,91].

O mecanismo de adsorção de um adsorvato em fase aquosa envolve geralmente quatro etapas[90,91,92]conforme a representação esquemática da Figura 4.

(1) **Transporte do interior da solução:** transporte do adsorvato ao interior da solução para a camada externa do filme líquido envolvendo a partícula do adsorvente.

(2) **Difusão externa:** difusão do adsorvato para a superfície do adsorvente através do filme líquido.

(3) **Difusão intrapartícula:** transferência do adsorvato da superfície da partícula do adsorvente para os sítios no interior da partícula, que pode ocorrer por difusão de poro, que é a difusão molecular do soluto em poros preenchidos com um fluido. Existe outro tipo de difusão intrapartícula, onde a difusão do soluto na superfície do adsorvente ocorre depois da adsorção, chamada de difusão de superfície.

(4) **Adsorção:** ocorre nos poros menores até que o equilíbrio seja atingido.

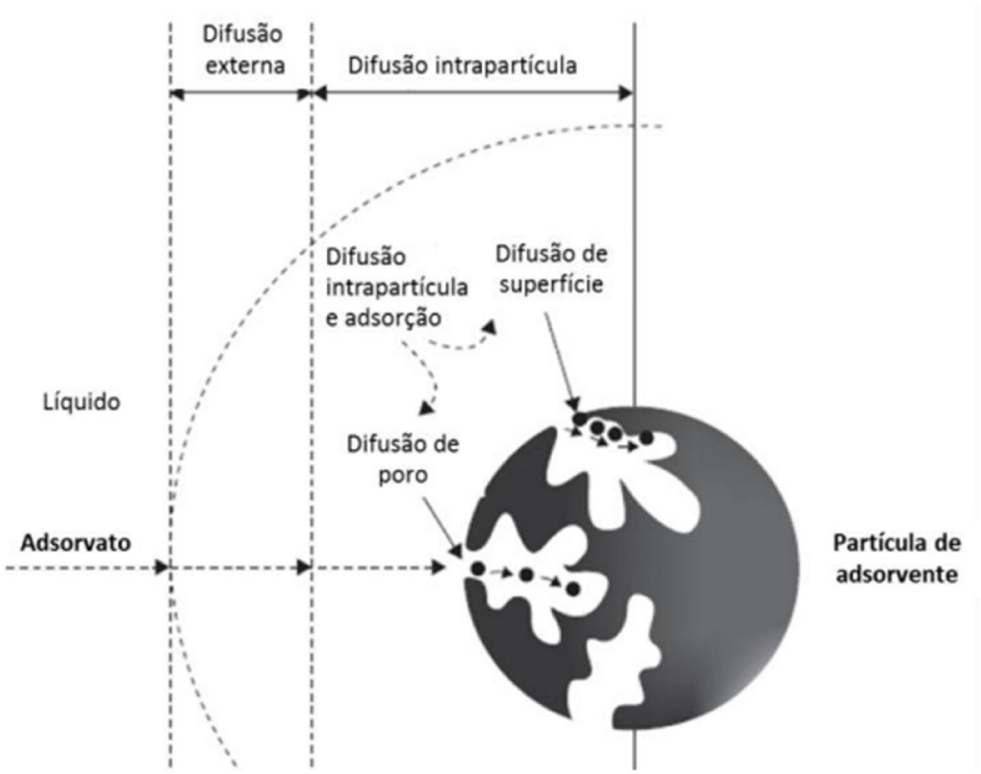

Figura 4. Representação do mecanismo de adsorção através dos processos de difusão externa e difusão intrapartícula de um adsorvato em uma partícula de adsorvente[90].

4.1. CARVÃO ATIVO

Os carvões ativos são materiais que possuem alta porosidade e sua estrutura é composta principalmente por carbono. Os mesmos são formados por espaços entre as moléculas, que estão contidos em uma rede tridimensional de camadas de grafeno, possuindo arranjos de anéis de carbono. A rede tridimensional possui algumas camadas que estão dispostas quase paralelamente umas às outras, apresentada na Figura 4[93].

Os carvões ativos possuem em sua estrutura heteroátomos como: oxigênio, hidrogênio, enxofre, nitrogênio e outros elementos na forma de grupos funcionais e/ou átomos ligados quimicamente à sua estrutura (Figura 4). Oxigênio é o principal heteroátomo, pois está presente em grupos funcionais como carboxila, carbonila, éter, fenol, lactona e outro[94]. Os grupos oxigenados são os mais importantes, pois podem alterar fortemente as propriedades do carvão ativo como polaridade e acidez, por exemplo[90].

Processos oxidativos, métodos de modificação bastante utilizados, introduzem átomos de oxigênio na matriz do carvão modificando a superfície química do carvão ativo[89]. No entanto, chegou-se à conclusão de que o carvão ativo tratado por processos oxidativos apresenta um caráter significativamente ácido e uma baixa capacidade de adsorção de compostos fenólicos[96].

O carvão ativo é um dos adsorventes industriais amplamente utilizados. Do ponto de vista industrial, o carvão ativo tem muitos aspectos importantes em aplicações como: filtração e purificação[97], super capacitores[98], entrega de drogas[99], armazenamento de hidrogênio[100], catalisadores[101] entre outras. As vantagens mais importantes do CA são sua alta área superficial, estrutura de poro interna bem desenvolvida e grupos funcionais químicos de superfície localizados em seu exterior e superfícies internas[102,103]. Entretanto, seu uso em grande escala é restrito devido ao elevado custo de produção[104]. A preparação de carvão ativo a partir de recursos renováveis como subprodutos agrícolas baseados em biomassa como casca de pinhão[105], casca de cupuaçu[106], caroço de pêssego[107], caroço de cereja[108], casca de laranja[109], casca de amêndoa[110] e caule de algodão[45] bambu[111], a casca de coco[112] e o resíduo de chá[113] é uma das maneiras mais empregadas pelos pesquisadores para reduzir o custo da matéria prima.

A produção de carvão ativo assistida por micro-ondas recebeu grande atenção nos últimos anos, devido a ser um processo rápido e por apresentar redução de energia[114]. Os grupos funcionais do carvão ativo podem ser alterados com métodos de modificação de superfície, como processos químicos[115], físicos[116], tratamentos com micro-ondas[111,117,118]e impregnação[119].

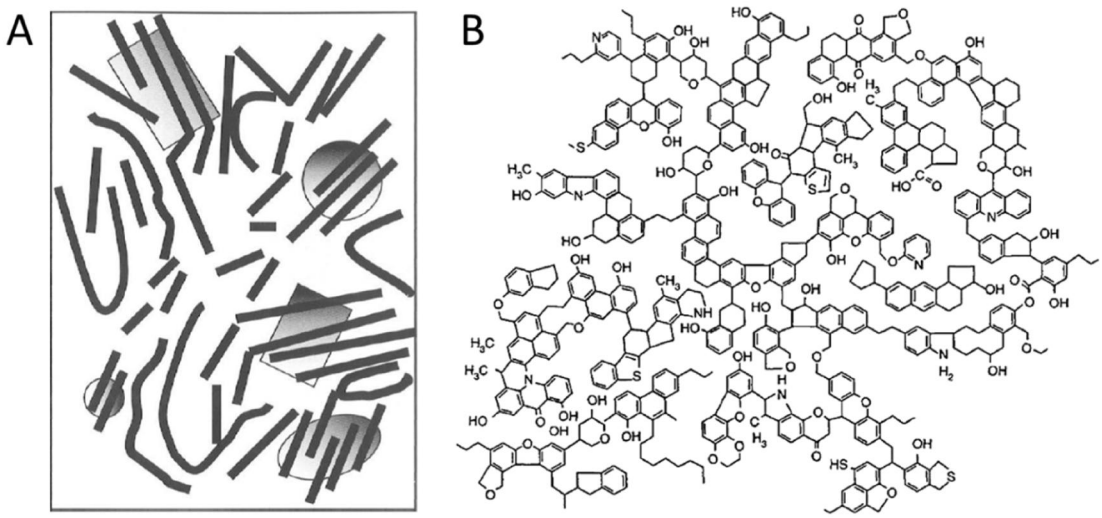

Figura 5. (A) Modelo estrutural de um carvão ativo formado por camadas de átomos de carbono dispostas de forma desordenada. (B) Modelo estrutural de um carvão ativo ilustrando a sua porosidade e os grupos funcionais em sua superfície (O, S, N)[120].

4.2 MODELOS DE ISOTERMAS DE ADSORÇÃO

As isotermas de adsorção expressam a quantidade de adsorvato (mg) removida por unidade de massa de adsorvente (g), e meio fluido (líquido ou gasoso) após a solução atingir o equilíbrio. As isotermas apresentam características específicas de acordo com uma dada temperatura em particular[121].

Com a aplicação de isotermas, é possível calcular-se a quantidade de adsorvato que um determinado adsorvente pode remover, o adsorvente mais apropriado para um adsorvato estabelecido[121], estabelecendo-se assim a relação de equilíbrio existente entre

a concentração de adsorvato e adsorvente de acordo com a temperatura empregada no processo[122].

Os parâmetros de equilíbrio de adsorção são úteis para o fornecimento das propriedades da superfície do adsorvente, mecanismo de adsorção entre adsorvente e adsorvato[121].

Existem diversas equações empregadas para descrever o equilíbrio existente entre adsorvente e adsorvato, dentre as mais conhecidas são: Langmuir, Freundlich e Liu, entre outros[122].

4.2.1. Isoterma de Langmuir

O modelo da isoterma de Langmuir[123] é baseado nas seguintes proposições[124,125,126]:

- Os adsorvatos são quimicamente adsorvidos em um número fixo de sítios bem definidos.
- Uma monocamada de adsorvato é formada sobre a superfície do adsorvente quando ocorre a saturação.
- Cada sítio pode conter somente uma espécie de adsorvato.
- Todos os sítios são energeticamente equivalentes.
- Não há interações entre as espécies de adsorvato.

A isoterma de Langmuir está descrita na **Equação 1**:

$$q_e = \frac{Q_{\max} \cdot K_L \cdot C_e}{1 + K_L \cdot C_e} \qquad (1)$$

onde q_e é a quantidade de adsorvato adsorvida no equilíbrio (mg g^{-1}), C_e é a concentração de adsorvato restante no equilíbrio (mg L^{-1}), K_L é a constante de equilíbrio de Langmuir (L mg^{-1}) e Q_{max} é a capacidade máxima de adsorção do adsorvente (mg g^{-1}).

4.2.2. Isoterma de Freundlich

O modelo de Freundlich[127] assume que a concentração de adsorvato na superfície do adsorvente aumenta indefinidamente com o aumento da concentração. Trata-se de um modelo empírico, utilizado amplamente em sistemas heterogêneos. O modelo também assume que a adsorção poderia acontecer em múltiplas camadas[106,124]. A isoterma de Freundlich é apresentada na **Equação (2)**:

$$q_e = K_F \cdot C_e^{1/n_F} \tag{2}$$

onde K_F é a constante de equilíbrio de Freundlich [mg g^{-1}(mg L^{-1})$^{-1/nF}$] e n_F é o expoente de Freundlich (adimensional).

4.2.3Isoterma de Liu

O modelo de Liu[128] é uma combinação das isotermas de Langmuir e de Freundlich, desconsiderando-se as hipóteses dos modelos de Langmuir e de Freundlich, monocamada e a hipótese da adsorção infinita, respectivamente. O modelo de Liu prevê que os sítios ativos do adsorvente possuem energias diferentes, podendo o adsorvente apresentar sítios ativos preferenciais para a adsorção[124]. A isoterma de Liu está representada na **Equação 3**:

$$q_e = \frac{Q_{\max} \cdot (K_g \cdot C_e)^{n_L}}{1 + (K_g \cdot C_e)^{n_L}} \tag{3}$$

onde K_g é a constante de equilíbrio de Liu (L mg^{-1}); n_L é o expoente de Liu (adimensional) e Q_{max} é a capacidade máxima de adsorção do adsorvente (mg g^{-1}).

4.3. MODELOS CINÉTICOS DE ADSORÇÃO

Estudos de cinética de adsorção são importantes, pois fornecem informações importantes sobre o mecanismo envolvido no processo de adsorção[124]. A partir da cinética de equilíbrio, é possível determinar-se a taxa com que um determinado adsorvato seja adsorvido em uma solução aquosa[129]. Muitos modelos cinéticos foram desenvolvidos com a finalidade de se encontrar as constantes envolvidas na cinética de adsorção[124].

4.3.1. Ordem geral

Os expoentes de leis de velocidade de reações químicas normalmente não dependem dos coeficientes das mesmas. Isso significa que a ordem da reação química deve ser determinada experimentalmente[1330,131]. Com o objetivo de estabelecer uma lei geral de velocidade, O processo de adsorção na superfície do adsorvente é determinado como a etapa determinante da velocidade, de modo a estabelecer-se uma lei de velocidade geral. Quando a lei universal de velocidade de reação é aplicada à **Equação 4**, a expressão da velocidade de adsorção é obtida[130-136].

$$\frac{dq}{dt} = k_N (q_e - q_t)^n \qquad (4)$$

onde k_N é a constante de velocidade, q_e é a quantidade de adsorvato adsorvida no equilíbrio, q_t é a quantidade de adsorvato adsorvida no tempo t e n é a ordem da adsorção em relação à concentração dos sítios ativos presentes na superfície do adsorvente. O expoente n pode ser um número inteiro ou racional. A **Equação 5** descreve o número de sítios ativos (θ_t) disponíveis na superfície do adsorvente:

$$\theta_t = 1 - \frac{q_t}{q_e} \tag{5}$$

A **Equação 6** descreve a relação entre a variável θ_t e a velocidade de adsorção:

$$\frac{d\theta_t}{dt} = -k\theta_t^n \tag{6}$$

onde $k = k_N(q_e)^{n-1}$. Para o adsorvente puro, $\theta_t = 1$. O valor de θ_t diminui durante o processo de adsorção. Quando o processo de adsorção atinge o equilíbrio, θ_t se aproxima de um valor fixo. Para um adsorvente saturado, $\theta_t = 0$.A **Equação 6** leva à **Equação 7** após integração:

$$\int_1^{\theta} \frac{d\theta_t}{\theta_t^n} = -k\int_0^t dt \tag{7}$$

A **Equação 7** leva à **Equação 8**:

$$\frac{1}{1-n} \cdot \left[\theta_t^{1-n} - 1\right] = -kt \tag{8}$$

Rearranjando a **Equação 8**, é obtida a **Equação 9**:

$$\theta_t = \left[1 - k\left(1-n\right) \cdot t\right]^{1/1-n} \tag{9}$$

Substituindo a **Equação 9** na **Equação 5** e considerando $k = k_N(qe)^{n-1}$, obtém-se a **Equação 10**:

$$q_t = q_e - \frac{q_e}{\left[k_N (q_e)^{n-1} \cdot t \cdot (n-1) + 1\right]^{1/1-n}} \tag{10}$$

A **Equação 10** é a equação de cinética de ordem geral de um processo de adsorção, sendo válida para$n \neq 1$[130-136].

4.3.2. Pseudo-primeira ordem

O modelo de cinética de pseudo-primeira ordem é um caso particular do modelo de ordem geral[102-104].Considerando-se a **Equação 6** quando $n = 1$:

$$\frac{d\theta_t}{dt} = -k \cdot \theta_t^1 \tag{11}$$

Pela integração da **Equação 11**, é obtida a **Equação 12**:

$$\theta_t = \exp(-k_1 \cdot t) \tag{12}$$

Quando a **Equação 5** é substituída na **Equação 12** e k é substituída por k_1, é obtida a **Equação 13** ou modelo de cinética de pseudo-primeira ordem.

$$q_t = q_e \left[1 - \exp(-k_1 \cdot t)\right] \tag{13}$$

4.3.3 Pseudo-segunda ordem

O modelo de cinética de pseudo-segunda ordem também é um caso particular do modelo de ordem geral[130-136]. Será considerada agora a **Equação 10** quando $n = 2$:

$$q_t = q_e - \frac{q_e}{\left[k_2(q_e) \cdot t + 1\right]} \tag{14}$$

Rearranjando a **Equação 14**, é possível obter a **Equação 15**:

$$q_t = \frac{q_e^2 k_2 t}{\left[k_2(q_e)\cdot t + 1\right]} \quad (15)$$

4.3.4.Difusão intrapartícula

A adsorção ocorre em quatro etapas básicas, sendo a terceira etapa a difusão intrapartícula, conforme explicado no **item 3.1**. A adsorção pode ser afetada de acordo com a resistência existente na etapa de difusão intrapartícula, de acordo com a **Equação 16**:

$$q_t = k_{id}\sqrt{t} + C \quad (16)$$

Onde *qt* é a quantidade de adsorvato adsorvia no tempo *t* (min), k_{id} é a constante de difusão intrapartícula (mg $g^{-1}min^{-0,5}$) e C é uma constante relacionada com a espessura da camada de difusão (mg g^{-1})[124].

4.4.FATORES QUE AFETAM A CAPACIDADE DE ADSORÇÃO

4.4.1. Propriedades morfológicas

Para que o processo de adsorção seja eficiente é necessário que seja realizada a escolha de um adsorvente adequado. Algumas características são fundamentais para que esse adsorvente seja determinado: capacidade de adsorção e seletividade assim como o custo, de forma que o processo seja viável economicamente[136].

O processo de adsorção é um fenômeno de superfície e dessa forma características como: área superficial e específica, volume e tamanho de poros, são fatores de grande importância nesse processo[136]. O tamanho dos poros do adsorvente apresenta papel extremamente importante na eficiência do processo de adsorção, visto que nesse processo o adsorvato pode ficar retido na superfície do adsorvente ou ocorrer um processo de difusão intra-partícula (difusão do adsorvato pelos poros do adsorvente). Neste segundo mecanismo, o tamanho dos poros está diretamente associado com a velocidade de difusão das espécies e com a quantidade das mesmas que pode ser adsorvida nos poros do material[136].

A porosidade total do adsorvente pode ser classificada de acordo com o diâmetro dos poros, conforme determinação da IUPAC, em: microporos, mesoporos e macroporos. Os microporos apresentam diâmetro inferior a 2 nm, os mesoporos possuem diâmetro entre 2 e 50 nm e os macroporos possuem poros com diâmetro superior a 50 nm[137].

4.4.2. Concentração inicial do adsorvato

De acordo com o aumento da concentração de adsorvato, a quantidade de adsorvida também aumenta. Esse efeito ocorre devido à maior quantidade de adsorvato para os sítios ativos do adsorvente, fornecendo uma força motriz que é capaz de superar toda a resistência de transferência de massa de adsorvato entre a fase aquosa e a fase sólida. Quando os sítios ativos do adsorvente se aproximam da saturação, a percentagem de remoção tende a diminuir[138]. Consequentemente, em adsorventes que possuam baixa capacidade de adsorção, o aumento da concentração inicial resulta em um aumento da quantidade adsorvida, tendo-se ao mesmo tempo, uma diminuição do percentual de remoção[139].

4.4.3. Efeito da temperatura

A variação da temperatura exerce grande influência na velocidade dos processos de adsorção, sendo desta forma, um parâmetro de grande importância. A elevação da

temperatura pode causar um aumento da energia cinética e da mobilidade das moléculas do adsorvato, assim como a elevação da taxa de difusão intra-partícula do adsorvato. Dessa forma, a variação de temperatura em um processo de adsorção leva a uma mudança na capacidade de adsorção[140].

Na realização de estudos de adsorção em diversas temperaturas, obtém-se o valor das constantes de velocidade, com o qual é possível calcular-se a energia de ativação do processo através da **Equação 17**:

$$\ln k = \ln A - \frac{Ea}{RT} \quad (17)$$

Onde k representa a constante de velocidade da reação, *A* a constante de Arrhenius, E*a* a energia de ativação de Arrhenius (KJ mol^{-1}) do processo de adsorção, T é a temperatura absoluta (Kelvin) e R a constante universal dos gases 8,134 $J.mol^{-1}.K^{-1}$. Ao plotar um gráfico $ln\ k$ versus 1/T deve-se obter uma relação linear com o coeficiente angular de - E*a*/*R*, permitindo assim o cálculo da E*a* do processo[141].

4.4.4. Efeito do pH

O parâmetro mais importante no estudo de adsorção é o efeito do pH, pois de acordo com o adsorvente, a variação do pH altera a capacidade de adsorção. Através do estudo do pH, é possível determinar se a superfície do adsorvente estará carregada positiva ou negativamente, esse estudo é o ponto de carga zero (pH_{pzc}), valor de pH na qual a carga líquida na superfície é igual a zero[139].

Para valores de pH menores que o pH_{pzc}, a carga na superfície do adsorvente é positiva, favorecendo portanto a adsorção de espécies aniônicas. Para valores de pH maiores que o pH_{pzc}, a carga na superfície do adsorvente é negativa, favorecendo a adsorção de espécies catiônicas[139].

4.5. PARÂMETROS TERMODINÂMICOS

Os parâmetros termodinâmicos apresentam informações sobre o processo de adsorção de acordo com a variação da temperatura. A mudança de energia livre de Gibbs (ΔG°, kJ mol^{-1}) é o critério fundamental para determinar a espontaneidade do sistema. Geralmente ΔG° para a fisissorção é menor do que para quimissorção. A variação de entalpia (ΔH°, kJ mol^{-1}) indica se o processo de adsorção é endotérmico ou exotérmico. A variação de entropia (ΔS°, J mol^{-1} K^{-1}) fornece informações sobre a desordem do sistema. Essa avaliação pode ser feita através das **Equações 18, 19 e 20**[133]:

$$\Delta G^o = \Delta H^o - T\Delta S^o \quad (18)$$

$$\Delta G^o = -RT \cdot Ln(K) \quad (19)$$

Combinando-se as **Equações 18 e 19**, obtém-se a **Equação 20**:

$$ln(k) = \frac{\Delta S^\circ}{R} - \frac{\Delta H^\circ}{R} . \frac{1}{T} \quad (20)$$

onde R é a constante universal dos gases (8,314 J K^{-1} mol^{-1}), T é a temperatura absoluta (Kelvin), e K representa a constante de equilíbrio de adsorção dos modelos de isoterma.

A partir constante de equilíbrio (K), pode-se estimar os parâmetros termodinâmicos de adsorção. O processo endotérmico é caracterizado pelo aumento do valor de K com o aumento da temperatura. Os valores de ΔS e ΔH podem ser calculados a partir da inclinação e do intercepto da reta ln (K) versus 1/T.

5. PROCEDIMENTO EXPERIMENTAL

5.1. REAGENTES E SOLUÇÕES

Todas as soluções foram preparadas com água deionizada. Os adsorvatos resorcinol e 3-aminofenol (**Apêndice 1**) foram fornecidos pela empresa Vetec (Rio de Janeiro, Brasil). Os fármacos amoxicilina, cafeína, captopril, enalapril, meloxicam, nimesulida, paracetamol, propanolol, diclofenaco de sódio, tetracilina e compostos

fenólicos 1-naftol, 2-naftol, 2-aminofenol, 3- aminofenol, 2-clorofenol, 2-nitrofenol, 4-nitrofenol, pirocatecol, resorcina, hidroquinona, o-cresol, m-cresol, 4-metoxifenol, bisfenol-A e timol foram fornecidos pela empresa Sigma-Aldrich (São Paulo, Brasil) (**Apêndice 2**). O corante ácido vermelho 1 foi fornecido pela empresa Vetec (São Paulo, Brasil), e os reagentes 3-aminopropiltrietoxisilano (APTES, 98%) (**Apêndice 3**).

Soluções estoque de 5000 mg L^{-1} foram preparadas conforme pesagem e dissolução das quantidades calculadas das soluções de trabalho em água deionizada. Através da solução estoque, foram realizadas diversas dissoluções para a obtenção das soluções de trabalho. O pH das soluções foi ajustado com o auxílio de um pHmetro (Schott Lab 850, Mainz, Alemanha), utilizando-se as soluções de NaOH 1,0 mol L^{-1} e HCl 1,0 mol L^{-1} (Neon, São Paulo, Brasil) para o ajuste do pH.

Para a ativação química dos carvões produzidos, foram empregados os reagentes $ZnCl_2$, etanol fornecido pela empresa Merck (Rio de Janeiro, Brasil) e hidróxido de amônio (28-30% v/v) fornecido pela empresa Sigma-Aldrich (São Paulo, Brasil)

Os reagentes resorcinol (RES), 3-aminofenol (AMP), 2-nitrofenol, 2-naftol, 2-clorofenol, 4-nitrofenol, hidroquinona, 3-cresol, bisfenol A, fenol, 2-cresol, ácido húmico, sulfato de sódio, cloreto de sódio, fosfato de sódio, carbonato de sódio e nitrato de potássio foram utilizados na preparação da simulação de efluentes. Todos os reagentes foram fornecidos pela empresa Vetec (Rio de Janeiro).

5.2. PREPARAÇÃO DOS ADSORVENTES

5.2.1. Carvão ativo de caroço de abacate em forno de micro-ondas

O carvão ativado foi preparado pesando-se 100,0 g $ZnCl_2$ e solubilizando o mesmo em 50,0 mL de água deionizada com posterior adição de 100,0 g de caroço de abacate (CA), previamente desidratado, moído (com um diâmetro < 250 μm), conforme apresentado na Figura 5 (proporção inorgânicos: orgânicos de 1:1) previamente seco em estufa a 105 ^{0}C durante 4 horas de modo a formar uma pasta homogênea. A pasta formada foi aquecida a 80 ^{0}C durante 30 minutos e após esse período a mesma foi seca em estufa a 90 ^{0}C durante 120 minutos. Posteriormente, 10,0 g da pasta (CA

impregnado com $ZnCl_2$) foram inseridos em um reator de quartzo em formato cilíndrico.

Abacate | Caroço de abacate | Caroço de abacate triturado

Figura 6. Abacate e caroço de abacate triturado.

O reator de quartzo foi inserido em um forno de micro-ondas adaptado com duas aberturas, uma na parte superior e outra na parte inferior, de modo que o reator ficasse em posição vertical e centralizado dentro do forno. A pirólise foi realizada sob atmosfera inerte (150 mL min^{-1}). Um frasco coletor de vidro foi acoplado na parte inferior do reator pra recolher o óleo gerado no processo de pirólise. A carbonização da pasta ocorreu em quatro ciclos de 80 s a 1200 W. Após a pirólise, o sistema foi resfriado durante 5 minutos sob 60 mL min^{-1} de nitrogênio. O tempo total de um ciclo de pirólise levou menos de 11 minutos, incluindo 5 minutos de resfriamento. Foram realizados outros ciclos de pirólise de modo a carbonizar todo o material preparado.

Figura 7. Fluxograma do processo de pirólise e lixiviação de carvão produzido em forno de micro-ondas.

Completando o processo de ativação química, foi realizada a lixiviação dos compostos inorgânicos, com HCl 6 mol L^{-1}. Foram misturados 10,0 g do material pirolisado com 200 mL de HCl 6 mol L^{-1} em um balão de fundo chato de 500 mL. A mistura foi agitada magneticamente e refluxada durante 2 h (70^0C – 80^0C). O material resultante foi resfriado à temperatura ambiente e filtrado sob vácuo utilizando-se uma membrana de 0,45 μm em um sistema Sartorius de policarbonato (Goettingen, Alemanha).

O filtrado foi descartado e o carvão foi lavado repetidas vezes até atingir o pH da água deionizada. Após, o carvão foi misturado com 200 mL de ácido etilenodiaminotetraacético (EDTA) 0,010 mol L^{-1} (pH 10), sob agitação durante 15 minutos. O carvão foi filtrado sob vácuo e depois misturado novamente à solução de EDTA (mesma concentração e pH) para eliminar traços de metais pesados no carvão. O adsorvente foi lavado repetidamente com água deionizada até atingir o pH da mesma. O carvão resultante foi seco em estufa a 105^0 C durante 5 h, com tamanho de partícula ≤106 μm e armazenado adequadamante até sua utilização. O adsorvente foi nomeado como ASAC.

Para verificar a lixiviação de Zn a partir do carvão preparado, 30,0 mg de ASAC foram misturados com 20,0 mL de água em um tubo do tipo Falcon de 50,0 mL e agitado durante 24 h. A fase sólida foi separada por centrifugação e a fase líquida foi analisada em um *Analyst 200 Flame Atomic Absorption Spectrometry* – PerkinElmer (Massachusetts, EUA) utilizando chama de ar-acetileno (10:2,5 L min^{-1}). Uma lâmpada de cátodo oco de Zn (l = 213,86 nm) foi utilizada como fonte de radiação.

5.2.2. Carvão ativo de caroço de abacate em forno convencional

Procedimento semelhante ao descrito no item 3.2.1 onde a pasta homogênea obtida foi transferida em um reator de quartzo tubular e o mesmo foi inserido em um forno de aquecimento convencional, Figura 7 (Sanchis, Porto Alegre, RS, Brasil). A programação de aquecimento das amostras seguiu as variações de temperatura e tempo de pirólise, conforme apresentado na Tabela 1:

Tabela 1: Programações das temperaturas de pirólise.

Experimento	Amostras	Temperaturas (^{0} C)	Tempo de pirólise (min)
1	ASAC 1	500	30
2	ASAC 2	700	30
3	ASAC 3	500	60
4	ASAC 4	700	60
5	ASAC 5	600	45
6	ASAC 6	600	45
7	ASAC 7	600	45

O processo de lixiviação dos carvões foi realizado conforme o item 3.2.1.

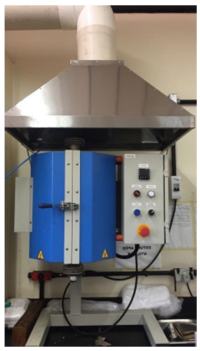

Figura 8. Forno convencional onde foram realizadas as pirólises referentes à Tabela 1.

5.2.3. Adsorventes híbridos

Os adsorventes híbridos de taninos e APTES foram preparados utilizando-se o catalisador básico NH_4OH (28-30% v/v) para a hidrólise do APTES em pH 10-11. Cerca de 5g de taninos foram dispersos em solução de 50 mL de etanol e amônia (100-250 µL). Então 2,5 g de APTES foram adicionadas a amostra foi agitada (300 rpm) sob refluxo 24 h a 75^0 C. Através desse procedimento em uma etapa, foram produzidos os híbridos de taninos e material silicatado. A adição da solução de amônia foi responsável para uma rápida reação de hidrólise e polimerização de APTES misturados com taninos (Apêndice 3). Posteriormente o material foi seco em estufa a 70^0 C por 16 horas em uma estufa. O material produzido nessa etapa foi chamado de Tan-Ap-0.5. Similarmente, as amostras Tan-Ap-1.0 e Tan-Ap-2.0 foram preparadas utilizando-se 5 g de taninos e 5g de APTES e 5 g de taninos e 10 g de APTES respectivamente.

5.2.4. Caracterização do adsorvente

A morfologia das superfícies dos carvões ativos e dos precursores *in natura* foram avaliadas através de microscopia eletrônica de varredura (SEM, do inglês *scanning electron microscopy*) empregando-se um microscópio JEOL, modelo JSM 6060 (Tóquio, Japão)[143]. A voltagem de aceleração empregada foi de 10 kV. A magnificação variou entre 1500 e 2500 vezes[144].

Os grupos funcionais nas superfícies dos carvões ativos foram caracterizados através de espectroscopia na região de infravermelho com transformada de Fourier (FTIR, do inglês *Fourier transform infrared spectroscopy*) em um equipamento Bruker, modelo alfa, (EUA). Os materiais AS e ASAC e o KBr foram secos em estufa a 120 ^{0}C durante 8 horas, armazenados em frascos fechados e mantidos em dessecador até a realização da análise. A resolução dos espectros foi de 4 cm^{-1} com 100 varreduras[145].

As isotermas de adsorção /dessorção de N_2 foram obtidas no ponto de ebulição do nitrogênio líquido (-196 ^{0}C) utilizando-se um analisador área de superficial Micromeritics Instrument, Tristar II 3020, (Norcross, EUA). Os adsorventes foram desgaseificados a 180 ^{0}C durante 12 h sob vácuo antes das análises. As propriedades texturais dos adsorventes foram avaliadas através dos métodos de BET (Brunauer, Emmett e Teller) e de BJH (Barret, Joyner e Halenda), respectivamente[144].

A determinação do potencial de carga zero (pH_{pzc}) dos carvões de abacate pirolisados em forno convencional foram determinados através do seguinte procedimento: 20,00 mL de solução de NaCl 0,050 mol L^{-1} foram adicionados a vários tubos Falcon de 50 mL contendo 50,0 mg de adsorvente. O pH das soluções foi ajustado para valores de 2,00 a 10,00 com soluções de HCl 0,10 mol L^{-1}e de NaOH 0,10 mol L^{-1}. As suspensões foram colocadas em uma câmara climatizada com agitação reciprocante (Oxylab, São Leopoldo, Brasil) de 150 rpm, a 25 °C, durante 24 h. A seguir, as amostras foram centrifugadas a 3500 rpm durante 5 min em uma centrífuga Excelsa II 206-BL (Fanem, São Paulo, Brasil). O procedimento de centrifugação foi repetido quando necessário. O pH_i (pH das soluções sem contato com o adsorvente) e o pH_f (pH

do sobrenadante depois do contato com o adsorvente) foi registrado. O valor do pH_{pzc} é o ponto onde a curva de ΔpH (pH_f-pH_i) *versus* pH_i cruza a linha do zero[146].

A reflectância difusa no infravermelho (DRUV, do inglês *diffuse reflectance UV–vis spectroscopy*) em um espectrofotômetro Shimadzu 2450 UV utilizando Integrador de ligação esférico ISR – 2200, na temperatura de 25^{0}C e faixa espectral de 200 – 800 nm.

Esta técnica foi empregada para avaliar as propriedades eletrônicas dos precursores, taninos e APTES, assim como a comparação da mistura dos mesmos para a obtenção dos adsorventes híbridos taninos/APTES. A linha de base foi obtida utilizando $BaSO_4$ (Indústrias de Químicas Pura Wako Ltda). As amostras foram pulverizadas para a realização de suas análises [147,148].

Para a determinação do índice de hidrofobicidade, 0,3 g de taninos e de taninos modificados foram secos em béqueres de 10 mL na temperatura de 70 ^{0}C durante 24 horas. As amostras foram resfriadas em dessecador antes da pesagem das mesmas. Posteriormente os béqueres foram expostos a uma atmosfera saturada com vapor de solvente (n-heptano ou água) em frascos Erlenmeyer, utilizando-se 60 mL de solvente. As amostras foram então colocadas nos béqueres de 10 mL e estes dentro dos frascos Erlemeyer contendo o solvente, de tal maneira que o conteúdo dos béqueres não estivesse em contato direto com o solvente ou a parede dos frascos Erlenmeyer[150]. O experimento foi realizado em uma câmara com a temperatura regulada em 25 ^{0}C. Após 24 horas, as amostras foram removidas dos frascos Erlenmeyer, secas cuidadosamente na parte externa dos béqueres e pesadas novamente. A razão hidrofílica-hidrofóbica foi calculada pela razão entre a quantidade adsorvida de vapor de n-heptano pela quantidade adsorvida de vapor de água, com o resultado expresso em $mg.g^{-1}$.

5.3. ESTUDOS DE ADSORÇÃO

5.3.1. Resorcinol e 3-aminofenol

A capacidade de adsorção do material ASAC foi avaliada para a remoção dos compostos fenólicos RES e AMP de soluções aquosas, com concentrações variando de

100,0 – 1800,0 mg L^{-1}. Alíquotas de 20,00 mL das soluções fenólicas foram adicionadas a 5,0 – 200,0 mg de ASAC em tubos Falcon de 50,0 mL. Diferentes condições de pH (2,0 – 10,0) foram avaliadas. Os tubos foram então tampados e colocados em uma câmara aclimatada com agitação reciprocante (150 rpm) durante 1 – 480 min. A temperatura foi variada de 25^0C 50^0C.

As amostras foram posteriomente centrifugadas (5 minutos) usando-se uma centrífuga Unicen M Herolab, para a separação do adsorvente da solução fenólica. O processo de centrifugação foi repetido até que o sobrenadante ficasse límpido. O sobrenadante (1 – 5 mL) foi então diluído para 10,0 – 50,0 mL em frascos padrão usando a solução branco com o pH adequado.

As concentrações de RES e AMP remanescentes em solução após o processo de adsorção foram determinadas em comprimentos de onda máximos de 273nm para RES e 282 nm para AMP utilizando-se um espectrofotômetro (T90 +PG Instruments UV-VIS; Londres, Inglaterra). A capacidade de adsorção e a remoção percentual de compostos fenólicos são obtidos pelas equações (21) e (22) respectivamente:

$$q = \frac{(C_0 - C_f)}{m} . V \tag{21}$$

$$\%\ Remoção = 100 . \frac{(C_0 - C_f)}{C_0} \tag{22}$$

Onde q é a quantidade de compostos fenólicos adsorvidos (mg g^{-1}); C_0 é a concentração inicial de adsorvato, RES e AMP, (mg L^{-1}); C_f são as concentrações dos fenóis em equilíbrio, após o processo de adsorção (mg L^{-1}); m é a massa seca de adsorvente (g) e V é o volume da solução de fenóis (L).

5.3.2. Contaminantes Emergentes

A capacidade de adsorção de compostos fenólicos e fármacos pelos carvões produzidos em forno convencional foi realizada utililzando-se 20,00 mL de compostos fenólicos (500 mg L^{-1}) e fármacos (200 mg L^{-1}) em tubos Falcon de 50,0 mL. Diferentes condições de pH (2,0 – 10,0) foram avaliadas. Os tubos foram então tampados e colocados em uma câmara aclimatada com agitação reciprocante (150 rpm) durante 1 – 480 min. A temperatura foi variada de 25^0C 50^0C.

O procedimento realizado seguiu-se conforme o item 4.3.1. Todos os experimentos foram realizados em triplicata.

5.3.3 Corante Vermelho Ácido 1

Alíquotas de 20,00 mL de 100,00 – 250,00 mg L^{-1} do corante vermelho ácido 1(variação de pH de 2,00 – 8,00) foram adicionados a tubos Falcon de 50,00 mL com massa de material adsorvente de 30,00 mg.Os tubos foram então tampados e colocados em uma câmara aclimatada com agitação reciprocante (150 rpm) durante 5 min – 24 h. Posteriormente, os adsorventes foram separados da solução através de centrifugação e as alíquotas de 1-5 mL foram diluídas e o pH dessas soluções foi medido.

As concentrações de corante vermelho ácido 1 remanescentes em solução após o processo de adsorção foram determinadas em comprimentos de onda máximos de 273nm para RES e 282 nm para AMP utilizando-se um espectrofotômetro (T90 +PG Instruments UV-VIS; Londres, Inglaterra).

5.4. AVALIAÇÃO ESTATÍSTICA E GARANTIA DE QUALIDADE

Os experimentos foram realizados em triplicata (n = 3) para garantir precisão e confiabilidade os dados. As corridas em branco foram realizadas em paralelo[144]. Todas as soluções foram armazenadas em frascos de vidro âmbar. Todos os materiais utilizados no experimento receberam uma limpeza prévia com solução HNO_3 10%[150], enxaguados com água deionizada, secos e armazenados em armários fechados.

Os dados das curvas padrão de calibração de RES e AMP (10,0 – 150,0 mg L^{-1}respectivamente) foram realizadas utilizando-se o *software* UV-Win T90 + Espectrofotômetro PG Instruments. Os limites de detecção de RES e AMP foram 0,013 e 0,011 mg L^{-1}, respectivamente. A relação sinal / ruído foi 3[138]. Uma solução de fenol (70,0 mg L^{-1}) foi utilizada como controle de qualidade para cada 10 determinações. Isso determinou que as leituras das concentrações de RES e AMP fossem precisas[151].

O aplicativo *Microcal Origin* 2015 foi empregado para avaliar o melhor ajuste dos dados cinéticos de equilíbrio, pelo método Simplex e o algoritmo Levenberg-Marquardt aplicando equações não-lineares. A adequação dos modelos de equilíbrio e cinética foi avaliada utilizando-se o coeficiente de determinação (R^2), o coeficiente de

determinação ajustado (R^2_{adj}) e o desvio padrão (SD, do inglês *standard deviation*). A diferença entre os valores teóricos e experimentais de RES e AMP adsorvidos pelo ASAC foram medidos usando-se SD. A expressão matemática para (R2), (R2adj) e SD são fornecidos pelas **Equações (23), (24) e (25), respectivamente**:

$$R^2 = \left(\frac{\sum_i^n (q_{i,exp} - \bar{q}_{exp})^2 - \sum_i^n (q_{i,exp} - q_{i,model})^2}{\sum_i^n (q_{i,exp} - \bar{q}_{exp})^2}\right) \quad (23)$$

$$R^2_{adj} = 1 - (1 - R^2).\left(\frac{n-1}{n-p-1}\right) \quad (24)$$

$$SD = \sqrt{\left(\frac{1}{n-p}\right).\sum_i^n (q_{i,exp} - q_{i,model})^2} \quad (25)$$

Onde q_i, model representa cada valor de q teórico individual de um dado modelo; $q_{i,exp}$representa cada valor de q experimental individual; q_{exp} expressa a média dos valores experimentais de q; n representa o numero de experimentos realizados; p representa o número de parâmetros do modelo[152].

6. CONCLUSÕES

As conclusões com esta tese foram divididas em três seções, de acordo com cada artigo publicado:

6.1. CARVÃO ATIVO DE CAROÇO DE ABACATE NA REMOÇÃO DE 3-AMINOFENOL E RESORCINA

Neste trabalho, o ASAC foi preparado por processo de aquecimento por micro-ondas após ativação química com $ZnCl_2$ como agente ativante. O carvão ativado produzido exibiu alta área específica superficial 1.433 m^2 g^{-1}. Os resultados do S_{BET} mostram que o ASAC possuía 19,48% de microporos e 80,52% de superfície. Em relação ao volume de poros, 26,74% do volume de poros correspondeu a microporos e

73,26% a mesoporos. Portanto, o ASAC sintetizado neste estudo de pesquisa pode ser classificado como predominantemente mesoporoso. A capacidade de adsorção do ASAC foi avaliada usando percentagens de remoção de RES e AMP. Os modelos de Avrami de ordem fracionária e modelo de isoterma Liu foram encontrados como os melhores ajustes para os dados experimentais. De acordo com o modelo de isoterma de Liu, a capacidade máxima de adsorção alcançada foi de 406,2 e 454,5 mg g^{-1} para RES e AMP a 50 ° C, respectivamente. Estes valores de capacidade de adsorção encontrados, foram os maiores entre os relatados na literatura. Foi visto que a partir do efeito da temperatura e de dados termodinâmica, que os processos de adsorção de RES e AMP no carvão ASAC foram dependentes da temperatura. O processo de adsorção foi exotérmico e espontâneo. O carvão ativado por abacate apresentou excelente remoção de efluentes fenólicos simulados; eles foram efetivamente removidos com percentual maior que 96,94% de uma mistura contendo altas concentrações de fenóis, matéria orgânica e alta salinidade. Pode ser concluído que, ASAC pode ser efetivamente usado em águas residuais reais contaminadas com compostos fenólicos.

6.2. CARVÕES ATIVOS DE CAROÇO DE ABACATE: OTIMIZAÇÃO E APLICAÇÃO NA REMOÇÃO DE CONTAMINANTES EMERGENTES

Neste estudo, caroços de abacate foram utilizados com sucesso como matéria-prima para produzir carvões ativados por pirólise convencional. A fim de determinar a melhor condição para produzir os carbonos ativados, empregou-se um experimento fatorial completo (DOE) variando-se a temperatura (500–700 ° C) e tempo de pirólise (30–60 min).Os dois fatores avaliados (temperatura e tempo de pirólise) influenciaram fortemente os valores de S_{BET} e volume de poros; ambos os fatores tiveram um efeito negativo, o que significa que o aumento dos valores levaram a diminuições na S_{BET} e nos valores de volume de poros. O carvão ativado produzido apresentou alta áreas de superficiais específicas na faixa de 1122-1584 m^2 g^{-1}.A caracterização da superfície revelou que os ASACs possuem características superficiais hidrofílica se possuem predominantemente grupos ácidos em suas superfícies. Os ASACs preparados foram empregados na adsorção de25 compostos orgânicos emergentes, como 10 produtos

farmacêuticos e 15 compostos fenólicos que apresentaram altos valores de absorção para todos os poluentes emergentes. Observou-se que o carvão ativado preparado à temperatura mais alta de pirólise(700 ° C), que gerou menos grupos funcionais totais e apresentou maior HI, foi o carvão ativado com maior capacidade de sorção para a adsorção de contaminantes orgânicos emergentes.Com base nos resultados deste trabalho, é possível concluir que o caroço de abacate pode ser empregado como matéria-prima para produzir carvões ativados de elevada área superficial e muito eficientes em relação ao tratamento de águas poluídas com produtos orgânicos poluentes emergentes.

6.3. ADSORVENTES HÍBRIDOS DE TANINOS E APTES (3-AMINOPROPILTRIETOXISILANO) E SUA APLICAÇÃO NA ALTA CAPACIDADE DE REMOÇÃO DO CORANTE VERMELHO ÁCIDO 1

Neste trabalho, materiais híbridos foram preparados misturando-se taninos e APTES, e os materiais modificados resultantes foram caracterizados e aplicados na remoção do corante vermelho ácido 1 de soluções aquosas por adsorção. Os dados de caracterização indicam a formação de um material híbrido tipo I, através de ligações covalentes provavelmente entre o derivado silícico e os grupos hidroxila presentes nas estruturas fenólicas do tanino. Os taninos modificados apresentam altas propriedades de adsorção com tanino não modificado. As melhores condições experimentais foram alcançadas em pH 2,0, tempo de8 h e a 50^0C. Os dados de adsorção cinética e de equilíbrio foram ajustados pelos modelos de Liu e de ordem geral, respectivamente. A capacidade máxima de adsorção obtida foi de 418,3 mg g^{-1} a 50 ° C por material tanino-APTES na proporção de 1: 1 (Tan-Ap-1.0). Baseado em dados experimentais verificou-se que as interações eletrostáticas e ligações de hidrogênio entre os adsorventes híbridos e corante vermelho ácido 1 têm desempenhado um importante papel no seu processo de adsorção. O efeito da temperatura demonstrou que o Q_{max} aumenta com um aumento da temperatura. As estimativas dos parâmetros termodinâmicos estabeleceram a adequação da adsorção de corante vermelho ácido 1 e os valores ΔG ° confirmam a viabilidade e espontaneidade do processo de adsorção. Os materiais modificados foram testados através do tratamento de efluentes de corantes sintéticos e apresentaram resultado satisfatório no tratamento desses efluentes.

7. REFERÊNCIAS BIBLIOGRÁFICAS

(1) S. Kottuparambil, Y.J. Kim, H. Choi, M.S. Kim, A. Park, J. Park, W. Shin, T. Han, A rapid phenol toxicity test based on photosynthesis and movement of the freshwater flagellate, *Euglena agilis* Carter, Aquat. Toxicol., **2014**, 155, 9–14.

(2) M.D. Erturk, M.T. Saçan, Assessment and modeling of the novel toxicity data set of phenols to Chlorella vulgaris, Ecotoxicol. Environ. Saf., **2013**, 90, 61–68.

(3) Fernández, M.; Fernández, M.; Laca, A.; Laca, A.; Díaz, M. Seasonal Occurrence and Removal of Pharmaceutical Products in Municipal Wastewaters. *J. Environ. Chem. Eng.* **2014**, *2* (1), 495–502.

(4) Kyzas, G. Z.; Deliyanni, E. Modified Activated Carbons from Potato Peels as Green Environmental-Friendly Adsorbents for the Treatment of Pharmaceutical Effluents. *Chem. Eng. Res. Des.* **2015**, *97*, 135–144.

(5) Rigobello, E. S.; Dantas, A. D. B.; Di Bernardo, L.; Vieira, E. M. Removal of Diclofenac by Conventional Drinking Water Treatment Processes and Granular Activated Carbon Filtration. *Chemosphere* **2013**, *92* (2), 184–191.

(6) Secondes, M. F. N.; Naddeo, V.; Belgiorno, V.; Ballesteros, F. Removal of Emerging Contaminants by Simultaneous Application of Membrane Ultrafiltration, Activated Carbon Adsorption, and Ultrasound Irradiation. *J. Hazard. Mater.* **2014**, *264*, 342–349.

(7) Alidina, M.; Li, D.; Ouf, M.; Drewes, J. E. Role of Primary Substrate Composition and Concentration on Attenuation of Trace Organic Chemicals in Managed Aquifer Recharge Systems. *J. Environ. Manage.* **2014**, *144*, 58–66.

(8) H.A.M. Bacelo, S.C.R. Santos, C.M.S. Botelho, Tannin-based biosorbents for environmental applications–a review, Chem. Eng. J. 303 (2016) 575–587.

(9) M.D. Erturk, M.T. Saçan, Assessment and modeling of the novel toxicity data

set of phenols to Chlorella vulgaris, Ecotoxicol. Environ. Saf., **2013**, 90, 61–68.

(10) Y. Liu, M. Meng, J. Yao, Z. Da, Y. Feng, Y. Yan, C. Li, Selective separation of phenol from salicylic acid effluent over molecularly imprinted polystyrene nanospheres composite alumina membranes, Chem. Eng. J., 286 (2016) 622–631.

(11) E.B. Estrada-Arriaga, J.A. Zepeda-Aviles, L. García-Sánchez, Post-treatment of real oil refinery effluent with high concentrations of phenols using photo-ferrioxalate and Fenton's reactions with membrane process step, Chem. Eng. J., 285 (2016) 508–516.

(12) N. Wang, T. Zheng, G. Zhang, P. Wanga, A review on Fentonlike processes for organic wastewater treatment, J. Environ. Chem. Eng., 4 (2016) 762–787.

(13) N. Jarrah, N.D. Múazu, Simultaneous electro-oxidation of phenol, CN^{-}, $S^{2-}$and NH^{4+}in synthetic wastewater using boron doped diamond anode, J. Environ. Chem.Eng., 4 (2016) 2656–2664.

(14) R. Boonchai, G. Seo, Microalgae membrane photobioreactor for further removal of nitrogen and phosphorus from secondary sewage effluent, Korean J. Chem. Eng., 32 (2015) 2047–2052.

(15) A. Hussain, S. K. Dubey, V. Kumar, Kinetic study for aerobic treatment of phenolic wastewater, Water Resour. Ind., 11 (2015) 81–90.

(16) R. Muppalla, S.K. Jewrajka, A.V.R. Reddy, Fouling resistant nanofiltration membranes for the separation of oil–water emulsion and micropollutants from water, Sep. Purif. Technol., 143 (2015) 125–134.

(17) J.J. Rueda-Márquez, M.G. Pintado-Herrera, M.L. Martín-Díaz, A. Acevedo-Merino, M.A. Manzano, Combined AOPs for potential wastewater reuse or safe discharge based on multibarrier treatment (microfiltration-H_2O_2 / UV-catalytic wet peroxide oxidation), Chem. Eng. J., 270 (2015) 80–90.

(18) L. Ma, J. Zhua, Y. Xi, R. Zhu, H. He, X. Liang, G.A. Ayoko, Adsorption of phenol, phosphate and Cd(II) by inorganic–organic montmorillonites: a

comparative study of single and multiple solute, Colloids Surf., A, 497 (2016) 63–71.

(19) Z. Luo, M. Gao, S. Yang, Q. Yang, Adsorption of phenols on reduced-charge montmorillonites modified by bispyridinium dibromides: mechanism, kinetics and thermodynamics studies, Colloids Surf., A, 482 (2015) 222–230.

(20) V. Makrigianni, A. Giannakas, Y. Deligiannakis, I. Konstantinou, Adsorption of phenol and methylene blue from aqueous solutions by pyrolytic tire char: equilibrium and kinetic studies, J. Environ. Chem. Eng., 3 (2015) 574–582.

(21) L.D.T. Prola, E. Acayanka, E.C. Lima, C.S. Umpierres, J.C.P. Vaghetti, W.O. Santos, S. Laminsi, P.T. Njifon, Comparison of Jatropha curcasshells in natural form and treated by non-thermal plasma as biosorbents for removal of Reactive Red 120 textile dye from aqueous solution, Ind. Crops Prod., 46 (2013) 328–340.

(22) M. Shirmardi, A.H. Mahvi, B. Hashemzadeh, A. Naeimabadi, G. Hassani, M.V. Niri, The adsorption of malachite green (MG) as a cationic dye onto functionalized multi walled carbon nanotubes, Korean J. Chem. Eng., 30 (2013) 1603–1608.

(23) D. Pérez-Quintanilla, A. Sánchez, I. Sierra, Preparation of hybrid organic-inorganic mesoporous silicas applied to Mercury removal from aqueous media: influence of the synthesis route on adsorption capacity and efficiency, J. Colloid Interface Sci., 472 (2016) 126–134.

(24) G.S. dos Reis, C.H. Sampaio, E.C. Lima, M. Wilhelm, Preparation of novel adsorbents based on combinations of polysiloxanes and sewage sludge to remove pharmaceuticals from aqueous solutions, Colloids Surf., A, 497 (2016) 304–315.

(25) L. Wanga, C. Han, M.N. Nadagouda, D.D. Dionysiou, An innovative zinc oxide-coated zeolite adsorbent for removal of humic acid, J. Hazard. Mater., 313 (2016) 283–290.

(26) G.S. dos Reis, M. Wilhelm, T.C.A. Silva, K. Rezwan, C.H. Sampaio, E.C. Lima, S.M.A.G.U. Souza, The use of design of experiments for the evaluation of the production of surface rich activated carbon from sewage sludge via microwave and conventional pyrolysis, Appl. Therm. Eng., 93 (2016) 590–597.

(27) M.J. Puchana-Rosero, M.A. Adebayo, E.C. Lima, F.M. Machado, P.S. Thue, J.C.P. Vaghetti, C.S. Umpierres, M. Gutterres, Microwave-assisted activated carbon obtained from the sludge of tannery-treatment effluent plant for removal of leather dyes, Colloids Surf., A, 504 (2016) 105–115.

(28) M.S. Bretanha, M.C. Rochefort, G.L Dotto, E.C. Lima, S.L.P. Dias, F.A. Pavan, Punica granatumhusk (PGH), a powdered biowaste material for the adsorption of methylene blue dye from aqueous solution, Desal. Wat. Treat., 57 (2016) 3194–3204.

(29) P.S. Thue, M.A. Adebayo, E.C. Lima, J.M. Sieliechi, F.M. Machado, G.L. Dotto, J.C.P. Vaghetti, S.L.P. Dias, Preparation, characterization and application of microwave-assisted activated carbons from wood chips for removal of phenol from aqueous solution, J. Mol. Liq., 223 (2016) 1067–1080.

(30) P.S. Thue, E.C. Lima, J.M. Sieliechi, C. Saucier, S.L.P. Dias, J.C.P. Vaghetti, F.S. Rodembusch, F.A. Pavan, Effects of first-row transition metals and impregnation ratios on the physicochemical properties of microwave-assisted activated carbons from wood biomass, J. Colloid Interface Sci., 486 (2017) 163–175.

(31) T. Calvete, E.C. Lima, N.F. Cardoso, S.L.P. Dias, E.S. Ribeiro, Removal of brilliant green dye from aqueous solutions using home made activated carbons, Soil Air Water, 38 (2010) 521–532.

(32) A. Takdastan, A.H. Mahvi, E.C. Lima, M. Shirmardi, A.A. Babaei, G. Goudarzi, A. Neisi, M.H. Farsani, M. Vosoughi, Preparation, characterization, and application of activated carbon from low-cost material for the adsorption of tetracycline antibiotic from aqueous solutions, Water Sci. Technol., 74 (2016) 2349–2363.

(33) C. Saucier, M.A. Adebayo, E.C. Lima, R. Cataluna, P.S. Thue, L.D.T. Prola, M.J. Puchana-Rosero, F.M. Machado, F.A. Pavan, G.L. Dotto, Microwave-assisted activated carbon from cocoa shell as adsorbent for removal of sodium diclofenac and nimesulide from aqueous effluents, J. Hazard. Mater., 289 (2015) 18–27.

(34) Z.Z. Qiang, X.H. Ying, C. Srinivasakannan, P.J. Hui, Z.L. Bo, Utilization of Crofton weed for preparation of activated carbon by microwave induced CO_2 activation, Chem. Eng. Process., 82 (2014) 1–8.

(35) N. Ferrera-Lorenzo, E. Fuente, I. Suárez-Ruiz, B. Ruiz, KOH activated carbon from conventional and microwave heating system of a macroalgae waste from the Agar–Agar industry, Fuel Process. Technol., 121 (2014) 25–31.

(36) R.H. Hesas, W.M.A.W. Daud, J.N. Sahu, A.A. Niya, The effects of a microwave heating method on the production of activated carbon from agricultural waste: a review, J. Anal. Appl. Pyrolysis, 100 (2013) 1–11.

(37) United States Environmental Protection Agency (EPA). Contaminants of Emerging Concern including Pharmaceuticals and Personal Care Productshttps://www.epa.gov/wqc/contaminants-emerging-concern-includingpharmaceuticals-and-personal-care-products (accessado em 17 ago2018).

(38) Aga, D. S. Fate of Pharmaceuticals in the Environment and in Water Treatment Systems. *CRC Press***2008**.

(39) P. Podkoscielny, A. Dabrowski, O.V. Marijuk, Heterogeneity of activated carbons in adsorption of phenol aqueous solutions, Appl. Surf. Sci. 205 (2003) 297–301.

(40) B.K. Korbahti, A. Tanyolac, Continuous electrochemical treatment

of phenolic wastewater in a tubular reactor, Water Res. 37 (2003) 1505–1514.

(41) L.R. Radovic, C. Moreno-Castilla, J. Rivera-Utrilla, Carbon materials as adsorbents in aqueous solutions, in: L.R. Radovic (Ed.), Chemistry and Physics of Carbon, vol. 27, Marcel Dekker, New York, 2001, pp. 227–406.

(42) A. D¸ abrowski, P. Podko´ scielny, Z. Hubicki, M. Barczak, Adsorption of phenolic compounds by activated carbon – a critical review, Chemosphere 58 (2005) 1049–1070.

(43) M.A. Khan, B.H. Hameed, J. Lawler, M. Kumar, B.H. Jeon, Developments in activated functionalized carbons and their applications in waterdecontamination: a review, Desalin. Water Treat. (2014), http://dx.doi.org/10.1080/19443994.2014.885397 (in press).

(44) H.H.P. Fang, O.C. Chan, Toxicity of phenol towards anaerobic biogranules, Water Res. 31 (1997) 2229–2242.

(45) Nollet, L. M. L.; Gelder, L. S. P. Handbook of Water Analysis, 2nd ed.; CRC: Boca Raton, FL,2007.

(46) Busca, G.; Berardinelli, S.; Resini, C.; Arrighi, L. Technologies for the removal of phenol from flid streams: a short review of recente developments. **Journal of Hazardous Materials**, 160, (2008), 265-288.

(47) Milhome, M.A.L. **Emprego de quitina e quitosana para adsorção de fenol de efluente de refinaria de petróleo**. 2006. 90 f. Dissertação (Mestrado em Saneamento Ambiental) – Universidade Federal do Ceará. Fortaleza, 2006.

(48) Sertori, F.C. **Proposição de um reator fotocatalítico para degradação de fenol**. 2008. 87 f. Dissertação (Mestrado em Engenharia Química) – Universidade Estadual de Campinas UNICAMP. Campinas, 2008.

(49) Namane, A.; Hellal, A. The dynamics adsorption characteristics of phenol by granular activated carbono. **Journal of Hazardous Mateials**, 137, 2006, 618-325.

(50) US-EPA, Environmental Protection Agency. Integrated Risk Information System (IRIS) on 4-Methylphenol, National Center for Environmental Assessment, Office of Research and Development, Washington, DC, 1999.

(51) Directive 2000/60/EC of the European Parliament and of the Council establishing a framework for the Community action in the field of water policy, Official Journal L 327 on 22 December 2000 (2000).

(52) R.W. Matthews, S.R. McEvoy, J. Photochem. Photobiol. A: Chem. 64 (1992) 231.

(53) S. Das, M. Muneer, K.R. Gopidas, J. Photochem. Photobiol. A: Chem. 77 (1992) 83.

(54) Y.T. Wei, C. Wan, J. Photochem. Photobiol. A: Chem. 69 (1992) 241.

(55) Y.T. Wei, Y.Y. Wang, C. Wan, J. Photochem. Photobiol. A: Chem. 55 (1990) 115.

(56) J.C. D'Oliveira, G. Al-Sayyed, P. Pichat, Environ. Sci. Technol. 24 (1990) 990.

(57) A. Huang, L. Cao, J. Chen, F.J. Spiess, S.L. Suib, T.N. Obee, S.O. Hay, J.D. Freihaut, J. Catal. 188 (1999) 40.

(58) U. Stafford, K.A. Gray, P. Kamat, J. Catal. 167 (1997) 25.

(59) Ikehata, K.; Naghashkar, N. J.; El-Din, M.G. Degradation of aqueous pharmaceuticals by ozonation and advanced oxidation processes: a review. Ozone: Sci. Technol., v.28, p.353-414, 2006.

(60) Rodriguez-Narvaez, O. M.; Peralta-Hernandez, J. M.; Goonetilleke, A.; Bandala, E. R. Treatment Technologies for Emerging Contaminants in Water: A Review. *Chem. Eng. J.***2017**, *323*, 361–380.

(61) Zenker, A.; Cicero, M. R.; Prestinaci, F.; Bottoni, P.; Carere, M. Bioaccumulation and Biomagnification Potential of Pharmaceuticals with a Focus to the Aquatic Environment. *J. Environ. Manage.***2014**, *133*, 378–387.

(62) Mills, L. J.; Chichester, C. Review of Evidence: Are Endocrine-Disrupting Chemicals in the Aquatic Environment Impacting Fish Populations? *Sci. Total Environ.***2005**, *343*, 1–34.

(63) Calderón-Preciado, D.; Matamoros, V.; Bayona, J. M. Occurrence and Potential Crop Uptake of Emerging Contaminants and Related Compounds in an Agricultural Irrigation Network. *Sci. Total Environ.***2011**, *412–413*, 14–19.

(64) Andersson, D. I.; Hughes, D. Evolution of Antibiotic Resistance at Non-Lethal Drug Concentrations. *Drug Resist. Updat.***2012**, *15* (3), 162–172.

(65) Hess-Wilson, J. K.; Knudsen, K. E. Endocrine Disrupting Compounds and Prostate Cancer. *Cancer Lett.***2006**, *241* (1), 1–12.

(66) Fowler, P. a.; Bellingham, M.; Sinclair, K. D.; Evans, N. P.; Pocar, P.; Fischer, B.; Schaedlich, K.; Schmidt, J. S.; Amezaga, M. R.; Bhattacharya, S.; Rhind, S. M.; O'Shaughnessy, P. J. Impact of Endocrine-Disrupting Compounds (EDCs) on Female Reproductive Health. *Mol. Cell. Endocrinol.***2012**, *355* (2), 231–239.

(67) Petrovic, M.; Barcelo, D.; Pérez, S. *Analysis, Removal, Effects and Risk of Pharmaceuticals in the Water Cycle*; Elsevier B.V.: Oxford, 2013.

(68) Santos, L. H. M. L. M.; Araújo, A. N.; Fachini, A.; Pena, A.; Delerue-Matos, C.; Montenegro, M. C. B. S. M. Ecotoxicological Aspects Related to the Presence of Pharmaceuticals in the Aquatic Environment. *J. Hazar Mater.***2010**, *175* (1–3), 45–95.

(69) Rivera-Utrilla, J.; Sánchez-Polo, M.; Ferro-García, M. Á.; Prados-Joya, G.; Ocampo-Pérez, R. Pharmaceuticals as Emerging Contaminants and Their

Removal from Water. A Review. *Chemosphere***2013**, *93* (7), 1268–1287.

(70) Kümmerer, K. The Presence of Pharmaceuticals in the Environment due to Human Use - Present Knowledge and Future Challenges. *J. Environ. Manage.***2009**, *90* (8), 2354–2366.

(71) Petrović, M.; Hernando, M. D.; Díaz-Cruz, M. S.; Barceló, D. Liquid Chromatography-Tandem Mass Spectrometry for the Analysis of Pharmaceutical Residues in Environmental Samples: A Review. *J. Chromatogr. A***2005**, *1067* (1–2), 1–14.

(72) Taylor, D.; Senac, T. Human Pharmaceutical Products in the Environment - The "problem" in Perspective. *Chemosphere***2014**, *115*, 95–99.

(73) Goldstein, W. E. *Pharmaceutical Accumulation in the Environment: Prevention, Control,Health Effects, and Economic Impact*; CRC Press-Taylor & Francis Group: Boca Raton, 2014.

(74) Dietrich, D. R.; Webb, S. F.; Petry, T. *Hot Spot Pollutants: Pharmaceuticals in the Environment*; Elsevier Academic Press publications: Burlington, 2005.

(75) Jjemba, P. K. *Pharma-Ecology: The Occurrence and Fate of Pharmaceuticals and Personal Care Products in the Environment*; John Wiley & Sons, Inc.: New Jersey, 2008.

(76) Den Berghe, H. Van; Garric, X.; Vert, M.; Coudane, J. New Amoxicillin-Poly(lactic Acid)-Based Conjugates: Synthesis and in Vitro Release of Amoxicillin. *Polym. Int.***2011**, *60* (3), 398–404.

(77) de Sousa, J. M.; Neto, M. F. A.; Partata, A. K. Ação Anti-Inflamatória Da Nimesulida E Seu Grau de Hepatotoxicidade. *Rev. Científica do ITPAC***2016**, *9*.

(78) Xu, J. J.; Hendriks, B. S.; Zhao, J.; de Graaf, D. Multiple Effects of Acetaminophen and p38 Inhibitors: Towards Pathway Toxicology. *FEBS Lett.***2008**, *582* (8), 1276–1282.

(79) Bosch, M. E.; Sánchez, A. J. R.; Rojas, F. S.; Ojeda, C. B. Determination of

Paracetamol: Historical Evolution. *J. Pharm. Biomed. Anal.***2006**, *42* (3), 291–321.

(80) Natarajan, S.; Bajaj, H. C.; Tayade, R. J. Recent Advances Based on the Synergetic Effect of Adsorption for Removal of Dyes from Waste Water Using Photocatalytic Process. *J. Environ. Sci.***2016**, 1–22.

(81) Ngulube, T.; Gumbo, J. R.; Masindi, V.; Maity, A. An Update on Synthetic Dyes Adsorption onto Clay Based Minerals: A State-of-Art Review. *J. Environ. Manage.***2017**, *191*, 35–57.

(82) Banat, I. M.; Nigam, P.; Singh, D.; Marchant, R. Microbial Decolorization of Textile-Dye-Containing Effluents: A Review. *Bioresour. Technol.***1996**, *58* (3), 217–227.

(83) Guaratini, C. C. I.; Zanoni, M. V. B. Corantes Têxteis. *Quím. Nova***2000**, 23, 71-78.

(84) Donadio, L. C. Abacate para exportação: aspectos técnicos da produção. Brasília: Frupex. MAPA, 1995. 53 p.

(85) Donadio, L. C.; Ferrari, L.; AVILÉS, T. C. Abacate. In: Donadio, L. C. (Ed). História da Fruticultura Paulista. Jaboticabal: SBF – Sociedade Brasileira de Fruticultura, 2010. P 33-63.

(86) Instituto Brasileiro de Qualidade em Horticultura. Disponível em http://www.hortibrasil.org.br, acessado em março de 2018.

(87) Kyzas, G. Z.; Deliyanni, E. Modified Activated Carbons from Potato Peels as Green Environmental-Friendly Adsorbents for the Treatment of Pharmaceutical Effluents. *Chem. Eng. Res. Des.***2015**, *97*, 135–144.

(88) Hashemian, S.; Salari, K.; Yazdi, Z. A. Preparation of Activated Carbon from Agricultural Wastes (Almond Shell and Orange Peel) for Adsorption of 2-Pic from Aqueous Solution. *J. Ind. Eng. Chem.***2013**, *20* (4), 1892–1900.

(89) ATKINS, P.W.; Físico-Química, volume 3, sexta edição, LTC – Livros Técnicos e Científicos, Rio de Janeiro, 1999.

(90) Cecen, F.; Aktas, O. *Activated Carbon for Water and Wastewater Treatment: Integration of Adsorption and Biological Treatment*; Wiley-VCH Verlag & Co. KGaA: Weinheim, 2012.

(91) Bansal, R. C. R. C.; Goyal, M.; Roop, C. B.; Meenakshi, G.; Bansal, R. C. R. C.; Goyal, M. *Activated Carbon Adsorption*; Taylor & Francis Group: Boca Raton, 2005.

(92) Cheung, W. H.; Szeto, Y. S.; McKay, G. Intraparticle Diffusion Processes during Acid Dye Adsorption onto Chitosan. *Bioresour. Technol.***2007**, *98* (15), 2897–2904.

(93) Plazinski, W.; Rudzinski, W. Kinetics of Adsorption at solid/Solution Interfaces Controlled by Intraparticle Diffusion: A Theoretical Analysis. *J. Phys. Chem. C***2009**, *113* (28), 12495–12501.

(94) Marsh, H.; Rodríguez-Reinoso, F. Activated Carbon; Elsevier Science & Technology Books: Oxford, 2006.

(95) Yahya, M. A.; Al-Qodah, Z.; Ngah, C. W. Z. Agricultural Bio-Waste Materials as Potential Sustainable Precursors Used for Activated Carbon Production: A Review. *Renew. Sustain. Energy Rev.***2015**, *46*, 218–235.

(96) G.D. Sheng, D.D. Shao, X.M. Ren, X.Q. Wang, J.X. Li, Y.X. Chen, X.K. Wang, Kinetics and thermodynamics of adsorption of ionizable aromatic compounds from aqueous solutions by as-prepared and oxidized multiwalled carbon nanotubes,J. Hazard. Mater. 178 (2010) 505–516.

(97) S. Liu, R. Wang, Modified activated carbon with an enhanced nitrobenzene adsorption capacity, J. Porous Mater. 18 (2011) 99–106

(98) H. Valdes, M. Sanchez-Polo, J. Rivera-Utrilla, C.A. Zaror, Effect of ozone treatment on surface properties of activated carbon, Langmuir 18 (2002) 2111–2116.

(99) B. Fang, Y.Z. Wei, K. Suzuki, M. Kumagai, Surface modification of carbonaceous materials for EDLCs application, Electrochim. Acta 50 (2005) 616–3621.

(100) J.X. He, S.B. Li, W.L. Shao, D.Y. Wang, M.Y. Chen, W.Q. Yin, W. Wang, Y.Y. Gu, B.L. Zhong, Activated carbon nanoparticles or methylene blue as tracer during video-assisted thoracic surgery for lung cancer can help pathologist find the detected lymph nodes, J. Surg. Oncol. 102 (2010) 676–682.

(101) Y.S. Lee, Y.H. Kim, J.S. Hong, J.K. Suh, G.J. Cho, The adsorption properties of surface modified activated carbon fibers for hydrogen storages, Catal. Today 120 (2007) 420–425.

(102) H.T. Gomes, S.M. Miranda, M.J. Sampaio, A.M.T. Silva, J.L. Faria, Activated carbons treated with sulphuric acid: catalysts for catalytic wet peroxide oxidation, Catal. Today 151 (2010) 153–158.

(103) Z.X. Jiang, Y. Liu, X.P. Sun, F.P. Tian, F.X. Sun, C.H. Liang, W.S. You, C.R. Han, C. Li, Activated carbons chemically modified by concentrated H2SO4 for the adsorption of the pollutants from waste water and the dibenzothiophene from fuel oils, Langmuir 19 (2003) 731–736.

(104) S.B. Wang, Z.H. Zhu, A. Coomes, F. Haghseresht, G.Q. Lu, The physical and surface chemical characteristics of activated carbons and the adsorption of methylene blue from wastewater, J. Colloid Interface Sci. 284 (2005) 440–446.

(105) N. Kannan, M.M. Sundaram, Kinetics and mechanism of removal of methylene blue by adsorption on various carbons-a comparative study, Dyes Pigments 51 (2001) 25–40.

(106) Cardoso, N. F.; Pinto, R. B.; Lima, E. C.; Calvete, T.; Amavisca, C. V.; Royer, B.; Cunha, M. L.; Fernandes, T. H. M.; Pinto, I. S. Removal of Remazol Black B Textile Dye from Aqueous Solution by Adsorption. *Desalination***2011**, *269* (1–3), 92–103.

(107) Cardoso, N. F.; Lima, E. C.; Pinto, I. S.; Amavisca, C. V.; Royer, B.; Pinto, R. B.; Alencar, W. S.; Pereira, S. F. P. Application of Cupuassu Shell as Biosorbent for the Removal of Textile Dyes from Aqueous Solution. *J. Environ. Manage.***2011**, *92* (4), 1237–1247.

(108) Attia, A. A.; Girgis, B. S.; Fathy, N. A. Removal of Methylene Blue by Carbons Derived from Peach Stones by H3PO4 Activation: Batch and Column Studies. *Dye. Pigment.***2008**, *76* (1), 282–289.

(109) Olivares-Marín, M.; Del Prete, V.; Garcia-Moruno, E.; Fernández-González, C.; Macías-García, a.; Gómez-Serrano, V. The Development of an Activated Carbon from Cherry Stones and Its Use in the Removal of Ochratoxin A from Red Wine. *Food Control***2009**, *20* (3), 298–303.

(110) Köseoğlu, E.; Akmil-Başar, C. Preparation, Structural Evaluation and Adsorptive Properties of Activated Carbon from Agricultural Waste Biomass. *Adv. Powder Technol.***2015**, *26*, 811–818.

(111) Hashemian, S.; Salari, K.; Yazdi, Z. A. Preparation of Activated Carbon from Agricultural Wastes (Almond Shell and Orange Peel) for Adsorption of 2-Pic from Aqueous Solution. *J. Ind. Eng. Chem.***2013**, *20* (4), 1892–1900.

(112) Bosch, M. E.; Sánchez, A. J. R.; Rojas, F. S.; Ojeda, C. B. Determination of Paracetamol: Historical Evolution. *J. Pharm. Biomed. Anal.***2006**, *42* (3), 291–321.

(113) Q.S. Liu, T. Zheng, N. Li, P. Wang, G. Abulikemu, Modification of bamboo-based activated carbon using microwave radiation and its effects on the adsorption of methylene blue, Appl. Surf. Sci. 256 (2010) 3309–3315.

(114) K.B. Yang, J.H. Peng, C. Srinivasakannan, L.B. Zhang, H.Y. Xia, X.H. Duan, Preparation of high surface area activated carbon from coconut shells using microwave heating, Bioresour. Technol. 101 (2010) 6163–6169.

(115) E. Yagmur, M. Ozmak, Z. Aktas, A novel method for production of activated carbon from waste tea by chemical activation with microwave energy, Fuel 87 (2008) 3278–3285.

(116) J.A. Menendez, A. Arenillas, B. Fidalgo, Y. Fernández, L. Zubizarreta, E.G. Calvo, J.M. Bermudez, Microwave heating processes involving carbon materials, Fuel Process. Technol. 91 (2010) 1–8.

(117) J.L. Figueiredo, M.F.R. Pereira, M.M.A. Freitas, J.J.M. Orfao, Modification of the surface chemistry of activated carbons, Carbon 37 (1999) 1379–1389.

(118) L. Pereira, R. Pereira, M.F.R. Pereira, F.P. van der Zee, F.J. Cervantes, M.M. Alves, Thermal modification of activated carbon surface chemistry improves its capacity as redox mediator for azo dye reduction, J. Hazard. Mater. 183 (2010) 931–939.

(119) J.A. Menendez, E.M. Menendez, M.J. Iglesias, A. Garcia, J.J. Pis, Modification of the surface chemistry of active carbons by means of microwave-induced treatments, Carbon 37 (1999) 1115–1121.

(120) J.M.V. Nabais, P.J.M. Carrott, M.M.L. RibeiroCarrott, J.A. Menendez, Preparation and modification of activated carbon fibres by microwave heating, Carbon 42 (2004) 1315–1320.

(121) C.K. Ahn, D. Park, S.H. Woo, J.M. Park, Removal of cationic heavy metal from aqueous solution by activated carbon impregnated with anionic surfactants, J. Hazard. Mater. 164 (2009) 1130–1136.

(122) Marsh, H.; Rodríguez-Reinoso, F. *Activated Carbon*; Elsevier Science & Technology Books: Oxford, 2006.

(123) Hernández-Hernández, K. A.; Solache-Ríos, M.; Díaz-Nava, M. C. Removal of Brilliant Blue FCF from Aqueous Solutions Using an Unmodified and Iron-Modified Bentonite and the Thermodynamic Parameters of the Process. *Water. Air. Soil Pollut.***2013**, *224* (5).

(124) Crini, G.; Peindy, H.N.; Dyes Pigm. **2005**, 70, 204.

(125) Le-Minh, N.; Khan, S. J.; Drewes, J. E.; Stuetz, R. M. Fate of Antibiotics during Municipal Water Recycling Treatment Processes. *Water Res.***2010**, *44* (15), 4295–4323.

(126) Langmuir, I. The Adsorption of Gases on Plane Surfaces of Glass, Mica and Platinum. *J. Am. Chem. Soc.***1918**, *40* (9), 1361–1403.

(127) Bergmann, C. P.; Machado, F. M. *Carbon Nanomaterials as Adsorbents for Environmental and Biological Applications*; Springer: New York.

(128) Foo, K. Y.; Hameed, B. H. Mesoporous Activated Carbon from Wood Sawdust by K2CO3 Activation Using Microwave Heating. *Bioresour. Technol.***2012**, *111*, 425–432.

(129) Vasanth Kumar, K.; Sivanesan, S. Isotherms for Malachite Green onto Rubber Wood (Hevea Brasiliensis) Sawdust: Comparison of Linear and Non-Linear Methods. *Dye. Pigment.***2007**, *72* (1), 124–129.

(130) Freundlich, H. Adsorption in Solution. *Phys. Chem. Soc.***1906**, *40*, 1361–1368.

(131) Liu, Y.; Xu, H.; Yang, S. F.; Tay, J. H. A General Model for Biosorption of Cd^{2+}, Cu^{2+} and Zn^{2+} by Aerobic Granules. *J. Biotechnol.***2003**, *102* (3), 233–239.

(132) Ho, Y. S.; McKay, G. Pseudo-Second Order Model for Sorption Processes. *Process Biochem.***1999**, *34* (5), 451–465.

(133) Liu, Y.; Liu, Y. J. Biosorption Isotherms, Kinetics and Thermodynamics. *Sep. Purif. Technol.***2008**, *61* (3), 229–242.

(134) Liu, Y.; Shen, L. A General Rate Law Equation for Biosorption. *Biochem. Eng. J.***2008**, *38* (3), 390–394.

(135) Alencar, W. S.; Lima, E. C.; Royer, B.; dos Santos, B. D.; Calvete, T.; da Silva, E.; Alves, C. N. Application of Aqai Stalks as Biosorbents for the Removal of

the Dye Procion Blue MX-R from Aqueous Solution. *Sep. Sci. Technol.***2012**, *47* (3), 513–526.

(136) Machado, F. M. Nanotubos de Carbono como Nanoadsorventes na Remoção de Corantes Sintéticos de Soluções Aquosas: Um Estudo Experimental e Teórico.Porto Alegre: Universidade Federal do Rio Grande do Sul, 2012.

(137) Dąbrowski, A. *Adv. Colloid Interface Sci*.**2001**, 93,135.

(138) Vasques, A.; Guelli, S.; Valleb, J.; Souza, A. *Chem. Technol. Biotechnol.***2009**, 84, 1146.

(139) Mishra, A. K.; Arockiadoss, T.; Ramaprabhu, S. *Chem. Eng. J.***2010**, 162, 1026.

(140) Robinson, T.; Chandran, B.; Nigam, P. *Bioresour. Technol.***2002**, 85, 119.

(141) Özcan, A. S.; Özcan, A.; *J. Colloid Interface Sci.***2004**, 276, 39.

(142) Calvete, T.; Lima, E. C.; Cardoso, N. F.; Vaghetti, J. C. P.; Dias, S. L. P.; Pavan, F. A. J. Environ. Manage, **2010**, 91, 1695.

(143) P.S. Thue, E.C. Lima, J.M. Sieliechi, C. Saucier, S.L.P. Dias, J.C.P. Vaghetti, F.S. Rodembusch, F.A. Pavan, Effects of first-row transition metals and impregnation ratios on the physicochemical properties of microwave-assisted activated carbons from wood biomass, J. Colloid Interface Sci., 486 (2017) 163–175.

(144) Prola, L. D. T.; Acayanka, E.; Lima, E. C.; Umpierres, C. S.; Vaghetti, J. C. P.; Santos, W. O.; Laminsi, S.; Djifon, P. T. Comparison of Jatropha Curcas Shells in Natural Form and Treated by Non-Thermal Plasma as Biosorbents for Removal of Reactive Red 120 Textile Dye from Aqueous Solution. Ind. Crops Prod. 2013, 46, 328–340.

(145) F. Barbosa Jr., E.C. Lima, F.J. Krug, Determination of arsenic in sediment and soil slurries by electrothermal atomic absorption spectrometry using W-Rh permanent modifier, Analyst, 125 (2000) 2079–2083.

(146) Cardoso, N. F.; Lima, E. C.; Royer, B.; Bach, M. V.; Dotto, G. L.; Pinto, L. A. A.; Calvete, T.; Comparison of Spirulina platensis microalgae and

commercial activated carbon as adsorbents for the removal of Reactive Red 120 dye from aqueous effluents J. Hazard. Mat. 2012, 241– 242,146.

(147) G.S. dos Reis, C.H. Sampaio, E.C. Lima, M. Wilhelm, Preparation of Novel adsorbents based on combinations of polysiloxanes and sewage sludge to remove pharmaceuticals from aqueous solutions, Colloids Surf. A 497 (2016) 304–315.

(148) G.S. dos Reis, M. Adebayo, S.T. Pascal, C.H. Sampaio, E.C. Lima, S.L.P. Dias, I.A.S. De Brum, F. Pavan, Removal of phenolic compounds from aqueous solutions using sludge-Based activated carbons prepared by conventional heating and microwave-assisted pyrolysis, Water Air Soil Pollut. 228 (33) (2017) 1–17.

(149) E.C. Lima, R.V. Barbosa, J.L. Brasil, A.H.D.P. Santos, Evaluation of different permanent modifiers for the determination of arsenic, cadmium and lead in environmental samples by electrothermal atomic absorption spectrometry, J. Anal. At. Spectrom., 17 (2002) 1523–1529

(150) Prola, L. D. T.; Acayanka, E.; Lima, E. C.; Umpierres, C. S.; Vaghetti, J. C. P.; Santos, W. O.; Laminsi, S.; Djifon, P. T. Comparison of Jatropha Curcas Shells in Natural Form and Treated by Non-Thermal Plasma as Biosorbents for Removal of Reactive Red 120 Textile Dye from Aqueous Solution. *Ind. Crops Prod.***2013**, *46*, 328–340.

(151) Prola, L. D. T.; Acayanka, E.; Tarley, C. R. T. Application of Aqai Stalks as Biosorbent for the Removal of Evans Blue and Vilmafix Red RR-2B Dyes from Aqueous Solutions. *Desalin. Water Treat.***2013**, *51*, 4582–4592.

(152) Leite, A.J.B.; Sophia A.C.; Thue, P.S.; Dos Reis,G.S.; Dias, S.L.P.; Lima, E.C.; Vaghetti, J.C.P.; Pavan, F.A.; Alencar, W.S. Activated carbon from avocado seeds for the removal of phenolic compounds from aqueous solutions. *Desalin. Water Treat.***2017**, 71, 168-181.

ANEXOS

Activated carbon from avocado seeds for the removal of phenolic compounds from aqueous solutions

Article *in* Desalination and water treatment · April 2017

DOI: 10.5004/dwt.2017.20540

9 authors, including:

Silvio Luis Pereira Dias
Universidade Federal do Rio Grande do Sul
26 PUBLICATIONS **297** CITATIONS

SEE PROFILE

Eder Claudio Lima
Universidade Federal do Rio Grande do Sul
140 PUBLICATIONS **4,419** CITATIONS

SEE PROFILE

Flávio A. Pavan
Universidade Federal do Pampa (Unipampa)
57 PUBLICATIONS **1,909** CITATIONS

SEE PROFILE

Desalination and Water Treatment
www.deswater.com

doi: 10.5004/dwt.2017.20540

71 (2017) 168–181
April

Activated carbon from avocado seeds for the removal of phenolic compounds from aqueous solutions

Anderson J.B. Leite[a], Carmalin Sophia A.[b], Pascal S. Thue[a], Glaydson S. dos Reis[a], Silvio L.P. Dias[a], Eder C. Lima[a,*], Julio C.P. Vaghetti[a], Flavio A. Pavan[c], Wagner Soares de Alencar[a,d]

[a]*Institute of Chemistry, Federal University of Rio Grande do Sul (UFRGS), Av. Bento Gonçalves 9500, P.O. Box 15003, 91501-970, Porto Alegre, RS, Brazil, Tel./Fax +55 (51) 3308 7175; emails: profederlima@gmail.com, eder.lima@ufrgs.br (E.C. Lima), barcellos2903@gmail.com (A.J.B. Leite), pascalsilasthue@gmail.com (P.S. Thue), glaydsonambiental@gmail.com (G.S. dos Reis), silvio.dias@ufrgs.br (S.L.P. Dias), juliovaghetti@gmail.com (J.C.P. Vaghetti), drwsa@yahoo.com.br (W.S. de Alencar)*
[b]*National Environmental Engineering Research Institute (NEERI), Chennai Zonal Laboratory, CSIR Campus, Taramani, Chennai 600113, India, email: ac_sophia@neeri.res.in*
[c]*Federal University of Pampa, UNIPAMPA, Bagé, RS, Brazil, email: flavio.pavan@unipampa.edu.br (F.A. Pavan)*
[d]*Institute of Exact Sciences, Federal University of South and Southeast of Pará (UNIFESSPA), Marabá, PA, Brazil*

Received 11 July 2016; Accepted 27 January 2017

ABSTRACT

Avocado seed activated carbon (ASAC) was synthesized by microwave-heating process using $ZnCl_2$ as an activating agent. The adsorbent ASAC was characterized using analytical techniques namely N_2 isotherms, Fourier transform infrared spectroscopy, and scanning electron microscopy. The surface area of ASAC was 1,432 $m^2\ g^{-1}$. The ASAC prepared was used for adsorption of resorcinol and 3-aminophenol from aqueous solutions. Kinetic models namely pseudo-first order, pseudo-second order, and Avrami fractional order and isotherms (Freundlich, Langmuir, and Liu) were applied to the experimental adsorption data. The results demonstrate maximum adsorption capacity for resorcinol (406.9 mg g^{-1}) and 3-aminophenol (454.5 mg g^{-1}) at 50°C. The thermodynamic analysis of data and the effect of temperature studies revealed that the adsorption processes of resorcinol and 3-aminophenol onto ASAC were temperature dependent. The adsorption processes were exothermic and spontaneous. The avocado carbon displayed excellent adsorption properties for the simulated effluents containing phenolic compounds.

Keywords: Avocado seed; Microwave-assisted pyrolysis; Activated carbons; Phenolic compounds; Isotherm and kinetic models; Adsorption

1. Introduction

Water pollution due to phenolic compounds has caused increasing environmental concerns in the last decades [1,2]. Numerous industries such as gas and coke plant's resins, paper and pulp, plywood, paints, pharmaceutical, petroleum, textile, plastic, etc., discharge wastewaters containing different types of phenolic contaminants [1,2]. Phenolic wastewaters are known to be toxic and carcinogenic. Hence, there is a growing awareness about the impact of these contaminants on water resource.

Phenolic compounds rapidly phototransform and form subproducts that may pose severe risks to aquatic organisms and human beings [1,2]. Ingestion of water contaminated with phenols may cause serious gastrointestinal damages, muscle tremors, difficulty in walking, and death in animals [1,2]. Due to the high environmental risks involved and toxicity of the effluents, it is important

* Corresponding author.

to remove phenol and phenolic compounds from contaminated industrial aqueous streams before being discharged into any water bodies [1,2].

Various treatment processes used for the removal of phenols from water and/or wastewaters are membrane separation [3], advanced oxidation process [4,5], electrochemical oxidation [6], biological processes [7,8], microfiltration and nanofiltration [9,10], and adsorption [11–13]. These chemical, biological, and physical treatment processes have their own advantages and disadvantages. The methods have found limited application, as they are either complex and/or not economical. However, adsorption has been found to be the most attractive method for removal of organic pollutants. The advantage with adsorption is: (i) the method is simple, (ii) adsorbents are reusable, and (iii) the process is highly economical [11–14].

Recently, several materials have been used as adsorbents or as precursors for preparation of adsorbents. Such materials include carbon nanotubes [15], silica [16] and polysiloxanes [17], zeolite [18], sewage sludge [17,19] and tannery sludge [20], and agroindustrial wastes such as *Punica granatum* husk [21], wood sawdust [22,23], Brazilian pine-fruit shell [24], oak shell [25], cocoa shell [26], etc. However, there is always a quest to find new materials with higher adsorption capacity so as to remove a spectrum of highly toxic pollutants from aqueous systems.

Due to textural properties, especially pore volume and specific surface area, activated carbons are widely used for the adsorption of organic pollutants from aqueous solutions [19,20,22–26]. Activated carbons may be prepared by pyrolysis using conventional thermal pyrolysis or microwave-assisted process [22,24]. The main difference among the methods is how the heat is generated. Microwave provides energy directly on the carbon bed [20,22,23] while conventional heating uses conduction and/or convection [24]. Microwave heating is advantageous over conventional pyrolysis, reason being its shorter pyrolysis time (<10 min) [20,26]. As a result, there is rapid temperature rise [20,26], and a remarkable decrease in energy consumption [20].

The main advantage and novelty of present study is that the microwave-induced activated carbons were prepared though a single stage of pyrolysis. The biomass impregnated with inorganics can only be carbonized in a microwave [23]. This is the main reason why researchers carbonize the organic precursors in a conventional furnace to produce carbonized material (i.e., microwave conductor), and subsequently, activated it through microwave induction [27–29]. On the other hand, in the present study, impregnation of the carbon material with inorganics is carried out before microwave-assisted pyrolysis. This task can be established in a single step [20,22,23,26]. This single step process reduces the total time for producing the activated carbons. Another novelty and advantage of this work is that, the total time of pyrolysis including the time for cooling down the quartz reactor was <11 min.

Therefore, the present study aims at the preparation and characterization of activated carbon from avocado seed (ASAC) by microwave-heating process. The prepared avocado shell carbon has been tried as an adsorbent for the removal of phenolics such as resorcinol (RES) and 3-aminophenol (AMP) from aqueous solutions.

2. Experimental

2.1. Chemicals and reagents

The adsorbate RES and AMP (Supplementary Figs. 1 and 2, respectively) were supplied by Vetec (Rio de Janeiro, Brazil). The $ZnCl_2$ was purchased from Synth (Diadema, SP, Brazil).

Reagents such as RES, AMP, 2-nitrophenol, 2-naphtol, 2-chlorophenol, 4-nitrophenol, hydroquinone, 3-cresol, bisphenol A, phenol, 2-cresol, humic acid, sodium sulfate, sodium chloride, potassium phosphate, sodium carbonate, potassium nitrate were used for the preparation of simulated effluents. All these reagents were supplied by Vetec (Rio de Janeiro, Brazil). 1.0 mol L^{-1} HCl and/or NaOH (Neon, São Paulo, Brazil) were used for pH adjustments.

2.2. Preparation of adsorbents

100.0 g of $ZnCl_2$ was weighed and dissolved in 50.0 mL of deionized water. 100.0 g of dried avocado seed (AS; milled at diameter < 250 μm) was added to the $ZnCl_2$ solution and mixed continuously at approximately 80°C for 30 min. After mixing, the paste was dried in an air oven at 90°C for 120 min. Pyrolysis of the AS (10.0 g) impregnated with $ZnCl_2$ was carried out in a quartz reactor as described elsewhere [20,22,23], under a nitrogen atmosphere (150 mL min^{-1}). The quartz reactor was placed in the microwave oven and the sample was carbonized in four cycles of 80 s at 1,200 W. Then, the system was cooled after pyrolysis for 5 min under 60 mL min^{-1} N_2. One pyrolysis cycle took <11 min, including 5 min of cooling time. Subsequently, other pyrolysis cycles were carried out.

10.0 g of pyrolyzed carbonaceous material was mixed with 200 mL of 6 mol L^{-1} HCl in a 500 mL boiling flask. The mixture was continuously stirred on a magnetic stirrer and refluxed for 2 h (70°C–80°C). The resultant slurry was cooled down to room temperature and filtered under vacuum using 0.45 μm membrane using a polycarbonate Sartorius system. The filtrate was discarded and the solid material was washed repeatedly until neutral pH with deionized water. Later, the solid material was again mixed with 200 mL of 0.010 mol L^{-1} Ethylenediaminetetraacetic acid (EDTA) (pH 10.0) solution and stirred for 15 min. The solid material was again filtered under vacuum, washed with 100 mL of 0.010 mol L^{-1} EDTA (pH 10.0) to eliminate trace heavy metals from the carbonaceous material. The solid material was again repeatedly washed with deionized water until neutral pH. The resultant carbon was oven dried at 105°C for 5 h, milled to particle sizes ≤106 μm and stored properly until use. The adsorbent was named as ASAC [20,22,26].

To check the leaching of Zn from the activated carbon prepared, 30.0 mg of ASAC was mixed with 20.0 mL of water in a 50.0 mL Falcon tube and stirred for 24 h. The solid phase was separated by centrifugation, and the liquid phase was analyzed in an Analyst 200 Flame Atomic Absorption Spectrometry – PerkinElmer (Massachusetts, USA) using air–acetylene flame (10:2.5 L min^{-1}). Hollow cathode lamp of Zn (λ = 213.86 nm) of the same manufacturer was used as radiation source.

2.3. Characterization of adsorbent materials

Several analytical techniques were used to understand how the microwave-heating process and the leaching out affected the structure of raw AS and ASAC. The surface

morphologies of ASAC were evaluated by employing a scanning electron microscope (JEOL microscope, model JSM 6060) [23]. The porous structure parameters of ASAC were determined through nitrogen adsorption/desorption isotherms by using a surface area analyzer (Micromeritics Instrument, TriStar II 3020, USA) [23]. The surface functional groups of AS and ASAC were characterized using a Fourier transform infrared spectroscopy (FTIR; Bruker, model alpha, USA) [22].

2.4. Adsorption studies

The adsorption experiments were performed to evaluate the adsorption capacity of ASAC. The concentration of RES and AMP was varied between 100.00–1,800.0 mg L^{-1}. Aliquots of 20.00 mL of adsorbate were taken in 50.0 mL flat Falcon tubes containing 5.0–200.0 mg of ASAC at varying pH conditions (2.0–10.0). The tubes were then capped and placed horizontally in an acclimatized agitator. The samples were agitated for 1–480 min at varied temperature (25°C–50°C).

The samples after a fixed time of agitation were centrifuged using a Unicen M Herolab centrifuge to separate the adsorbent. 1–5 mL of the supernatant was then diluted to 10.0–50.0 mL in standard flasks using the blank solution at suitable pH. The concentration of the unadsorbed RES and AMP was analyzed using a spectrophotometer (T90+ PG Instruments) at wavelengths 273 and 282 nm, respectively.

The sorption capacity and the percentage removal of phenolic compounds are given by Eqs. (1) and (2), respectively:

$$q = \frac{(C_0 - C_f)}{m} \cdot V \tag{1}$$

$$\%\text{Removal} = 100 \cdot \frac{(C_0 - C_f)}{C_0} \tag{2}$$

where q is the sorption capacity of phenolic compounds adsorbed (mg g^{-1}); C_0 is the initial adsorbate concentration (mg L^{-1}); C_f is the adsorbate concentrations in equilibrium (mg L^{-1}); m is the weight of ASAC (g); and V is the volume of the adsorbate in solution (L).

2.5. Statistical evaluation and quality assurance

The experiments were performed in triplicates to assure precision, accuracy, and reliability of data. Blank runs were conducted in parallel [30].

RES and AMP solutions were stored in amber colored glass bottles. All the glassware used in the experiment were precleaned using 10% HNO_3 [31], rinsed with deionized water, dried, and stored in closed cabinets.

Standard calibration graphs of RES and AMP (10.0–150.0 mg L^{-1}) were prepared using UV-Win software of T90+ PG Instruments spectrophotometer. Triplicate analytical analysis was performed, and the precision was maintained (n = 3). The detection limits of RES and AMP were 0.013 and 0.011 mg L^{-1}, respectively. The signal/noise ratio was 3 [32]. A spiked phenol solution (70.0 mg L^{-1}) was used as quality control at every 10 determinations. This determined that the readings of the RES and AMP concentrations were accurate [33].

Microcal Origin 2015 application was used to evaluate the best fitting equilibrium and kinetic data, by simplex method and the Levenberg–Marquardt algorithm applying nonlinear equations. The suitability of the equilibrium and kinetic models was evaluated using determination coefficient (R^2), the adjusted determination coefficient (R^2_{adj}), and standard deviation (SD) of residues [34]. The difference between the theoretical and experimental quantities of RES and AMP adsorbed by ASAC was measured using SD. The mathematical expression for R^2, R^2_{adj}, and SD are given by Eqs. (3), (4), and (5), respectively.

$$R^2 = \left(\frac{\sum_i^n \left(q_{i,exp} - \bar{q}_{exp}\right)^2 - \sum_i^n \left(q_{i,exp} - q_{i,model}\right)^2}{\sum_i^n \left(q_{i,exp} - \bar{q}_{exp}\right)^2} \right) \tag{3}$$

$$R^2_{adj} = 1 - \left(1 - R^2\right).\left(\frac{n-1}{n-p-1}\right) \tag{4}$$

$$SD = \sqrt{\left(\frac{1}{n-p}\right).\sum_i^n \left(q_{i,exp} - q_{i,model}\right)^2} \tag{5}$$

where $q_{i,exp}$ is the distinct experimental q value; $\bar{q}_{exp}$ represents the mean experimental q values; $q_{i,model}$ is the distinct theoretical q value predicted by the model; n is the number of experiments; p is the number of variables in the model [34].

2.6. Kinetics of adsorption

Pseudo-first order, pseudo-second order, and Avrami fractional order models were used to fit the kinetic data. The mathematical equations of these respective models are shown in Eqs. (6), (7), and (8) [34,35].

$$q_t = q_e \cdot \left[1 - \exp(-k_1 \cdot t)\right] \tag{6}$$

$$q_t = \frac{q_e^2 k_2 t}{\left[k_2 (q_e) \cdot t + 1\right]} \tag{7}$$

$$q_t = q_e . \left\{1 - \exp\left[-\left(k_{AV} . t\right)\right]^{nAV}\right\} \tag{8}$$

2.7. Equilibrium of adsorption

The Langmuir, Freundlich, and Liu isotherm models were applied to fit the experimental equilibrium data. The mathematical expression for these models is presented in Eqs. (9)–(11), respectively [34,35].

$$q_e = \frac{Q_{max} \cdot K_L \cdot C_e}{1 + K_L \cdot C_e} \tag{9}$$

$$q_e = K_F \cdot C_e^{1/n_F} \quad (10)$$

$$q_e = \frac{Q_{\max} \cdot \left(K_g \cdot C_e\right)^{n_L}}{1 + \left(K_g \cdot C_e\right)^{n_L}} \quad (11)$$

2.8. Synthetic effluents

Two synthetic industrial effluent mixtures were prepared. The effluent consisted of 11 different phenols, humic acid, and inorganics usually present in industrial effluents. The composition of the effluents (A and B) is presented in Table 1. The purpose of using synthetic effluents is to evaluate the sorption capacities of the ASAC for removal of mixed phenolic compounds in the presence of high concentrations of organic matter and salts.

3. Results and discussion

3.1. Characterization of activated carbons

The chemical modification of the AS with $ZnCl_2$ and further pyrolysis assisted by microwave generated ASAC with great structural properties and adsorption capacity when compared with the raw biomass. Among the main characteristics of the adsorbent, the surface area, and volume of pores play an influential role during adsorption processes. Textural (surface area, porosity, etc.) characterization of the AS and ASAC was performed by N_2 adsorption–desorption isotherms at –196°C and their results are shown in Table 2.

Table 1
Chemical composition of simulated industrial effluents

Phenols	Concentration (mg L^{-1})	
	Effluent A	Effluent B
Resorcinol (RES)	50.00	100.0
3-Amino phenol (AMP)	50.00	100.0
Phenol	5.00	10.0
2-Cresol	5.00	10.0
3-Cresol	5.00	10.0
2-Chlorophenol	5.00	10.0
Bisphenol A	5.00	10.0
2-Nitrophenol	5.00	10.0
4-Nitrophenol	5.00	10.0
2-Naphtol	5.00	10.0
Hydroquinone	5.00	10.0
Organic matter		
Humic acid	10.0	20.0
Inorganic components		
Sodium sulfate	20.0	40.0
Sodium carbonate	20.0	40.0
Sodium chloride	20.0	40.0
Potassium nitrate	20.0	40.0
Potassium phosphate	20.0	40.0
pH[a]	7.0	7.0

[a]pH was adjusted with 1.0 mol L^{-1} HCl and/or NaOH.

Table 2 presents the surface area, external surface area, micropore area, total pore volume, micropore volume and mesopore volume of the precursor (AS), and ASAC. The porosity characterization displayed that ASAC is composed mainly of mesopores (pores whose diameter are within 2–50 nm) [36]. The total surface area (S_{BET}) of ASAC was 1,433 $m^2\ g^{-1}$, the surface area due to micropores (S_{micro}) was 279.1 $m^2\ g^{-1}$, and the external surface was 1,153 $m^2\ g^{-1}$. It can be seen that only 19.48% of the area of the ASAC is due to the micropores. The total pore volume (V_{tot}) was 0.4447 $cm^3\ g^{-1}$, the volume of micropore (V_{mic}) was 0.1189 $cm^3\ g^{-1}$, and the volume of mesopores (V_{mes}) was 0.3258 $cm^3\ g^{-1}$. The ratio V_{mic}/V_{tot} is 26.74% and the V_{mes}/V_{tot} is 73.26%. It may be observed from these results that the obtained ASAC is predominantly mesoporous with a 26% contribution of micropores [36]. The raw material (AS) presented an S_{BET} value of only 2.776 $m^2\ g^{-1}$, and it was not possible to measure the area of micropores and volume of micropores and mesopores.

The process of production of activated carbon by chemical activation consists in impregnation of the biomass with $ZnCl_2$. This is followed by a pyrolysis that could occur in a conventional muffle furnace [24,25] or in a microwave oven [22,23] forming a pyrolyzed material containing inorganics [20,23,26,35]. The chemical activation process is conducted using 6.0 mol L^{-1} HCl [35]. This process increases the porosity of the activated carbon [23]. The role of $ZnCl_2$ in the carbonization of the biomass may be a complexation of this metal with the biomass, followed by a dehydration of the biomass at high temperatures [23,37]. $ZnCl_2$ can melt at >300°C and diffuse to occupy the cavities of the pyrolyzed material. After the pyrolysis, refluxing with 6.0 mol L^{-1} HCl, would remove the zinc compounds from the cavities of the activated carbon, producing an activated carbon with high porosity and surface area [23,35,37].

It may be noted that the S_{BET} value obtained in this study was higher than other activated carbons reported in the literature reporting different carbon sources as precursor. Dos Reis et al. [19] pyrolyzed sewage sludge, chemically activated it with $ZnCl_2$ and generated an activated carbon with a surface area of 192 $m^2\ g^{-1}$. Puchana-Rosero et al. [20] produced activated

Table 2
Textural properties of AS and ASAC

Sample	ASAC	AS
S_{BET} ($m^2\ g^{-1}$)	1,433	2.776
S_{micro} ($m^2\ g^{-1}$)	279.1	–
S_{ext} ($m^2\ g^{-1}$)	1,153	–
S_{mic}/S_{BET} (%)	19.48	–
V_{tot} ($cm^3\ g^{-1}$)	0.4447	0.0069
V_{mic} ($cm^3\ g^{-1}$)	0.1189	–
V_{mes} ($cm^3\ g^{-1}$)	0.3258	–
D_p (nm)	2.105	9.918

carbon by microwave pyrolysis of tannery sludge and the S_{BET} of the same was 491 $m^2 g^{-1}$. Saucier et al. [26] produced activated carbon from cocoa shell by microwave-assisted pyrolysis and obtained a material with S_{BET} of 619 $m^2 g^{-1}$. Ribas et al. [35] synthesized biochar from cocoa shell using a conventional furnace and obtained S_{BET} of 522 $m^2 g^{-1}$. The S_{BET} values obtained may depend on the characteristics of the organic precursors, activation method, and the heating procedure. In addition, when chemical activation is used, $ZnCl_2$ is the most efficient activating agent compared with other metals such as $FeCl_3$ [26,35], $CuCl_2$, $CoCl_2$, and $NiCl_2$ [23]. In order to eliminate the inorganic salts/oxides formed during pyrolysis, the contents were leached out using 6.0 mol L^{-1} HCl [20,22,23,26,35]. Several authors have reported washing with 1.0 mol L^{-1} HCl, leading to formation of an activated carbon with lower surface area, and the carbons may release toxic inorganics when in contact with aqueous solutions. On the other hand, the ASAC synthesized in this work was treated with 6.0 mol L^{-1} HCl for leaching inorganics. This was later followed by the treatment with 0.010 M EDTA solution (pH 10.0). The synthesized activated carbon did not release high quantities of Zn into the aqueous solution. The total concentration of Zn leached out from 30.0 mg of ASAC in 20.0 mL of deionized water during 24 h of contact was 0.0240 ± 0.0006 mg L^{-1}. Considering the permissible limit for Zn that could be available in drinking water is 5.0 mg L^{-1} [38], the concentration of Zn released from the activated carbon was meagre (208 times lower than the permissible limit) [38].

The surface morphology of the materials before (AS) and after pyrolysis (ASAC) was characterized using scanning electron microscopy (SEM). The SEM images of the AS and the ASAC are presented in Fig. 1. The surface of AS is fibrous and smooth (Fig. 1(A)). However, ASAC sample showed a brick of carbon with irregular dimension containing some fissures which may be from the mortar (Fig. 1(B)). SEM technique does not clearly display the pores on the surface of the material because the scale of the figure is micrometers (μm) while, the scale of the pores are in nanometers. Therefore, the N_2 adsorption–desorption curves are a better analytical technique to evaluate the porosity of the adsorbent.

FTIR analysis helps in the identification of the surface functional groups which may contribute toward enhanced adsorption of the pollutant onto the adsorbent [17,22–24]. AS might contain lignin, hemicellulose, cellulose, and tannin as the major components [39]. Thus, a vast numbers of functional groups such as amines, phenolic, carboxyl, and alcohols may exists on the surface and may be involved during the adsorption process [26,39]. The results of FTIR for AS and ASAC are presented in Fig. 2. The AS samples showed the following bands: a band at 3,268 cm^{-1} is due to the OH stretching vibrations from the intermolecular hydrogen bonding [39]; a band at 2,919 cm^{-1} is due to the asymmetric C–H stretching, 1,617 cm^{-1} is due to the asymmetric stretching in (C=O) carboxylates [39], 1,521 and 1,439 cm^{-1} may be assigned to the sp^2 hybridized C=C stretching band of the aromatic ring [39]. The band at 1,144 and 1,003 cm^{-1} could be assigned to C–O stretching of alcohols or phenols [39], and the band at 762 cm^{-1} could be assigned to C–H out of plane bending in the aromatic rings [39].

FTIR analysis of ASAC showed a broad band at 3,441 cm^{-1}. This band is due to O–H stretching [39]. The bands at 2,921 and 2,849 cm^{-1} are due to the asymmetric and symmetric C–H stretching [39]. The band at 1,638 cm^{-1} is due to the asymmetric stretching in (C=O) carboxylates [39]. The bands at 1,540 and 1,460 cm^{-1} could be due to sp^2 hybridized C=C stretching band of the aromatic rings [39], 1,161 and 1,035 cm^{-1} may be assigned to C–O stretching in alcohols or phenols [39], and 877 cm^{-1} could be due to C–H out of plane bending mode of the aromatic rings [39].

It could be inferred from the FTIR analysis that the microwave-heating process increased the intermolecular hydrogen bonding otherwise did not bring about much change in the surface groups on ASAC. The major functional groups found in the carbon adsorbent includes: (i) O–H likely from alcohols, phenols, (ii) aromatic rings, (iii)

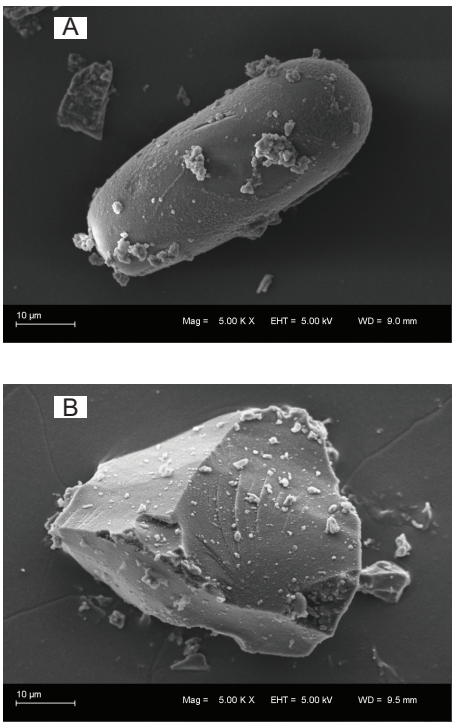

Fig. 1. SEM images of AS and ASAC.

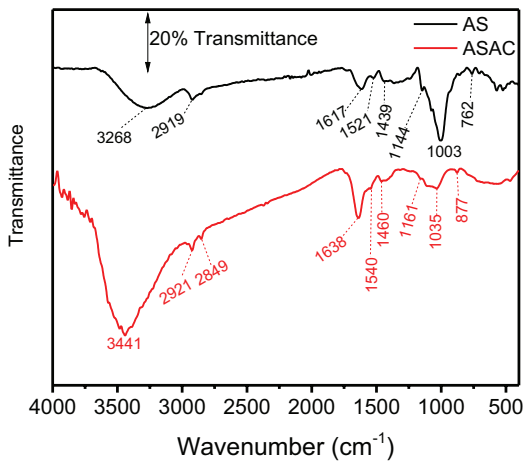

Fig. 2. FTIR spectra of ASAC.

C=O likely from carboxylic acids, esters, and (iv) CH from aromatic and aliphatic compounds may be responsible for the adsorption process.

3.2. Study of adsorbent dosage and initial pH

Preliminary adsorption experiments were carried out with 300 mg L^{-1} of RES and AMP in order to study higher dosage (0.25–10.0 g L^{-1}) of the ASAC adsorbent. The other conditions such as initial pH was maintained at 6.0 and temperature at 25°C (Supplementary Fig. 3(A)). It was observed for adsorbent dosages ≥1.50 g L^{-1} the percentage of removal of AMP and RES onto ASAC became practically constant. Therefore, this adsorbent dose (1.50 g L^{-1}) was fixed for further experiments (30.0 mg of the adsorbent for 20.0 mL of adsorbate solution). This adsorbent dose is similar to the results reported in our previous studies [20,22,23].

During optimization of pH, the concentration of RES and AMP was kept at 300 mg L^{-1}, adsorbent dosage was 1.5 g L^{-1}, temperature was 25°C, and the pH was varied between 2.0 and 10.0 (Supplementary Fig. 3(B)). It may be seen from Fig. 3(B) that between pH 4 and 9, removal of AMP and RES was practically constant. Hence, it may be concluded that for effluent treatment, it is best to keep the pH close to neutral. Initial pH was maintained at 7.0 in all further experiments.

3.3. Adsorption kinetics

The successful adsorption process depends on proper understanding of the kinetic parameters. Knowledge of the adsorption kinetics helps to design a process with high efficiency. Kinetic analysis gives us an insight about the interaction/contact between the adsorbate and adsorbent and its significance in the process to attain equilibrium [20,22,39]. After equilibrium is attained, the system reaches a stationary state [20,22,39]. Once stationary state is reached, for practical application, the adsorption may be stopped.

In order to study the kinetics of adsorption of RES and AMP on ASAC, pseudo-first order, pseudo-second order and Avrami fractional order models were applied. The graphical representations of the kinetic models are presented in Fig. 3 and Table 3, respectively.

In order to explain the suitability of the models, their adjusted determination coefficients (R^2_{adj}) and SD of residues were considered. Higher R^2_{adj} and lower SD values mean smaller difference between theoretical and experimental q_t values [19–22,24,26].

On the basis of discussions given above, fractional model has presented the highest R^2_{adj} (varying from 0.9980 to 0.9999) and lowest SD values (varying from 0.6782 to 2.769) for RES and AMP (Table 3) at both initial concentrations, which means that q_t predicted by fractional order model is closer to the values of q_t measured experimentally.

Fractional order model presents a complex or multipathway variations in adsorption mechanism [20,22,40]. The results suggest that the adsorption of RES and AMP onto ASAC, follows multiple kinetic orders instead of an integer-kinetic order [20,22,34,40]. Occurrence of multiple kinetic order of the adsorption is further confirmed by the n_{AV} exponent factor [20,22,34,40].

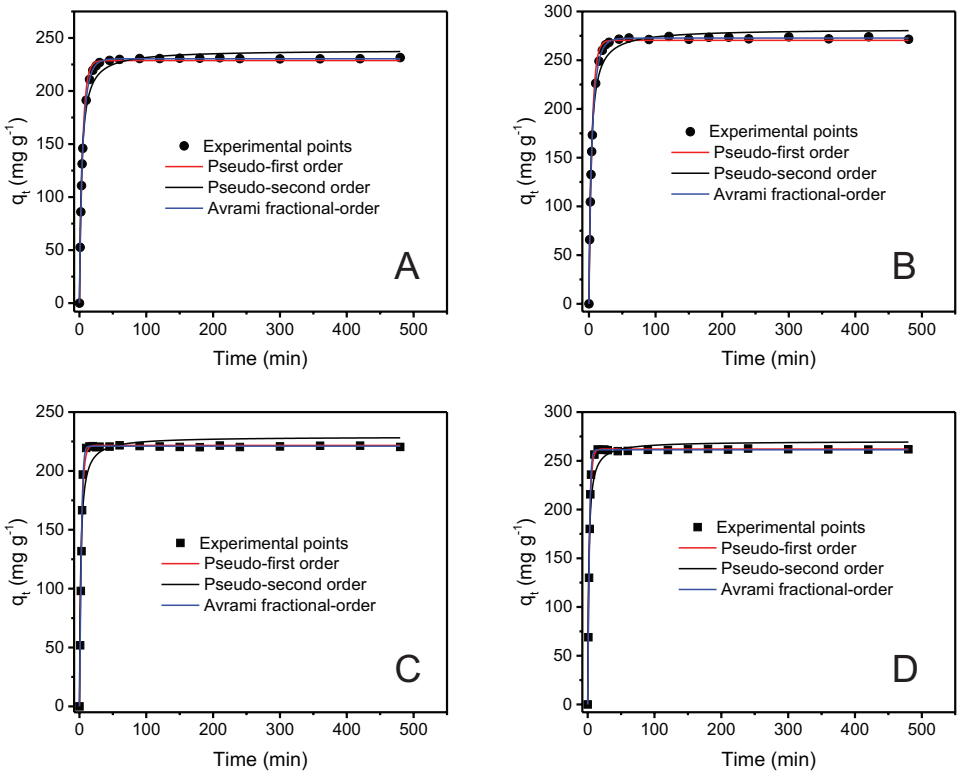

Fig. 3. Adsorption kinetics of AMP at 400 mg L^{-1} (A) and 900 mg L^{-1} (B), and RES at 400 mg L^{-1} (C) and 900 mg L^{-1} (D) onto ASAC. Conditions: temperature – 25°C, adsorbent mass – 30.0 mg, and initial pH of adsorbate – 7.0.

Table 3
Kinetic parameters for adsorption of RES and AMP onto ASAC

	RES		AMP	
	400.0 mg L^{-1}	900.0 mg L^{-1}	400.0 mg L^{-1}	900.0 mg L^{-1}
Pseudo-first order				
k_f (min^{-1})	0.3287	0.3826	0.2110	0.2149
q_e (mg g^{-1})	221.7	262.1	228.7	270.4
$t_{1/2}$	2.109	1.812	3.285	3.226
$t_{0.95}$	9.114	7.831	14.20	13.94
R^2 adjusted	0.9921	0.9943	0.9957	0.9945
SD (mg g^{-1})	5.492	5.274	4.443	5.916
Pseudo-second order				
k_s (g mg^{-1} min^{-1})	0.002367	0.002406	0.001373	0.01191
q_e (mg g^{-1})	229.0	270.1	238.7	282.0
$t_{1/2}$	1.845	1.539	3.052	2.977
$t_{0.95}$	35.05	29.24	57.98	56.57
R^2 adjusted	0.9513	0.9558	0.9890	0.9894
SD (mg g^{-1})	13.62	14.73	7.098	8.190
Avrami fractional order				
k_{AV} (min^{-1})	0.3310	0.3810	0.1999	0.2027
q_e (mg g^{-1})	221.0	261.3	230.4	272.7
n_{AV}	1.296	1.270	0.8232	0.8043
$t_{1/2}$	2.277	1.967	3.206	3.128
$t_{0.95}$	7.046	6.226	18.97	19.30
R^2 adjusted	0.9980	0.9996	0.9999	0.9999
SD (mg g^{-1})	2.769	1.452	0.6782	0.8730

Conditions: Initial pH of adsorbate – 7.0, adsorbent mass – 30 mg.

Considering that the kinetic models present different rate constants with different units, it is difficult to compare the rate constants of these models. Considering $t_{1/2}$ and $t_{0.95}$ are the time necessary to attain 50% and 95% of the saturation, respectively [22,26], the kinetic equation constants were calculated based on the nonlinear interpolation of their respective kinetic curves of Fig. 3 (Table 3). Considering the above discussion, Avrami fractional model is the best fit for the experimental data. In the case of RES, the $t_{1/2}$ values ranged from 1.967 to 2.277 min, and $t_{0.95}$ ranged from 6.226 to 7.046 min. While, in the case of AMP, the $t_{1/2}$ values ranged from 3.128 to 3.206 min and $t_{0.95}$ ranged from 18.97 to 19.30 min. Based on these values of $t_{1/2}$ and $t_{0.95}$ it is possible to infer that the kinetics of adsorption of RES is more rapid than AMP. The increase of initial adsorbate concentration could increase the time required to reach equilibrium [34]. Based on these results, the contact time between the adsorbent and adsorbate for the experiments was fixed at 30 min for RES and 60 min for AMP.

3.4. Adsorption isotherms

The adsorption isotherms play a significant role in understanding how the adsorbates interact with adsorbents and it helps with the enhanced use of the adsorbent. An adsorption isotherm defines the interaction between the quantity of adsorbate adsorbed and the concentration of adsorbate that was left unadsorbed in solution, at a fixed temperature. Nonlinear forms of Langmuir, Freundlich, and Liu isotherm models were used to study the adsorption data of RES and AMP [34], and the results are presented in Fig. 4 and Table 4.

As done in the previous kinetic studies [20,22], the most suited equilibrium model was determined using the adjusted determination coefficient (R^2_{adj}) and SD of residues.

On the basis of R^2_{adj} and SD values, the best fitting model for both RES and AMP onto ASAC was the Liu isotherm model. The model presented R^2_{adj} closer to 1.00 and the lowest SD values, which interprets that the q predicted by the Liu isotherm model is closer to the experimentally

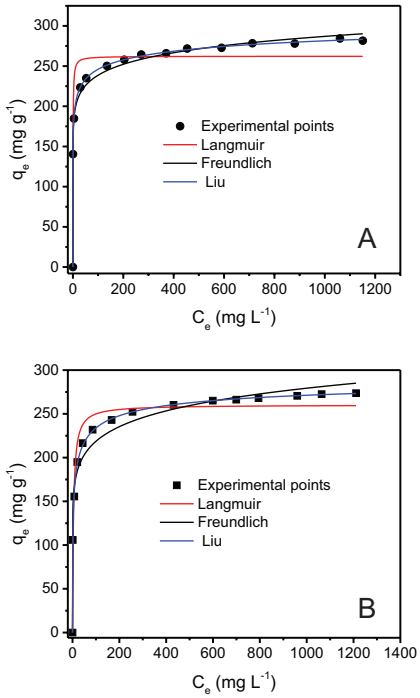

Fig. 4. Adsorption isotherms of AMP (A) and RES (B) onto ASAC at 25°C. Conditions: adsorbent mass – 30.0 mg, initial pH of adsorbate – 7.0, time of contact between the adsorbent and adsorbate – 30 min for RES and 60 min for AMP.

measured q. At all studied range temperatures, both RES and AMP followed Liu isotherm model [20,22,34].

The maximum adsorption capacity calculated by using the Liu model was observed to be 299.7, 317.4, 332.1, 349.0, 366.8, and 406.2 mg g^{-1} at 25°C, 30°C, 35°C, 40°C, 45°C, and 50°C for RES, respectively. The maximum adsorption capacity values observed for AMP were 352.4, 372.1, 390.4, 410.6, 432.0, and 454.5 mg g^{-1} at 25°C, 30°C, 35°C, 40°C, 45°C, and 50°C, respectively. These values are closest to experimental data because presented highest R^2_{adj} and lowest SD values (Table 4).

3.5. Comparative evaluation of adsorption of phenolic compounds on activated carbons and other adsorbents

The maximum adsorption efficiency of ASAC was compared with various others adsorbents reported in literature [41–50] and presented in Table 5. It is obvious from Table 5 that the ASAC exhibited higher adsorption capacities for both adsorbates RES and AMP. Among the 12 different adsorbents presented in the table, ASAC exhibited a Q_{max} value >400 mg g^{-1} which is higher than 11 other materials presented in the table. Although the Q_{max} values of the carbons presented in the table were derived at different experimental conditions, the values were obtained in their best-optimized conditions and are being compared with the best-optimized conditions of this work. These results are significant from a scientific point of view, because the adsorbents proposed in this present study show very good performance when matched with

Table 4
Langmuir, Freundlich, and Liu isotherm parameters for the adsorption of RES and AMP onto ASAC

	Resorcinol						3-Aminophenol					
	25°C	30°C	35°C	40°C	45°C	50°C	25°C	30°C	35°C	40°C	45°C	50°C
Langmuir												
Q_{max} (mg g^{-1})	260.3	278.4	280.6	293.0	312.2	315.2	262.3	271.5	289.0	338.8	311.8	314.2
K_L (L mg^{-1})	0.2403	0.2530	0.1296	0.1630	0.1408	0.2077	1.687	0.8502	0.6203	0.2930	0.6140	0.2173
R^2_{adj}	0.9417	0.9589	0.9728	0.9606	0.9595	0.9419	0.9179	0.9210	0.9576	0.9203	0.9243	0.9799
SD (mg g^{-1})	18.73	17.58	12.39	16.90	18.71	22.77	21.72	21.65	16.23	28.82	24.17	11.54
Freudlich												
K_F (mg g^{-1} (mg L^{-1})$^{-1/nF}$)	133.9	130.4	151.5	138.3	139.1	147.1	164.9	172.6	181.4	177.8	190.1	207.1
n_F	9.394	7.980	10.15	8.121	7.507	7.911	12.47	13.17	12.57	9.136	11.51	14.62
R^2_{adj}	0.9710	0.9649	0.9907	0.9824	0.9729	0.9872	0.9922	0.9954	0.9966	0.9759	0.9949	0.9993
SD (mg g^{-1})	13.20	16.24	7.235	11.29	15.30	10.68	6.686	5.230	4.614	15.84	6.260	2.128
Liu												
Q_{max} (mg g^{-1})	299.7	317.4	332.1	349.0	366.8	406.2	352.4	372.1	390.4	410.6	432.0	454.5
K_g (L mg^{-1})	0.1922	0.1579	0.1308	0.1088	0.09326	0.07958	0.3576	0.2903	0.2593	0.2186	0.1842	0.1549
n_L	0.4289	0.4910	0.4052	0.4349	0.4853	0.3662	0.2344	0.2182	0.2371	0.3652	0.2466	0.1918
R^2_{adj}	0.9990	0.9998	0.9997	0.9998	0.9999	0.9997	0.9997	0.9999	0.9999	0.9999	0.9999	0.9999
SD (mg g^{-1})	2.428	1.152	1.234	1.231	1.137	1.585	1.389	0.3177	0.3353	0.4664	0.03385	0.03534

Conditions: Adsorbent mass – 30.0 mg, initial pH of adsorbate – 7.0, time of contact – 30 min for RES and 60 min for AMP.

adsorbents already reported in the literature [41–50]. This shows that the AS raw material can generate an efficient activated carbon for removal of phenolic compounds from aqueous solutions.

3.6. Effect of temperature and thermodynamic parameters

The effect of temperature is another essential physicochemical variable that can influence adsorption. Variation in temperature of the reaction would directly impact change in the adsorption efficiency and the adsorption capacity of the adsorbent [34,35,39].

The effect of temperature on the removal of the phenolic compounds by ASAC was investigated by varying the temperature from 25°C to 50°C (Table 6). Adsorption of both the phenolic compounds seemed to be significantly affected by temperature and the same influenced the Q_{max} values (Table 4). During RES adsorption, the Q_{max} at 25°C was 299.7 mg g^{-1}. It increased to 406.2 mg g^{-1} at 50°C, an enhancement of 35.53% was observed on the maximum adsorption

Table 5
Maximum sorption capacities of different adsorbents used for removal of various phenolic compounds

Adsorbent	Phenolic adsorbate	Q_{max} (mg g^{-1})	References
Mesoporous SBA-15	Resorcinol	128	[41]
Mesoporous carbon	Resorcinol	37	[42]
Mesoporous carbon	Resorcinol	39.2	[43]
Activated carbon coal	3-Aminophenol	110	[44]
Mesoporous carbons	Resorcinol	40.6	[45]
Activated carbon from waste rubber	*p*-Cresol	250	[46]
Eggshell activated carbons	Phenol	192	[47]
Activated carbon	2-Chlorophenol	549.5	[48]
Aminated activated carbons	Phenol	227.27	[49]
Granular activated carbon	Catechol	100	[49]
Granular activated carbon	Resorcinol	113	[50]
ASAC	Resorcinol	406.2	This work
ASAC	3-Aminophenol	454.5	This work

Table 6
Thermodynamic parameters of the adsorption of resorcinol (RES) and 3-aminophenol (AMP) onto ASAC

	Temperature (K)					
	298	303	308	313	318	323
Resorcinol						
K_g (L mol^{-1})	2,116	1,738	1,440	1,198	1,027	876.2
$\Delta G°$ (kJ mol^{-1})	–24.68	–24.60	–24.52	–24.44	–24.42	–24.38
$\Delta H°$ (kJ mol^{-1})	–28.25	–	–	–	–	–
$\Delta S°$ (J K^{-1} mol^{-1})	–12.06	–	–	–	–	–
R^2_{adj}	0.9991	–	–	–	–	–
3-Aminophenol						
K_g (L mol^{-1})	3,902	3,168	2,830	2,386	2,010	1,690
$\Delta G°$ (kJ mol^{-1})	–26.19	–26.11	–26.25	–26.23	–26.20	–26.14
$\Delta H°$ (kJ mol^{-1})	–26.14	–	–	–	–	–
$\Delta S°$ (J K^{-1} mol^{-1})	0.1346	–	–	–	–	–
R^2_{adj}	0.9942	–	–	–	–	–

capacity (Table 4). The same trend was observed for the AMP. At 25°C, the Q_{max} for AMP was 352.4 and when the temperature was raised to 50°C the maximum adsorption capacity achieved was 454.5 mg g^{-1}. An enhancement of 28.97% on the maximum adsorption capacity was observed. Although there is an increase in the Q_{max} values of both adsorbates with the increase of temperature, there is no relationship of this parameter with the thermodynamics of adsorption, as reported in an earlier publication [34]. On the other hand, the equilibrium constant of the Liu model decreased uniformly with the increase in temperature, demonstrating that the adsorption in AMP and RES were exothermic. In order to validate the above statement, the thermodynamic parameters for RES and AMP adsorption are presented in Table 6.

Change in enthalpy and entropy ($\Delta H°$ and $\Delta S°$) can be calculated from the slope and the intercept of the plot of $\ln K_g$ vs. $1/T$ [34,35,39]. The R^2_{adj} values of the plots are 0.9942 and 0.9991 for AMP and RES, respectively.

The interactions of adsorbent with adsorbate can be chemical or physical. This may be explained using the magnitude of enthalpy. The enthalpy value for physical adsorption is <40 kJ mol^{-1} [51]. The enthalpy values of adsorption of RES and AMP onto the activated carbon is compatible with the physical adsorption [51]. $\Delta H°$ has negative values, which signify that the interactions of the activated carbon with RES and AMP are exothermic. Since $\Delta G°$ values are negative the adsorption of RES and AMP onto ASAC is spontaneous, and a favorable process.

3.7. Removal of simulated mixed phenolic effluent using ASAC

Two mixtures of synthetic effluents containing various phenolic compounds, humic acid, and some inorganic salts with different compositions were prepared. The efficacy of the ASAC as an adsorbent to treat synthetic effluents was investigated (Table 1).

The UV–Vis spectra of the untreated and treated effluents were observed from 190 to 500 nm (Fig. 5). The percentage removal of the phenolic compounds from the synthetic effluents was calculated using the area under the absorption bands. ASAC displayed great adsorption performance on the removal of both the synthetic effluent mixtures. The removal percentages were 99.33% and 96.94% for effluent A and effluent B, respectively.

Based on the above results obtained from simulated effluent, ASAC may be an efficient adsorbent for the removal of phenolic compounds from simulated wastewaters as well as industrial effluents contaminated with organic compounds [52–55].

4. Conclusion

In this work, ASAC was prepared by microwave-heating process after chemical activation with $ZnCl_2$ as activating agent. The produced activated carbon exhibited high specific surface area 1,433 m^2 g^{-1}. The S_{BET} results show that ASAC possessed 19.48% of micropores and 80.52% of external surface. In relation to volume of pores, 26.74% of pore volume corresponded to micropores and 73.26% to mesopores. Therefore, the ASAC synthesized in this research study may be classified as predominantly mesoporous.

The adsorptive capacity of ASAC was evaluated using RES and AMP removal percentages. Avrami fractional order and Liu isotherm model were found to be best fit to the experimental data. According to Liu isotherm model, the maximum adsorption capacity achieved were 406.2 and 454.5 mg g^{-1} for RES and AMP at 50°C, respectively. This adsorption capacity values were found to be highest among the ones reported in literature [41–50].

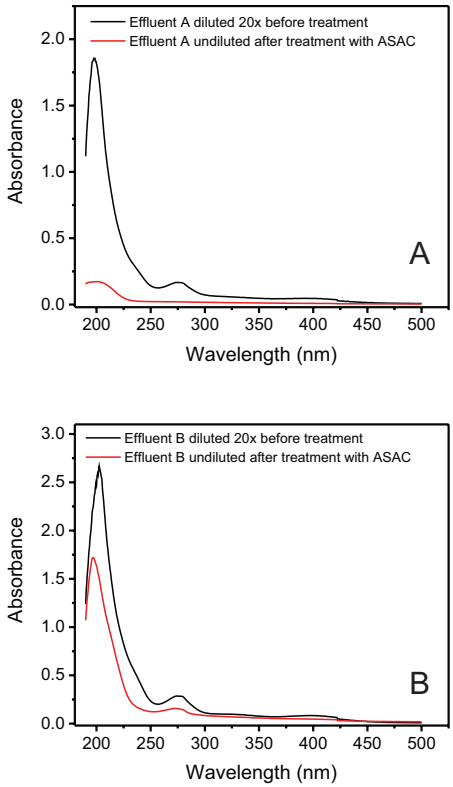

Fig. 5. UV/Vis spectra of simulated effluents A and B before and after treatment with ASAC activated carbon. See Table 1 for the composition of the effluents.

It was seen from the effect of temperature and thermodynamic data, that the adsorption processes of RES and AMP onto ASAC were dependent on temperature. The adsorption process was exothermic and spontaneous.

The avocado-activated carbon displayed excellent removal of simulated phenolic effluents; they effectively removed >96.94% of a mixture containing high concentrations of phenols, organic matter, and salinity. It may be concluded that, ASAC can be effectively used in real wastewater contaminated with phenolic compounds.

Acknowledgments

The authors are grateful to The Coordination of Improvement of Higher Education Personnel (CAPES, Brazil), to The Academy of Sciences for Developing World (TWAS, Italy), and to The National Council for Scientific and Technological Development (CNPq, Brazil), to Clean Water Mission Project (ESC – 00306), CSIR-NEERI, India for sponsorship and fellowships. We are also grateful to Centre of Electron Microscopy (CME-UFRGS) for the use of the SEM microscope. We are grateful to Chemaxon for giving us an academic research license for the MarvinSketch software,

Version 16.6.6.0, (http://www.chemaxon.com), 2016 used for phenols physical–chemical properties.

Symbols and acronyms

AS	—	Avocado seed
ASAC	—	Avocado seed activated carbon
RES	—	Resorcinol
AMP	—	3-Aminophenol
FTIR	—	Fourier transform infrared spectroscopy
SEM	—	Scanning electron microscopy
BET method	—	Brunauer, Emmett and Teller method for determination of surface area
S_{BET}	—	Total Surface area determined by BET method, $m^2\ g^{-1}$
S_{micro}	—	Surface area of micropores obtained by *t* plot, $m^2\ g^{-1}$
$S_{external}$	—	External surface area, $m^2\ g^{-1}$
S_{BET}	—	$S_{micro} + S_{external}$
V_{tot}	—	Total volume of pores, $cm^3\ g^{-1}$
V_{micro}	—	Volume of micropores, $cm^3\ g^{-1}$
V_{meso}	—	Volume of mesopores, $cm^3\ g^{-1}$
V_{tot}	—	$V_{micro} + V_{meso}$
R^2	—	Coefficient of determination
R^2_{adj}	—	Adjusted coefficient of determination
SD	—	Standard deviation of the residues
q	—	Sorption capacity of phenolic compounds adsorbed, mg g^{-1}
C_0	—	Initial adsorbate concentration, mg L^{-1}
C_f	—	Adsorbate concentrations in equilibrium, mg L^{-1}
m	—	Weight of ASAC, g
V	—	Volume of the adsorbate in solution, L
$q_{i,\,exp}$	—	Distinct experimental q value
$\overline{q}_{exp}$	—	Mean experimental q values
$q_{i,\,model}$	—	Distinct theoretical q value predicted by the model
n	—	Number of experiments
p	—	Number of variables in the model
q_e	—	Amount of adsorbate adsorbed at the equilibrium, mg g^{-1}
C_e	—	Supernatant adsorbate concentration at the equilibrium, mg L^{-1}
K_L	—	Langmuir equilibrium constant, L mg^{-1}
Q_{max}	—	Maximum adsorption capacity of the adsorbent, mg g^{-1}
K_F	—	Freundlich equilibrium constant, mg g^{-1} (mg $L^{-1})^{-1/n}$
n_F	—	Freundlich exponent, dimensionless
K_g	—	Liu equilibrium constant, L mg^{-1}
n_L	—	Dimensionless exponent of the Liu equation
q_t	—	Amount of adsorbate adsorbed at time *t*, mg g^{-1}
q_e	—	Equilibrium adsorption capacity, mg g^{-1}
k_f	—	Pseudo-first-order rate constant, min^{-1}
t	—	Contact time, min
k_s	—	Pseudo-second-order rate constant, g $mg^{-1}\ min^{-1}$
k_{AV}	—	Avrami kinetic constant, min^{-1}
n_{AV}	—	Fractional adsorption order, which is related to the adsorption mechanism
$t_{1/2}$	—	Time necessary to attain 50% of the saturation
$t_{0.95}$	—	Time necessary to attain 95% of the saturation

References

[1] S. Kottuparambil, Y.J. Kim, H. Choi, M.S. Kim, A. Park, J. Park, W. Shin, T. Han, A rapid phenol toxicity test based on photosynthesis and movement of the freshwater flagellate, *Euglena agilis* Carter, Aquat. Toxicol., 155 (2014) 9–14.

[2] M.D. Erturk, M.T. Saçan, Assessment and modeling of the novel toxicity data set of phenols to *Chlorella vulgaris*, Ecotoxicol. Environ. Saf., 90 (2013) 61–68.

[3] Y. Liu, M. Meng, J. Yao, Z. Da, Y. Feng, Y. Yan, C. Li, Selective separation of phenol from salicylic acid effluent over molecularly imprinted polystyrene nanospheres composite alumina membranes, Chem. Eng. J., 286 (2016) 622–631.

[4] E.B. Estrada-Arriaga, J.A. Zepeda-Aviles, L. García-Sánchez, Post-treatment of real oil refinery effluent with high concentrations of phenols using photo-ferrioxalate and Fenton's reactions with membrane process step, Chem. Eng. J., 285 (2016) 508–516.

[5] N. Wang, T. Zheng, G. Zhang, P. Wanga, A review on Fenton-like processes for organic wastewater treatment, J. Environ. Chem. Eng., 4 (2016) 762–787.

[6] N. Jarrah, N.D. Múazu, Simultaneous electro-oxidation of phenol, CN^-, S^{2-} and NH_4^+ in synthetic wastewater using boron doped diamond anode, J. Environ. Chem. Eng., 4 (2016) 2656–2664.

[7] R. Boonchai, G. Seo, Microalgae membrane photobioreactor for further removal of nitrogen and phosphorus from secondary sewage effluent, Korean J. Chem. Eng., 32 (2015) 2047–2052.

[8] A. Hussain, S. K. Dubey, V. Kumar, Kinetic study for aerobic treatment of phenolic wastewater, Water Resour. Ind., 11 (2015) 81–90.

[9] R. Muppalla, S.K. Jewrajka, A.V.R. Reddy, Fouling resistant nanofiltration membranes for the separation of oil–water emulsion and micropollutants from water, Sep. Purif. Technol., 143 (2015) 125–134.

[10] J.J. Rueda-Márquez, M.G. Pintado-Herrera, M.L. Martín-Díaz, A. Acevedo-Merino, M.A. Manzano, Combined AOPs for potential wastewater reuse or safe discharge based on multi-barrier treatment (microfiltration-H_2O_2/UV-catalytic wet peroxide oxidation), Chem. Eng. J., 270 (2015) 80–90.

[11] L. Ma, J. Zhua, Y. Xi, R. Zhu, H. He, X. Liang, G.A. Ayoko, Adsorption of phenol, phosphate and Cd(II) by inorganic–organic montmorillonites: a comparative study of single and multiple solute, Colloids Surf., A, 497 (2016) 63–71.

[12] Z. Luo, M. Gao, S. Yang, Q. Yang, Adsorption of phenols on reduced-charge montmorillonites modified by bispyridinium dibromides: mechanism, kinetics and thermodynamics studies, Colloids Surf., A, 482 (2015) 222–230.

[13] V. Makrigianni, A. Giannakas, Y. Deligiannakis, I. Konstantinou, Adsorption of phenol and methylene blue from aqueous solutions by pyrolytic tire char: equilibrium and kinetic studies, J. Environ. Chem. Eng., 3 (2015) 574–582.

[14] L.D.T. Prola, E. Acayanka, E.C. Lima, C.S. Umpierres, J.C.P. Vaghetti, W.O. Santos, S. Laminsi, P.T. Njifon, Comparison of *Jatropha curcas* shells in natural form and treated by non-thermal plasma as biosorbents for removal of Reactive Red 120 textile dye from aqueous solution, Ind. Crops Prod., 46 (2013) 328–340.

[15] M. Shirmardi, A.H. Mahvi, B. Hashemzadeh, A. Naeimabadi, G. Hassani, M.V. Niri, The adsorption of malachite green (MG) as a cationic dye onto functionalized multi walled carbon nanotubes, Korean J. Chem. Eng., 30 (2013) 1603–1608.

[16] D. Pérez-Quintanilla, A. Sánchez, I. Sierra, Preparation of hybrid organic-inorganic mesoporous silicas applied to mercury

removal from aqueous media: influence of the synthesis route on adsorption capacity and efficiency, J. Colloid Interface Sci., 472 (2016) 126–134.
[17] G.S. dos Reis, C.H. Sampaio, E.C. Lima, M. Wilhelm, Preparation of novel adsorbents based on combinations of polysiloxanes and sewage sludge to remove pharmaceuticals from aqueous solutions, Colloids Surf., A, 497 (2016) 304–315.
[18] L. Wanga, C. Han, M.N. Nadagouda, D.D. Dionysiou, An innovative zinc oxide-coated zeolite adsorbent for removal of humic acid, J. Hazard. Mater., 313 (2016) 283–290.
[19] G.S. dos Reis, M. Wilhelm, T.C.A. Silva, K. Rezwan, C.H. Sampaio, E.C. Lima, S.M.A.G.U. Souza, The use of design of experiments for the evaluation of the production of surface rich activated carbon from sewage sludge via microwave and conventional pyrolysis, Appl. Therm. Eng., 93 (2016) 590–597.
[20] M.J. Puchana-Rosero, M.A. Adebayo, E.C. Lima, F.M. Machado, P.S. Thue, J.C.P. Vaghetti, C.S. Umpierres, M. Gutterres, Microwave-assisted activated carbon obtained from the sludge of tannery-treatment effluent plant for removal of leather dyes, Colloids Surf., A, 504 (2016) 105–115.
[21] M.S. Bretanha, M.C. Rochefort, G.L Dotto, E.C. Lima, S.L.P. Dias, F.A. Pavan, *Punica granatum* husk (PGH), a powdered bio-waste material for the adsorption of methylene blue dye from aqueous solution, Desal. Wat. Treat., 57 (2016) 3194–3204.
[22] P.S. Thue, M.A. Adebayo, E.C. Lima, J.M. Sieliechi, F.M. Machado, G.L. Dotto, J.C.P. Vaghetti, S.L.P. Dias, Preparation, characterization and application of microwave-assisted activated carbons from wood chips for removal of phenol from aqueous solution, J. Mol. Liq., 223 (2016) 1067–1080.
[23] P.S. Thue, E.C. Lima, J.M. Sieliechi, C. Saucier, S.L.P. Dias, J.C.P. Vaghetti, F.S. Rodembusch, F.A. Pavan, Effects of first-row transition metals and impregnation ratios on the physicochemical properties of microwave-assisted activated carbons from wood biomass, J. Colloid Interface Sci., 486 (2017) 163–175.
[24] T. Calvete, E.C. Lima, N.F. Cardoso, S.L.P. Dias, E.S. Ribeiro, Removal of brilliant green dye from aqueous solutions using home made activated carbons, Soil Air Water, 38 (2010) 521–532.
[25] A. Takdastan, A.H. Mahvi, E.C. Lima, M. Shirmardi, A.A. Babaei, G. Goudarzi, A. Neisi, M.H. Farsani, M. Vosoughi, Preparation, characterization, and application of activated carbon from low-cost material for the adsorption of tetracycline antibiotic from aqueous solutions, Water Sci. Technol., 74 (2016) 2349–2363.
[26] C. Saucier, M.A. Adebayo, E.C. Lima, R. Cataluna, P.S. Thue, L.D.T. Prola, M.J. Puchana-Rosero, F.M. Machado, F.A. Pavan, G.L. Dotto, Microwave-assisted activated carbon from cocoa shell as adsorbent for removal of sodium diclofenac and nimesulide from aqueous effluents, J. Hazard. Mater., 289 (2015) 18–27.
[27] Z.Z. Qiang, X.H. Ying, C. Srinivasakannan, P.J. Hui, Z.L. Bo, Utilization of Crofton weed for preparation of activated carbon by microwave induced CO_2 activation, Chem. Eng. Process., 82 (2014) 1–8.
[28] N. Ferrera-Lorenzo, E. Fuente, I. Suárez-Ruiz, B. Ruiz, KOH activated carbon from conventional and microwave heating system of a macroalgae waste from the Agar–Agar industry, Fuel Process. Technol., 121 (2014) 25–31.
[29] R.H. Hesas, W.M.A.W. Daud, J.N. Sahu, A.A. Niya, The effects of a microwave heating method on the production of activated carbon from agricultural waste: a review, J. Anal. Appl. Pyrolysis, 100 (2013) 1–11.
[30] F. Barbosa Jr., E.C. Lima, F.J. Krug, Determination of arsenic in sediment and soil slurries by electrothermal atomic absorption spectrometry using W-Rh permanent modifier, Analyst, 125 (2000) 2079–2083.
[31] E.C. Lima, R.V. Barbosa, J.L. Brasil, A.H.D.P. Santos, Evaluation of different permanent modifiers for the determination of arsenic, cadmium and lead in environmental samples by electrothermal atomic absorption spectrometry, J. Anal. At. Spectrom., 17 (2002) 1523–1529.
[32] E.C. Lima, J.L. Brasil, A.H.D.P. Santos, Evaluation of Rh, Ir, Ru, W–Rh, W–Ir and W–Ru as permanent modifiers for the determination of lead in ashes, coals, sediments, sludges, soils, and freshwaters by electrothermal atomic absorption spectrometry, Anal. Chim. Acta, 484 (2003) 233–242.
[33] E.C. Lima, F.J. Krug, J.A. Nóbrega, A.R.A. Nogueira, Determination of ytterbium in animal faeces by tungsten coil electrothermal atomic absorption spectrometry, Talanta, 47 (1998) 613–623.
[34] E.C. Lima, M.A. Adebayo, F.M. Machado, Kinetic and Equilibrium Models of Adsorption, Chapter 3, C.P. Bergmann, F.M. Machado, Ed., Carbon Nanomaterials as Adsorbents for Environmental and Biological Applications, Springer (Springer International Publishing, Switzerland), 2015, pp. 33–69.
[35] M.C. Ribas, M.A. Adebayo, L.D.T. Prola, E.C. Lima, R. Cataluña, L.A. Feris, M.J. Puchana-Rosero, F.M. Machado, F.A. Pavan, T. Calvete, Comparison of a homemade cocoa shell activated carbon with commercial activated carbon for the removal of reactive violet 5 dye from aqueous solutions, Chem. Eng. J., 248 (2014) 315–326.
[36] P.B. Balbuenat, K.E. Gubbins, Theoretical interpretation of adsorption behavior of simple fluids in slit pores, Langmuir, 9 (1993) 1801–1814.
[37] H. Shang, Y. Lu, F. Zhao, C. Chao, B. Zhang, H. Zhang, Preparing high surface area porous carbon from biomass by carbonization in a molten salt medium, RSC Adv., 5 (2015) 75728–75734.
[38] Drinking Water Contaminants – Standards and Regulations – Secondary Drinking Water Standards: Guidance for Nuisance Chemicals, United States Environmental Protection Agency. Available at: https://www.epa.gov/dwstandardsregulations/secondary-drinkin (Accessed January 18, 2017).
[39] A. Bazzo, M.A. Adebayo, S.L.P. Dias, E.C. Lima, J.C.P. Vaghetti, E.R. de Oliveira, A.J.B. Leite, F.A. Pavan, Avocado seed powder: characterization and its application for crystal violet dye removal from aqueous solutions, Desal. Wat. Treat., 57 (2016) 15873–15888.
[40] E.C. Lima, A.R. Cestari, M.A. Adebayo, Comments on the paper: a critical review of the applicability of Avrami fractional kinetic equation in adsorption-based water treatment studies, Desal. Wat. Treat., 57 (2016) 19566–19571.
[41] Q. Li, H. Yu, J. Song, X. Pan, J. Liu, Y. Wang, L. Tang, Synthesis of SBA-15/polyaniline mesoporous composite for removal of resorcinol from aqueous solution, Appl. Surf. Sci., 290 (2014) 260–266.
[42] W. Shou, B. Chao, Z.U. Ahmad, D.D. Gang, Ordered mesoporous carbon preparation by the in situ radical polymerization of acrylamide and its application for resorcinol removal, J. Appl. Polym. Sci., 133 (2016). doi: 10.1002/app.43426.
[43] R. Guo, J. Guo, F. Yu, D.D. Gang, Synthesis and surface functional group modifications of ordered mesoporous carbons for resorcinol removal, Microporous Mesoporous Mater., 175 (2013) 141–146.
[44] B. Petrova, B. Tsyntsarski, T. Budinovaa, N. Petrova, L.F. Velasco, C.O. Ania, Activated carbon from coal tar pitch and furfural for the removal of p-nitrophenol and m-aminophenol, Chem. Eng. J., 172 (2011) 102–108.
[45] H. Ren, W. Shou, C. Ren, D.D. Gang, Preparation and post-treatments of ordered mesoporous carbons (OMC) for resorcinol removal, Int. J. Environ. Sci. Technol., 13 (2016) 1505–1514.
[46] V.K. Gupta, A. Nayak, S. Agarwal, I. Tyagi, Potential of activated carbon from waste rubber tire for the adsorption of phenolics: effect of pre-treatment conditions, J. Colloid Interface Sci., 417 (2014) 420–430.
[47] L. Giraldo, J.C. Moreno-Piraján, Study of adsorption of phenol on activated carbons obtained from eggshells, J. Anal. Appl. Pyrolysis, 106 (2014) 41–47.
[48] P. Strachowski, M. Bystrzejewski, Comparative studies of sorption of phenolic compounds onto carbon-encapsulated iron nanoparticles, carbon nanotubes and activated carbon, J. Mol. Liq., 213 (2016) 351–359.
[49] G. Yang, H. Chen, H. Qin, Y. Feng, Amination of activated carbon for enhancing phenol adsorption: effect of nitrogen-containing functional groups, Appl. Surf. Sci., 293 (2014) 299–305.
[50] S. Suresh, V.C. Srivastava, I.M. Mishra, Study of catechol and resorcinol adsorption mechanism through granular activated

carbon: characterization, pH and kinetic study, Sep. Sci. Technol., 46 (2011) 1750–1766.
[51] C.L. Sun, C.S. Wang, Estimation on the intramolecular hydrogen-bonding energies in proteins and peptides by the analytic potential energy function, J. Mol. Struct., 956 (2010) 38–43.
[52] M. Shirmardi, N. Alavi, E.C. Lima, A. Takdastan, A.H. Mahvi, A.A. Babaei, Removal of atrazine as an organic micro-pollutant from aqueous solutions: a comparative study, Process Saf. Environ. Prot., 103 (2016) 23–35.
[53] A.A. Babaei, E.C. Lima, A. Takdastan, N. Alavi, G. Goudarzi, M. Vosoughi, G. Hassani, M. Shirmardi, Removal of tetracycline antibiotic from contaminated water media by multi-walled carbon nanotubes: operational variables, kinetics, and equilibrium studies, Water Sci. Technol., 74 (2016) 1202–1216.
[54] M. Shirmardi, A.H. Mahvi, A. Mesdaghinia, S. Nasseri, R. Nabizadeh, Adsorption of acid red 18 dye from aqueous solution using single-wall carbon nanotubes: kinetic and equilibrium, Desal. Wat. Treat., 51 (2013) 6507–6516.
[55] N.F. Cardoso, E.C. Lima, B. Royer, M.V. Bach, G.L. Dotto, L.A.A. Pinto, T. Calvete, Comparison of *Spirulina platensis* microalgae and commercial activated carbon as adsorbents for the removal of Reactive Red 120 dye from aqueous effluents, J. Hazard. Mater., 241–242 (2012) 146–153.

Supplementary information

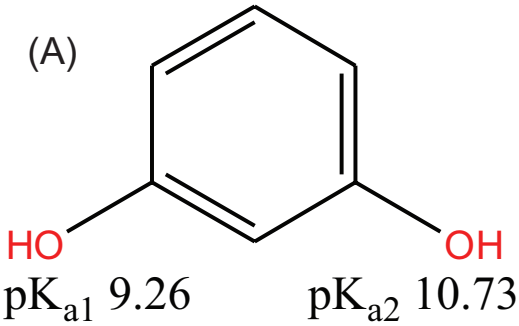

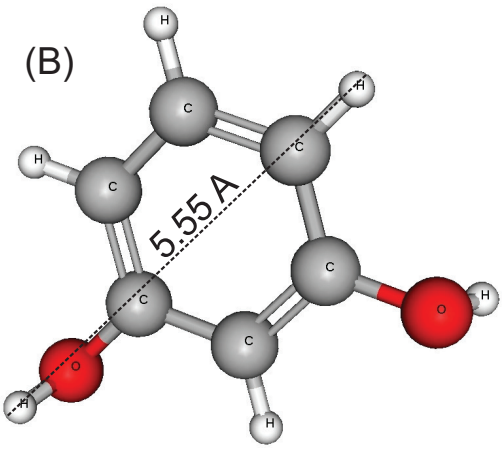

Supplementary Fig. 1. (A) Structural formula of RES; pK_a values are expressed in the molecule. (B) Optimized three-dimensional structural formula of RES. The dimensions of the chemical molecule were calculated using MarvinSketch Version 16.6.6.0. Van der Waals surface area 158.58 A^2 (pH 4.4–9.9); polar surface area 40.46 A^2 (pH 0–9.1); dipole moment 0.33 Debye; log$P$ 1.37; Davies hydrophilic–lipophilic balance (HLB) = 7.95.

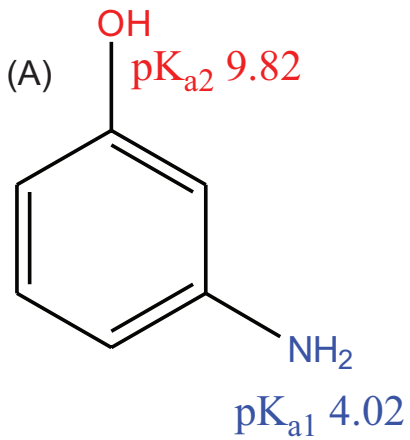

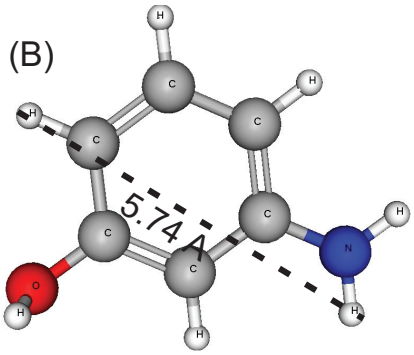

Supplementary Fig. 2. (A) Structural formula of AMP; pK_a values are expressed in the molecule. (B) Optimized three-dimensional structural formula of AMP. The dimensions of the chemical molecule were calculated using MarvinSketch Version 16.6.6.0. Van der Waals surface area 161.92 A^2 (pH 4.4–9.9); polar surface area 46.25 A^2 (pH 4.4–9.9); dipole moment 4.09 Debye; log$P$ 0.84; Davies hydrophilic–lipophilic balance (HLB) = 6.05.

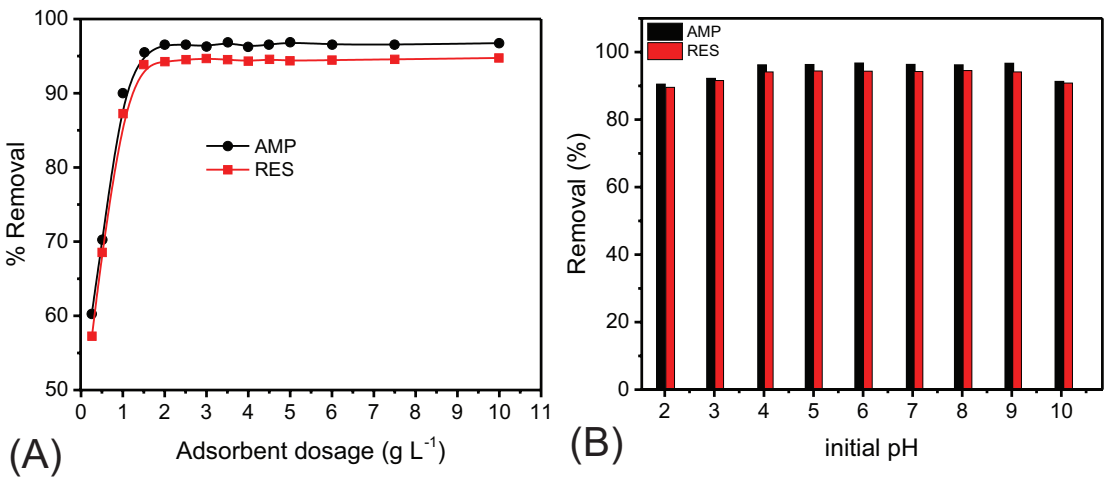

Supplementary Fig. 3. (A) Effect of ASAC dosage and (B) effect of initial pH, on the adsorption of AMP and RES onto ASAC activated carbon. Conditions of (A): 300 mg L^{-1} AMP and RES, 25°C, pH 6.0. Conditions of (B): 300 mg L^{-1} AMP and RES, 25°C, adsorbent dosage 1.50 g L^{-1}.

RESEARCH ARTICLE

Activated carbons from avocado seed: optimisation and application for removal of several emerging organic compounds

Anderson B. Leite[1] · Caroline Saucier[1] · Eder C. Lima[1] · Glaydson S. dos Reis[1,2] · Cibele S. Umpierres[1] · Beatris L. Mello[1] · Mohammad Shirmardi[3] · Silvio L.P Dias[1] · Carlos H. Sampaio[2]

Received: 21 August 2017 / Accepted: 19 December 2017 / Published online: 28 December 2017

Abstract

In this study, avocado seed was successfully used as raw material for producing activated carbons by conventional pyrolysis. In order to determine the best condition to produce the activated carbons, a 2^2 full-factorial design of experiment (DOE) with three central points was employed by varying the temperature and time of pyrolysis. The two evaluated factors (temperature and time of pyrolysis) strongly influenced the S_{BET}, pore volumes, hydrophobicity–hydrophilicity ratio (HI) and functional groups values; both factors had a negative effect over S_{BET}, pore volumes and functional groups which means that increasing the values of factors leads to decrease of these responses; on the other hand, with regards to HI, both factors caused a positive effect which means that increasing their values, the HI has an enhancement over its values. The produced activated carbon exhibited high specific surface areas in the range of 1122–1584 $m^2\ g^{-1}$. Surface characterisation revealed that avocado seed activated carbons (ASACs) have hydrophilic surfaces and have predominantly acidic groups on their surfaces. The prepared ASACs were employed in the adsorption of 25 emerging organic compounds such as 10 pharmaceuticals and 15 phenolic compounds which presented high uptake values for all emerging pollutants. It was observed that the activated carbon prepared at higher temperature of pyrolysis (700 °C), which generated less total functional groups and presented higher HI, was the activated carbon with higher sorption capacity for uptaking emerging organic contaminants. Based on results of this work, it is possible to conclude that avocado seed can be employed as a raw material to produce high surface area and very efficient activated carbons in relation to treatment of polluted waters with emerging organic pollutants.

Keywords Avocado seed · Design of experiments · Activated carbons · Emerging pollutants · Adsorption process

Responsible editor: Philippe Garrigues

Electronic supplementary material The online version of this article (https://doi.org/10.1007/s11356-017-1105-9) contains supplementary material, which is available to authorized users.

✉ Glaydson S. dos Reis
glaydson.simoes@ufrgs.br; glaydsonambiental@gmail.com

[1] Institute of Chemistry, Federal University of Rio Grande do Sul (UFRGS), Av. Bento Gonçalves 9500, P.O. Box 15003, Porto Alegre, RS 91501-970, Brazil

[2] School of Engineering, Department of Metallurgy, Federal University of Rio Grande do Sul (UFRGS), Av. Bento Gonçalves 9500, Porto Alegre, RS, Brazil

[3] Department of Environmental Health Engineering, Faculty of Paramedical Sciences, Babol University of Medical Sciences, Babol, Iran

Introduction

Every year, large quantities of dangerous emerging organic pollutants are generated by many types of industries such petrochemical, medicines, textile, paper and plastics which consume a substantial number of phenolic compounds and pharmaceuticals which ends to produce a large amount of polluted water with their products (Ahmed et al. 2016; Geissena et al. 2015; Jiang et al. 2013).

These organic substances are delivered into wastewaters, and this brings serious issues for water contamination and its treatment, because it tends to persist even after the conventional removal processes in the wastewater treatment plants (Fatta-Kassinos and Michael 2013; Geissena et al. 2015). Therefore, their removal from industrial effluents has been a major environmental issue in recent years.

Several methods, such as advanced oxidation procedures (AOP) (Ba-Abbad et al. 2017; Gil et al., 2017, Lin et al. 2017a, b), biological treatment (Besha et al. 2017; Ghattas, et al., 2017), coagulation (Kishimoto and Kobayashi 2016), flocculation (Kishimoto and Kobayashi, 2016; Matamoros and Salvado 2013), filtration (Zhang et al. 2017b) and adsorption (Bhatnagar and Anastopoulos 2017; Zhuo et al. 2017) processes have been applied to remove this kind of pollutants from the effluents (Besha et al. 2017; Carmalin et al. 2016). Some of these methods have been shown to be effective; however, some of them presented some drawbacks and limitations such as an excess amount of chemical reagent, high implemental costs and high sludge production that has serious disposal problems. Among these methods, adsorption is a preferred route because of its low initial cost for implementation, simplicity and relatively low residue production (dos Reis et al. 2016a, b, 2017).

Adsorption technology using different adsorbents has been considered as one of the most efficient and economic method for treatment of effluents containing emerging organic pollutants such phenols and pharmaceuticals (Saucier et al. 2015, 2017; Thue et al. 2016, 2017). Accordingly, a large variety of adsorbent materials have been proposed and studied for their ability to remove emerging organic pollutants (Takdastan et al. 2016; Rossner et al. 2009; Prola et al. 2013b; Rovani et al. 2016). Among these adsorbents, activated carbon is one of the most employed adsorbents for adsorption of organic compounds simply because it has well-developed pore structures with high specific area that favours high adsorption ability (dos Reis et al. 2016c; Calvete et al. 2010; Ribas et al. 2014).

Nowadays, there is a great interest in finding effective adsorbents prepared from waste biomass (Leite et al. 2017; Prola et al. 2013a; Puchana-Rosero et al. 2017). Exploring efficiency and adding value to waste biomass may contribute to environmental sustainability and offer benefits for future commercial applications (Leite et al. 2017; Prola et al. 2013a; Puchana-Rosero et al. 2017).

For instance, Saucier et al. (2015) prepared an activated carbon (AC) from cocoa shell by using a mixture of zinc chloride plus iron chloride as agents of activation by using microwave-assisted pyrolysis. Then, the carbons were used for removal of sodium diclofenac and nimesulide from aqueous solutions; the maximum sorption capacities (Q_{max}) obtained were 63.47 and 74.81 $m^2\ g^{-1}$, for diclofenac and nimesulide, respectively, at 25 °C. In another study, Thue et al. (2016) reported the preparation of an AC from wood waste using microwave-assisted pyrolysis and the adsorbents were used for removal of o-cresol from aqueous solutions obtaining a Q_{max} of 222.2 mg g^{-1} at 25 °C. Ahmed et al. (2017) produced an AC from human hair using potassium hydroxide as activating agent, using a conventional furnace system for the pyrolysis. The prepared AC was used for the adsorption of tetracycline, and the Q_{max} obtained was 128.52 $m^2\ g^{-1}$. Saucier et al. (2017) produced magnetic activated carbons by using iron and cobalt carboxylates, and the resulting adsorbents were used for removal of amoxicillin and paracetamol from aqueous solutions, obtaining Q_{max} values of 339.4 and 302.2 $m^2\ g^{-1}$ for amoxicillin and paracetamol, respectively, at 25 °C.

Leite et al. (2017) prepared an AC from avocado seed using microwave-assisted pyrolysis, and the adsorbent was employed for removal of resorcinol and 3-aminophenol from aqueous solutions. The values of Q_{max} obtained were 299.7 and 352.4 mg g^{-1} for resorcinol and 3-aminophenol, respectively, at 25 °C. Although the microwave-assisted pyrolysis could present some advantages over the conventional furnace system (Puchana-Rosero et al. 2016), the microwave oven used for producing activated carbons is not commercially available, and it is usually an adaptation of domestic microwave oven that is used for pyrolysis of the biomass (Leite et al. 2017; Puchana-Rosero et al. 2016; Saucier et al. 2015, 2017; Thue et al. 2016, 2017). Therefore, these oven systems do not have available temperature control, and all the pyrolysis should be performed in the maximum power of the furnace. However, the conventional furnace for thermal pyrolysis is available, being possible to optimize several parameters, such as ramp heating rate, final temperature of pyrolysis, holding time at the final temperature and several steps of temperature for performing the pyrolysis.

However, for the preparation of activated carbons using pyrolysis of the biomass (Calvete et al. 2010; Ribas et al. 2014), there are some factors that might affect the final quality (porosity, surface chemistry and therefore the performance of adsorption) of the materials such as hold temperature and time (dos Reis et al. 2016c; Thue et al. 2017; Ribas et al. 2014). Then, a multivariate technique extensively and usefully is needed for applying in optimisation of procedures through fast, economic and effective pathway and allows more than one variable to be optimized simultaneously (Bruns et al. 2016; dos Reis et al. 2016c; Ennaciri et al. 2014). A good selection of design and optimisation models makes possible to simultaneously evaluate the variable contribution (main and interaction) on the preparation of a material with good adsorption properties (dos Reis et al. 2016c; Ennaciri et al. 2014).

In this work, the use of avocado seed has been studied for preparation of activated carbons (avocado seed activated carbon (ASACs)) and their preparations were optimized by using a 2^2 full-factorial design of experiment (DOE) by varying two factors (temperature and time of pyrolysis) with three central points (total of seven experiments). The ASAC materials were characterized by N_2 adsorption–desorption isotherms, vibrational spectroscopy in the infrared region (FTIR), point of zero charge (pH_{pzc}), total acidic and basic groups, hydrophobicity–hydrophilicity ratio (HI). The quantitative parameters obtained were used as responses of the DOE, and then, the prepared ASACs were employed for adsorption of several emerging

organic compounds (10 pharmaceuticals and 15 phenolic compounds) from aqueous solutions.

Material and method

Statistics–experimental design

The design of experiment optimisation concerning the full-factorial design was carried out using Minitab version 17.3. Individual and synergetic effects of two operational parameters (see Table 1) including temperature of pyrolysis (A) and holding time (B) were investigated using a 2^2 full-factorial design with three central points. The analysis of variance (ANOVA) was performed to justify the significance and adequacy of the developed regression model. The adequacy of the response surface models was evaluated by calculation of the adjusted determination coefficient (R^2_{Adj}), coefficient of variation, adequate precision and also by testing it for the lack of fit.

Preparation of activated carbon

The preparation of the ACs followed the procedures described by Ribas et al. (2014) and Leite et al. (2017): 100.0 g of avocado seed (AS) was milled at diameter < 250 μm; 100.0 g of $ZnCl_2$ and 30.0 mL of water were added and mixed until they form a homogeneous paste (Leite et al. 2017). The resulting paste was placed in a quartz tube reactor inside conventional heating furnace (Sanchis, Porto Alegre, RS, Brazil). The heating treatment was carried out by heating the sample from room temperature until final temperature (T_f), according to data of Table 1, and N_2 flow (150 mL/min). Then, the system was cooled down, also under N_2 atmosphere, until the temperature attain values < 150 °C.

Afterwards, the pyrolysed materials were treated with a 6 mol L^{-1} HCl solution under reflux at 80 °C (Ribas et al. 2014; Saucier et al. 2015; Leite et al. 2017). The resulting activated carbons were labelled according to the experiments performed in the full 2^2 factorial design as ASAC1 to ASAC7 for experiments from 1 to 7 (see Table 1).

ASAC characterisation

Nitrogen adsorption isotherms were recorded with a Micrometrics Instrument, TriStar II 3020 at − 196 °C after drying for 3 h at 120 °C under reduced pressure (< 2 mbar) (Umpierres et al. 2017). The specific surface areas were determined from the Brunauer, Emmett and Teller (BET) method (Thommes et al. 2015). Pore size was calculated by the Barrett–Joyner–Halenda (BJH) method from desorption curves (Thommes et al. 2015).

Table 1 Optimisation of pyrolysis of avocado seed (AS) on conventional heating furnace. The N_2 flow was kept at 150 mL min^{-1} during all the heating. When the heating program was cooled down, the N_2 was kept until the temperature was < 150 °C. Ramp temperature was used at 10 °C min^{-1} from the room temperature until the final temperature (T_f)

Experiment	Samples	T_f (°C)	Hold time (min)
1	ASAC1	500	30
2	ASAC2	700	30
3	ASAC3	500	60
4	ASAC4	700	60
5	ASAC5	600	45
6	ASAC6	600	45
7	ASAC7	600	45
	Levels		
	− 1	0	1
T_f (°C)	500	600	700
Hold time (min)	30	45	60

Surface images were observed with a scanning electron microscope (SEM) (TESCAN 3, Sweden) (Lemraski et al. 2017).

The functional groups of the hybrid materials were determined using a Bruker spectrometer and alpha model fourier transform infrared spectroscopy (FTIR). The spectrum was recorded with 64 cumulative scans over the range of 4000–400 cm^{-1} with a resolution of 4 cm^{-1} (Zhang et al. 2017a).

Thermogravimetric analyses (TGA) were obtained on a TA Instruments model SDT Q600 (New Castle, USA) with a heating rate of 20 °C min^{-1} at 100 mL min^{-1} of synthetic air flow. Temperature was varied from 20 to 1000 °C with an acquisition time of 1 point per 5 s using 10.00–15.00 mg of solid (Wang et al. 2017).

For determination of hydrophobicity/hydrophilicity of the surfaces, the ACs were dried in 10-mL beakers at 70 °C for 24 h (dos Reis et al. 2016b; Prenzel et al. 2014). Then, the samples were cooled down in a desiccator before the accurate weight (ca. 0.3 g) of each sample was obtained. Afterwards, the beakers were disposed into capped Erlenmeyer flasks, containing 60 mL of solvent (water or *n*-heptane) inside a temperature-regulated shaker at 25.0 ± 0.1 °C in static condition. The samples were placed in such a way that they were not in contact with the solvent or wall of the Erlenmeyer. After 24 h, the sample was removed from the Erlenmeyer, dried carefully from the outside with laboratory tissues and weighed again. The maximal vapour amount adsorbed on the ACs was obtained by the difference between the final and initial weight and expressed in milligrammes per gramme (dos Reis et al. 2016b; Prenzel et al. 2014). The hydrophobicity/hydrophilicity balances (HI) were calculated as the ratio of

adsorbed *n*-heptane vapour (mg g^{-1}) to adsorbed water vapour amount (mg g^{-1}).

The pH_{pzc} values were determined through the procedure described in the literature (Prola et al. 2013a). The total acidity and basicity of the ACs were determined using a modified Boehm titration (Goertzen et al. 2010; Thue et al. 2017).

Chemicals, reagents and solutions

Deionized water was used for preparation of all solutions.

All phenolic compounds and pharmaceuticals used in the adsorption processes were purchased from Sigma-Aldrich (São Paulo, Brazil) and are listed in the Table 2 (Pubchem 2017), and their chemical structures are depicted on Supplementary Fig. 1 and Supplementary Fig. 2.

The solutions used for the experiments of adsorption were 200 mg L^{-1} of pharmaceuticals and 500 mg L^{-1} of phenols that were prepared from stock solutions of 1000 mg L^{-1}. The pH of these solutions was 7.0 for the majority of these compounds, with exception of nimesulide (pH 8.5), tetracycline (pH 8.5), 1-naphtol (pH 10.5), 2-naphthol (pH 10.5), bisphenol A (pH 10.5) and thymol (pH 11.5).

Batch adsorption studies and quality assurance

The batch adsorption processes for the phenolic compounds and pharmaceuticals on seven ASACs materials were performed using 20.00 mL of phenolic (500 mg L^{-1}) and pharmaceutical (200 mg L^{-1}) solutions at a suitable pH, which were quantitatively transferred to 50.0-mL flat Falcon tubes containing 30.0 mg of ASAC adsorbent (1.5 g L^{-1}). The flasks were capped and placed horizontally in a thermostatic reciprocating shaker (25.0 ± 0.1 °C) model Oxy-303T, furnished by Oxylab (Novo Hamburgo, RS, Brazil), using a contact time of 120 min. After the stipulated time, the flasks were removed and centrifuged to separate the adsorbents from the aqueous solutions, and aliquots of 1–5 mL of the supernatants were properly diluted to 10.0–100.0 mL in calibrated flasks using aqueous solution at suitable pH.

The residual solutions of each adsorbate after adsorption were measured using a UV-visible spectrophotometer at their respective wavelengths, and the adsorption capacity (q_e) was determined using the relation shown in Eq. (1).

$$q = \frac{(C_0 - C_f)}{m} V \quad (1)$$

where q (mg g^{-1}) is the amount of the used adsorbate adsorbed per unit adsorbent; C_0 and C_f (mg/L) are the initial and equilibrium liquid phase concentrations, respectively; V (L) is the volume of the adsorbate solution; and m (g) is the adsorbent amount.

All of the experiments were carried out in triplicate to ensure reproducibility, reliability and accuracy of data. The relative standard deviations of all measurements were < 4.5%. Blanks were run in parallel and corrected when necessary (Barbosa-Jr et al. 2000).

The solutions of adsorbates were stored in glass bottles, which were cleaned by immersing in 1.4 mol L^{-1} HNO_3 for 24 h (Lima et al. 2001), rinsing with deionized water, drying and keeping them in cabinets.

Adsorbate solutions (between 2.00–100.0 mg L^{-1}), in parallel with a blank, were used for linear analytical calibration. The calibration curves were performed on the UV-Win software of the T90+ PG Instruments spectrophotometer. All of the analytical measurements were repeated thrice, and the precisions of the standards were better than 5.0% ($n = 3$) (Lima et al. 2000). The adsorbate solutions (15.0 mg L^{-1}) were used as quality control after every five measurements to ensure accuracy of the solutions (Barbosa-Jr et al. 1999).

Results and discussion

SEM analysis

Analysis such as SEM, in view of its ability to directly view the surface of activated carbons at high magnification, has demonstrated enormous potential for use in the study and characterisation of activated carbons (Thue et al. 2016, 2017; Lemraski et al. 2017). SEM was used to observe the physical surface of the all ASAC samples (see Fig. 1). Such images show that the activation stage produced carbon surfaces which were very irregular in relation to its format and present high roughness. At the amplification of × 1000 (at micrometric scale), it is not possible to distinguish the ASAC samples from each other.

Specific surface area and porosity

Specific surface area and porosity are two important physical properties of a material that impact its quality and utility for a certain application, especially for adsorption process. These physical characteristics are important because they are deeply related to adsorptive capacity of the materials (Thue et al. 2016, 2017; dos Reis et al. 2016a, c). Many works have addressed that the success in the application of adsorbents is closely linked with specific surface area and porosity characteristics of these adsorbents (Leite et al. 2017; Thue et al. 2016, 2017; Lin et al. 2017c).

The physical features of the avocado seed activated carbons made by different pyrolysis conditions are shown in Table 3. By analysing Table 3, it is easy to see that the textural properties of the obtained activated carbons differ in relation to its pyrolysis conditions.

Table 2 Physico-chemical properties of the molecules

Compound	Molecular formula	λ_{max} (nm)	Molecular weight (g mol^{-1})	Solubility in water (g L^{-1})[a]	Van der Waals surface area (A^2, pH 7.0)[b]	Polar surface area (A^2, pH 7.0)[b]	Van der Waals volume (A^3)[b]	Polar surface area/Van der Waals surface area ratio	Log P[b]
Pharmaceuticals									
Amoxicillin	$C_{16}H_{19}N_3O_5S$	227.0	365.404	3.430	476.14	162.71	307.13	0.3417	0.87
Caffeine	$C_8H_{10}N_4O_2$	273.0	194.194	21.60	269.07	58.44	164.20	0.2172	−0.07
Captopril	$C_9H_{15}NO_3S$	200.0	217.283	4.52	318.05	99.24	196.51	0.3120	0.34
Enalapril	$C_{20}H_{28}N_2O_5$	270.5	376.453	16.40	591.12	98.77	357.31	0.1671	0.07
Meloxicam	$C_{14}H_{13}N_3O_4S_2$	359.0	351.395	15.40 (pH 7.0)[b]	421.52	139.05	275.99	0.3299	3.54
Nimesulide	$C_{13}H_{12}N_2O_5S$	392.5	308.308	2.19 (pH 8.5)[b]	407.92	104.12	249.17	0.2552	2.60
Paracetamol	$C_8H_9NO_2$	243.0	151.165	14.00	251.37	49.33	159.08	0.1962	0.46
Propanolol	$C_{16}H_{21}NO_2$	289.5	259.349	24.09 (pH 7.0)[b]	430.03	46.07	257.37	0.1071	3.48
Sodium diclofenac	$C_{14}H_{10}Cl_2NO_2Na$	275.5	318.129	6.02 (pH 7.0)[b]	359.64	52.16	234.43	0.1450	−2.31
Tetracycline	$C_{13}H_{12}N_2O_5S$	357.0	308.308	2.19 (pH 8.5)[b]	407.92	104.12	249.17	0.2552	−1.37
Phenols									
1-Naphthol	$C_{10}H_8O$	292.5	144.173	1.79 (pH 10.5)[b]	209.50	20.23	133.72	0.0966	2.85
2-Naphthol	$C_{10}H_8O$	273.5	144.173	1.25 (pH 10.5)[b]	209.70	20.23	133.65	0.0965	2.70
2-Aminophenol	C_6H_7NO	283.0	109.128	20.00	161.26	46.25	101.48	0.2868	0.62
3-Aminophenol	C_6H_7NO	281.0	109.128	19.39 (pH 7.0)[b]	161.99	46.25	101.50	0.2855	0.21
2-Chlorophenol	C_6H_5ClO	273.5	128.555	2.75 (pH 7.0)[b]	162.88	20.23	104.48	0.1242	2.15
2-Nitrophenol	$C_6H_5NO_3$	278.0	139.110	2.10	181.86	66.20	113.52	0.3640	1.79
4-Nitrophenol	$C_6H_5NO_3$	226.0	139.110	11.60	185.14	63.37	113.43	0.3423	1.91
Pyrocatechol	$C_6H_6O_2$	275.0	110.112	33.24	158.06	40.46	99.01	0.2560	0.88
Resorcinol	$C_6H_6O_2$	273.0	110.112	33.42	158.57	40.46	99.03	0.2552	0.80
Hydroquinone	$C_6H_6O_2$	288.0	110.112	6.72	158.58	40.46	99.04	0.2551	0.59
o-Cresol	C_7H_8O	270.0	108.140	6.67	179.02	20.23	107.37	0.1130	1.95
m-Cresol	C_7H_8O	271.0	108.140	3.94	179.31	20.23	107.32	0.1128	1.96
4-Methoxyphenol	$C_7H_8O_2$	287.5	124.139	13.24	195.05	29.46	116.49	0.1510	1.58
Bisphenol A	$C_{15}H_{16}O_2$	276.0	228.291	1.96 (pH 10.5)[b]	359.75	40.46	221.44	0.1125	3.32
Thymol	$C_{10}H_{14}O$	273.0	150.221	2.39 (pH 11.5)[b]	271.49	20.23	158.40	0.0745	3.30

[a] Pubchem: https://pubchem.ncbi.nlm.nih.gov/. Site visited on September 27, 2017

[b] Chemical properties were calculated using the plug-in of Marvin Sketch 17.16.0 (www.chemaxon.com 2017)

For the S_{BET}, it should be noted that their values are high-presenting values ranging from 1122 to 1584 m^2 g^{-1} (see Table 3). The high values of S_{BET} might implicate in high uptakes of adsorbates by ASACs (Lin et al. 2017c; Thue et al. 2016, 2017). Therefore, it should be pointed out that avocado seed is an excellent precursor for preparation of highly porous activated carbons.

Other parameters that are useful for analysis of the textural properties of these ASAC materials are micropore area and external surface area and total, micropore and mesopore volumes. As can be seen in Table 3, all these parameters have followed the same S_{BET} trend, as earlier observed for other activated carbons (Thue et al. 2016, 2017; Ahmed et al. 2017). It is noted that the samples pyrolysed at 500 °C reached higher textural parameter values compared with those samples pyrolysed at 700 °C.

It is also valuable to classify the activated carbons by their relationship between microporosity and

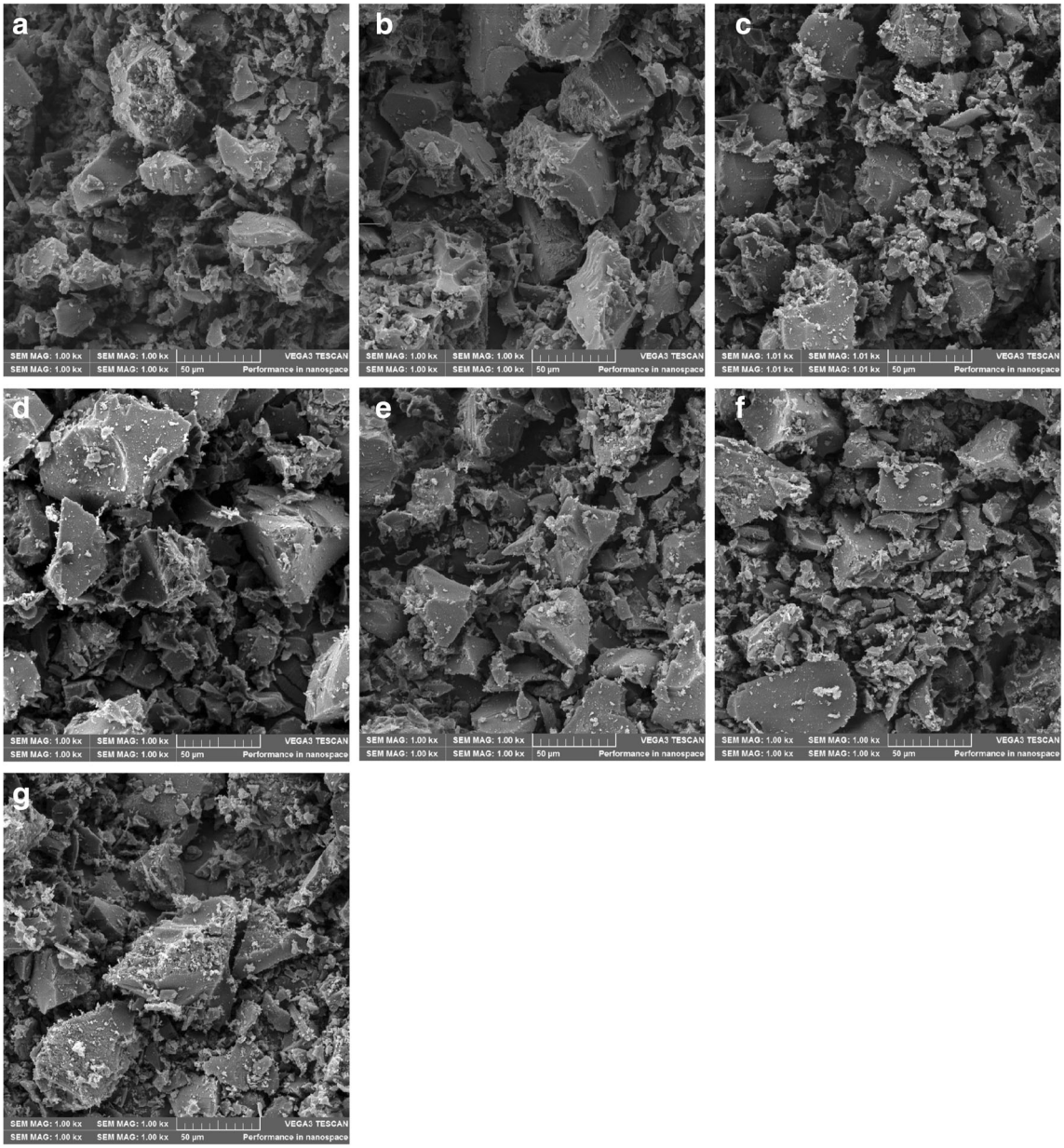

Fig. 1 SEM images of avocado seed activated carbon (ASACs). **a** ASAC1. **b** ASAC2. **c** ASAC3. **d** ASAC4. **e** ASAC5. **f** ASAC6. **g** ASAC7. All images correspond to a magnification of × 1000

Table 3 Textural properties of avocado seed activated carbons

Sample	BET surface area ($m^2\ g^{-1}$)	*t*-plot micropore area ($m^2\ g^{-1}$)	*t*-plot extern. surface area ($m^2\ g^{-1}$)	Total pore volume ($cm^3\ g^{-1}$)	*t*-plot micropore volume ($cm^3\ g^{-1}$)	Mesopore volume ($cm^3\ g^{-1}$)
ASAC1	1584	360	1224	0.8469	0.1563	0.6906
ASAC2	1230	201	1029	0.6685	0.0838	0.5847
ASAC3	1370	263	1107	0.7664	0.1120	0.6544
ASAC4	1122	284	838	0.6002	0.1249	0.4753
ASAC5	1343	316	1027	0.7354	0.1354	0.6000
ASAC6	1300	250	1050	0.7248	0.1261	0.5987
ASAC7	1310	237	1073	0.7232	0.1376	0.5856

mesoporosity. Therefore, the volumes of mesopores were divided by the total pore volume and the values were multiplied by 100%. The percentages of mesopores obtained were 81.54, 87.46, 85.39, 79.19, 81.59, 82.60 and 80.97% for ASAC1, ASAC2, ASAC3, ASAC4, ASAC5, ASAC6 and ASAC7, respectively. Based on these values, clearly, it is seen that all of the obtained activated carbons are predominantly mesoporous materials which could facilitate their uses in adsorption processes, in which adsorbate molecules diffuses through the pores of the ASACs (Leite et al. 2017; Thue et al. 2016, 2017).

Observing the values of specific surface area and total pore volume of the obtained ASAC adsorbents (Table 3), the values of surface area are ranging from 1122 to 1584 $m^2\ g^{-1}$ and for total pore volume ranging from 0.6002 to 0.8469 $cm^3\ g^{-1}$, which are very good values when compared with data already published in the literature. Rovani et al. (2016) produced activated carbon from agro-industrial wastes such as coffee, wood and apple pomace wastes; the highest surface area was achieved by apple pomace wastes with a specific area of 176.4–209.9 $m^2\ g^{-1}$ and total pore volume of 0.2571 to 0.2822 g cm^{-3}; Dos Reis et al. (2016a) produced activated carbon from sewage sludge obtaining specific surface area ranging from 387.7 to 679.3 $m^2\ g^{-1}$ and total pore volume ranging from 0.379 to 0.690 g cm^{-3}; Calvete et al. (2010) produced activated carbon from pinon wastes and obtained surface area of 1035 to 1425 $m^2\ g^{-1}$ and total pore volumes ranging from 0.43 to 0.50 g cm^{-3}; Ahmed et al. (2017) produced activated carbon from human hair and obtained surface area of 1505 $m^2\ g^{-1}$ and total pore volume of 0.798 g cm^{-3}. Based on these data, it can be inferred that the ASAC activated carbons presented higher surface area and higher total pore volume, which are good characteristics for adsorption of different adsorbates (Thue et al. 2016, 2017).

Fourier transform infrared spectroscopy, point of zero charge, total acidity and basicity (Boehm titration) and hydrophobicity index

FTIR analysis contributes in the identification of functional surface groups present on a solid surface which may contribute for explaining the adsorption of adsorbate molecules onto the carbon surfaces (Ribas et al., 2014; Saucier et al. 2015; Thue et al. 2016, 2017). The FTIR spectra of all ASACs are displayed in Fig. 2. Although some differences in the spectra of ASACs can be seen, it seems that the different conditions in the pyrolysis process did not cause large differences in the spectra of ASACs which presented almost the same group of vibrational FTIR bands, such as the following: The band at 3443–3419 cm^{-1} is due to the OH stretching vibrations from the intermolecular hydrogen bonding (Calvete et al. 2010; Leite et al. 2017; Thue et al. 2016); bands at 2920–2924 and 2853–2858 cm^{-1} are due to the asymmetric and symmetric C–H stretching, respectively (Prola et al. 2013a, b); a small shoulder at 1736–1708 cm^{-1} could assigned to C=O stretching of carboxylic acids (Ribas et al. 2014;); that at 1614–1630 cm^{-1} is due to the asymmetric stretching in of carboxylates (O=C=O) (Thue et al. 2016, 2017); and those at 1409–1410 and 1460 cm^{-1} may be assigned to the aromatic ring mode (Leite et al. 2017; Thue et al. 2016). The bands at 1262–1163 and 1030–1040 cm^{-1} could be assigned to C–O stretching of phenols and alcohols, respectively, and the band at 799–806 cm^{-1} could be assigned to C–H out-of-plane bending in the aromatic rings (Leite et al. 2017; Thue et al. 2016). The most important functional groups present in all ACs include (i) O–H likely from alcohols and phenols, (ii) aromatic rings, (iii) C=O likely from carboxylic acids and esters and (iv) CH from aromatic and aliphatic compounds.

The surface chemistry and functionality of a solid material (specially a functional material such carbon material) are determined by the presence of basic and acidic groups on its surface. The pH_{pzc} is the pH at which the surface of an adsorbent is globally neutral, i.e. contains as much positively charged as negatively charged surface functions. Below this value, the surface is positively charged, making it able to attract anions; beyond this value, it is negatively charged which would attract cations.

It can be seen from Table 4 that the pH_{pzc} values of all samples are between 6.11 and 6.80. These values of pH_{pzc} reveal that the surfaces of these ASACs are close to neutrality; however, it reveals that there are a small excess of acidic groups in relation to basic groups.

The total acidity and total basicity of the ASACs were determined using modified Boehm titration (Goertzen et al. 2010; Thue et al. 2017); see Table 4. This method was preferred in relation to fractionated acidic groups (carboxylic acids, phenolic, lactonic) because the CO_2 generated with the use of carbonate and hydrogen carbonate in the aqueous solution leads to wrong results of these groups, which are usually neglected by the majority of authors, who use standard coloured indicator to detect the end point of the titration (Goertzen et al. 2010). It is also observed that the total amount of acidic groups present on the ASAC samples is a little bit higher than that of the basic groups, and this result is consistent with the values of pH_{pzc} reported earlier (Table 4). Samples with higher amount of acidic groups presented lower values of pH_{pzc}. Therefore, the values of pH_{pzc} are in complete agreement with the total amounts of acidic and basic groups present in the activated carbon samples.

In relation to the polarity of the surface of the obtained ASAC adsorbents, it was also observed that samples with higher total amount of functional groups (acidic and basic groups) presented lower values of HI (see Table 4). The HI values were calculated as the ratio of the amount of adsorbed *n*-heptane vapour (mg g^{-1}) by the ASAC samples divided by

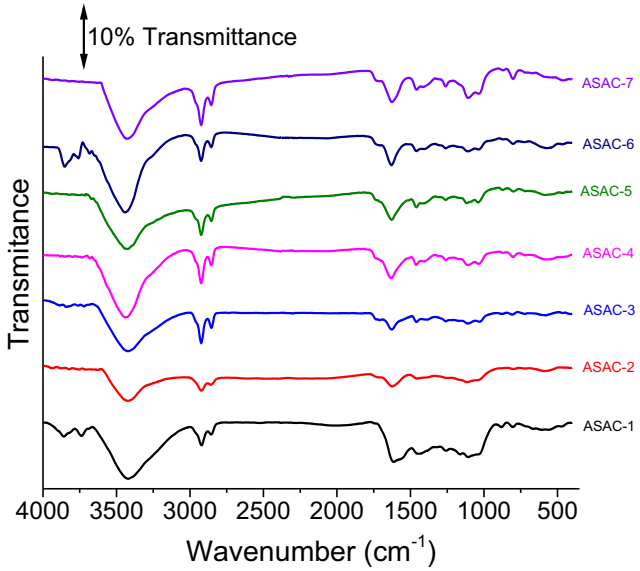

Fig. 2 FTIR spectra of ASACs

the amount of adsorbed water vapour (mg g^{-1}) by the carbon samples (dos Reis et al. 2016b; Prenzel et al. 2014). It is observed that all ASAC surfaces are predominantly hydrophilic in nature (see Table 4), since all HI values are lower than 1.00.

It should be highlighted that the values of pH_{pzc}, total amount of functional groups and HI are completely in agreement, reinforcing that these results should be correct.

The presences of hydrophilic groups on ASAC surfaces are related to H– bonding and oxygen groups that are present on the ASAC surfaces (see Fig. 2). Taking into account these set of results presented until here, it differentiates the better pyrolysis conditions to be carried out, in order to obtain activated carbons with higher sorption capacity for removal of organic emerging contaminants. Therefore, it is necessary to use a statistical tool, to differentiate the textural, functional, polarities and surface acidity of activated carbon samples obtained from the conventional pyrolysis of avocado seed which will be presented in the next section.

Evaluation of the influence variables by statistical analysis

When analysing the effects of multiple variables in an experiment, it is useful to see the normal probability plots of the standardized effects at a given probability level ($p = 0.05$, in this case) to verify what is the variable that has the main effect over a determined response, as well as if the variation of a given parameter will increase or decrease the responses and also it is possible to detect if there are some synergistic or antagonistic effect of varying two or more variables simultaneously. Based on that, in this study, normal probability plots of the standardized effects at $p = 0.05$ for the responses, surface area (Supplementary Fig. 3A), total volume of pores (Supplementary Fig. 3B), total functional groups (Supplementary Fig. 3C) and HI (Supplementary Fig. 3D) for producing activated carbons from avocado seed using the experimental conditions are depicted on Table 1. These graphs could be divided in two regions: at the left of zero standardized effect, where the factors and their interactions presented negative coefficients, and at the right of zero standardized effect where the factors presented positive coefficients. All these factors and interactions which were represented as a square were significant figures, and they were out of the central line that crosses the zero value at the abscissa at 50%. The effects positioned in this line were represented by a circle and correspond to the estimate of errors of the effects, being not significant (Bruns et al. 2006; Montgomery 2017). As the probability level was established at 95% of confidence level ($p = 0.05$), all factors and interactions with values of probability lower than 0.05 are significant (see Supplementary Table 1) and all parameters or interactions of two factors with probability > 0.05 are not significant. Also, the contribution of each factor and its interaction in the overall responses were also given (see Supplementary Table 1).

For the response of surface area (S_{BET}), it was observed that the parameters' final temperature (A) and time of holding the pyrolysis at the final temperature (B) presented both negative coefficients and for this response, there is no interaction of the

Table 4 Chemical surface properties of avocado seed activated carbons

Sample	pH_{pzc}	Total acidity (mmol g^{-1})	Total basicity (mmol g^{-1})	Total of functional groups (mmol g^{-1})	HI
ASAC1	6.11	0.2950	0.1885	0.4835	0.7884
ASAC2	6.80	0.2054	0.1568	0.3622	0.8750
ASAC3	6.32	0.2831	0.1475	0.4306	0.7889
ASAC4	6.85	0.1907	0.1590	0.3497	0.9146
ASAC5	6.48	0.2145	0.1547	0.3692	0.8047
ASAC6	6.55	0.2245	0.1547	0.3792	0.8045
ASAC7	6.52	0.2137	0.1608	0.3745	0.8041

HI amount of adsorbed vapour of *n*-heptane (mg g^{-1}) divided by amount of adsorbed vapour of water (mg g^{-1})

two factors. The contribution of the parameter temperature of pyrolysis corresponds to 77.90% of the overall response (in standardized effects), followed by the time of holding pyrolysis (20.71%). The contributions of interaction of two factors (A × B), central point and error were 0.27, 0.24 and 0.88%, respectively. Based on these results (Supplementary Fig. 3A and Supplementary Table 1A), when the temperature of pyrolysis of avocado seed passes from 500 to 700 °C, a decrease in the surface area will be observed. Also, the increase of time of pyrolysis, from 30 to 60 min, also led to a decrease in surface area. The effect of increase in temperature of pyrolysis and time of holding temperature on the surface area was already reported in the literature by Botomé et al. (2017), and the authors also observed a decrease in the surface area.

For the response total pore volume, all the factors (A and B) and the interactions of two factors (A × B) were significant (see Supplementary Fig. 3B and Supplementary Table 1B). Also, it was observed that increases in the temperature of pyrolysis (A) and holding time at the final temperature (B) as well as the interaction A × B presented negative coefficients, meaning that its increases in their values lead to a decrease in the total pore volume. The contributions of each factor on the overall response were 71.28% (A), 16.40% (B), 5.23% (A × B), 6.96% (central point) and only 0.13% (pure error). Considering that there was significant central point in the response total pore volume, it is possible to highlight that a curvature occurred for this response. Also, interactions of temperature of pyrolysis and time of holding at final temperature also decreased the total pore volume (negative coefficient). Although these two parameters were observed (A × B and central point), the final temperature of pyrolysis (A) is the factor that contributes the most with the total pore volume.

There is a direct relationship between surface area and total pore volume of an activated carbon (Thue et al. 2016, 2017). As the total surface area of ASACs increases, it would lead to increases in the total pore volume. The increase in temperature and holding time at final temperature led to decreases in the surface area (Supplementary Fig. 3A) and total pore volume (Supplementary Fig. 3B).

For the response of total functional groups present on the surface of ASACs, an interesting effect of the parameters was obtained. The temperature of pyrolysis (A) and holding time (B) present negative coefficients; on the other hand, the interactions of temperature of pyrolysis multiplied by holding time (A × B) present a positive coefficient. In addition, the magnitude of A × B is very close to that of A (see Supplementary Table 1C). The overall response (total amount of functional groups) follows a decreasing order, temperature (41.42%), holding time (21.37%), interaction A × B (20.82%), central point (16.39%) and pure error (0.00%). Again, the presence of a central point indicates the curvature when the temperature and the holding time are increased from 500 to 700 °C and 30 to 60 min, respectively. The increase in temperature leads to a decrease in the total functions present on the surface of activated carbons as expected (dos Reis et al. 2016a, c). The increase in temperature during the pyrolysis leads to the elimination of the most volatile organic groups of the pyrolysed lignocellulosic material (Saucier et al. 2015) that will render low contents of organic groups onto the surface of ASAC samples. Also, the increase in the holding time will increase the releases of volatile organic groups (dos Reis et al. 2016a, c). However, the synergistic effect of temperature of pyrolysis multiplied by the holding time (A × B) is not expected in the univariate analysis, and just this result justifies the 2^2 full-factorial design with three central points carried out in this work.

The hydrophobic/hydrophilic ratio (HI) was the fourth response explored in this work. Contrary to all the responses shown until now, all the coefficients presented positive values (see Supplementary Fig. 3D and Supplementary Table 1D). The increase in the temperature of pyrolysis as well as the holding time of the final temperature of pyrolysis led to increase in the HI values, which means that the ASAC surfaces of the carbon adsorbents became less hydrophilic (since all values of HI are lower than 1.00). This achievement is compatible with total organic functional groups. The increase in temperature leads to releases of oxygen functional groups, and therefore, the carbon surfaces become more hydrophobic (dos Reis et al. 2016b; Prenzel et al. 2014). The overall HI response for the factorial design followed a decreasing order, temperature of pyrolysis (36.47%), holding time (24.01%), the interaction of two factors temperature of pyrolysis multiplied by holding time (24.00%) and central point (15.52%).

Based on the DOE of the four responses studied, the following could be drawn:

- For obtaining activated carbons with higher surface area and higher total pore volumes, it would be better to use lower pyrolysis temperatures and holding times;
- For obtaining activated carbons with higher number of total functional groups, it would be better also to use lower pyrolysis temperatures and holding times.

However, it should be mentioned that higher surface area, higher total pore volume and higher functional groups are not a guarantee that the activated carbon will be a good adsorbent for removal of emerging organic contaminants from aqueous solutions, because the adsorption does not take into account the physical characteristics of the adsorbent (higher surface area, higher total pore volume). It also considers the chemical nature of adsorbate and adsorbent and the chemical composition of the medium (Lima et al. 2015).

Adsorption of emerging pollutants

Among the different types of organic pollutants in wastewater, phenolic and several pharmaceutical compounds are considered as priority pollutants since they cause several issues for the living organisms, even at very low concentrations. Removal of these emerging compounds by adsorption onto activated carbon is one of the most applied methods for treating polluted waters. In this work, avocado seed was used as raw material for preparation of activated carbons and they were used for uptake of 15 phenolic compounds and 10 pharmaceuticals in aqueous solutions as shown in Table 5. The ASACs exhibited very high adsorption capacity for all organic emerging contaminants.

It is well-known in the literature that the adsorption characteristics of different phenolic and pharmaceutical compounds are influenced by their physicochemical properties, such as water solubility and octanol–water partition coefficients (dos Reis et al. 2017, Thue et al. 2016, 2017; Yang et al. 2017). However, in this study, the affinity of each organic emerging contaminant compared with others does not follow a logical pattern with respect to their physical chemical properties, reported in Table 2, in order to differentiate the reason for the differences on sorption capacities of different emerging organic contaminants. We tried to make some correlation of amount adsorbed of the organic compound with its molecular weight, its Van der Waals and polar surface areas, its ratio of polar surface area divided by the Van der Waals surface area, its Van der Waals volume and its Log *P*. However, all these parameters did not follow a logical pattern to explain why the ASACs presented differences in the sorption capacity for these 25 emerging organic contaminants. Therefore, the statistical analysis, described below, helped to understand these differences.

The results shown in Table 5 suggest that the ASACs could be successfully employed for removal of organic emerging compounds from aqueous solutions. The reasons for this could be several. However, what better explains the efficiency in the removal of such adsorbates is the mechanism of adsorption. To better understand the possible mechanisms that might play key roles in phenolic compound adsorption on ASACs, some mechanisms, such as π–π interactions, dispersion interactions, electron donor–acceptor and hydrogen bonds (dos Reis et al. 2016c; Thue et al. 2016), are proposed.

In the ASACs, surfaces are expected to contain large amounts of polar groups such as –OH, –COO, –O and –NH, (as can be seen in the FTIR analysis) and exhibit mostly polar (hydrophilic) behaviour.

The organic emerging contaminant adsorption on ASACs could also be determined by π–π interactions (between the π electrons present in the rings of phenols with the π electrons of the aromatic rings present on ASACs) and "donor–acceptor complex" formation between the surface carbonyl groups (electron donors) and the aromatic ring of phenol acting as the acceptor.

It is clearly seen that although the ASAC-1 has the highest S_{BET} and total pore volume (1584 $m^2\ g^{-1}$ and 0.8469 $cm^3\ g^{-1}$, respectively) among the others, it does not present the highest uptake, which suggests that the adsorption of emerging pollutants such phenols and pharmaceuticals is not totally influenced by physical features of the ASACs (see Table 5). The differences between the values of q might also be linked by the physical–chemical properties of the emerging pollutants; however, no logical pattern was followed as can be seen by the physical–chemical properties shown in Table 2 as well as in the Supplementary Fig. 1 and Supplementary Fig. 2.

However, observing Table 5 as well as the results of Table 4, the decreasing sorption capacity of the ASAC for all organic emerging contaminants was as follows: ASAC4 > ASAC2 > ASAC7 ≈ ASAC6 ≈ ASAC5 > ASAC3 > ASAC1. This order is exactly the opposite order of total functional groups, whose decreasing order was ASAC1 > ASAC3 > ASAC6 ≈ ASAC7 ≈ ASAC5 > ASAC2 > ASAC4. Also, the sorption decreasing order of ASACs also agrees with that of the HI ratio, whose decreasing order is ASAC4 > ASAC2 > ASAC5 ≈ ASAC6 ≈ ASAC7 > ASAC3 > ASAC1. Based on these results, it can be concluded that the sorption capacity of the emerging organic contaminants decreased as the number of total basic and acidic groups increased, and the sorption capacity also increased with the increase in HI ratio, and this analysis was observed based on the statistical results of the factorial design.

Considering that all activated carbons prepared in this work presented surface area higher than 1000 $m^2\ g^{-1}$ (see Table 3) and considering that a pyrolysis temperature of avocado seed carried out at 700 °C led to a decrease in functional groups (acidic and basic functional groups) onto the surface of activated carbon, which resulted in the most hydrophobic surface, when compared with the activated carbons (see Table 4), whose final pyrolysis temperature was 500 °C, it could be stated that for adsorption of 25 emerging contaminants, the best activated carbon was ASAC4. However, all other activated carbons also could be successfully employed for adsorption of organic compounds from aqueous solutions.

Comparison of adsorption capacities of different adsorbents

In order to compare the effectiveness of the avocado activated carbons for removal of phenolic compounds, Table 6 brings some results of some works reported in literature in relation to adsorption of some phenolic compounds and pharmaceuticals over many types of ACs. The results found in literature might enable a comparison analysis about the effectiveness the avocado ACs prepared in this work (see Table 5) with many other adsorbents.

Table 5 Sorption capacity of 25 emerging organic contaminants

	Sorption capacity (mg g^{-1})				
	Amoxicillin	Caffeine	Captopril	Enalapril	Meloxicam
ASAC1	71.94	116.86	122.58	99.56	180.26
ASAC2	109.97	129.43	131.58	119.08	199.87
ASAC3	74.52	119.56	123.25	100.32	182.36
ASAC4	110.00	131.85	132.01	121.74	201.36
ASAC5	95.85	126.15	129.58	110.12	196.25
ASAC6	97.83	127.12	127.58	110.68	195.25
ASAC7	94.56	125.58	128.25	112.36	194.25
	Nimesulide	Paracetamol	Propanolol	Sodium diclofenac	Tetracycline
ASAC1	117.56	95.56	69.25	121.25	188.52
ASAC2	133.85	121.69	102.58	131.05	197.85
ASAC3	119.25	105.21	71.25	124.25	191.25
ASAC4	134.01	122.56	104.03	132.52	200.36
ASAC5	127.25	99.95	99.62	126.89	196.52
ASAC6	126.36	98.65	98.91	127.58	198.52
ASAC7	127.52	97.25	99.67	129.99	197.25
	2-Aminophenol	3-Aminophenol	1-Naphtol	2-Naphtol	Thymol
ASAC1	297.36	147.25	301.58	270.69	278.52
ASAC2	330.87	268.25	331.39	317.73	301.50
ASAC3	299.34	149.71	305.52	275.58	280.56
ASAC4	331.08	270.58	332.58	319.29	302.25
ASAC5	325.24	187.69	318.25	305.25	290.52
ASAC6	327.58	189.07	317.25	306.53	291.52
ASAC7	329.32	184.69	316.54	304.26	292.36
	2-Nitrophenol	4-Nitrophenol	Cathecol	Resorcinol	Hydroquinone
ASAC1	275.35	238.37	141.25	99.52	130.25
ASAC2	306.58	261.64	229.58	170.53	305.05
ASAC3	277.56	242.62	142.21	101.95	133.78
ASAC4	307.43	266.03	231.71	172.91	307.98
ASAC5	292.54	264.86	181.02	142.35	226.75
ASAC6	295.24	267.01	183.88	145.54	224.56
ASAC7	294.61	265.25	180.48	144.25	226.45
	2-Chlorophenol	*o*-Cresol	*m*-Cresol	4-Methoxyphenol	Bisphenol A
ASAC1	202.38	148.24	135.58	197.35	314.56
ASAC2	239.98	201.57	182.59	272.58	327.25
ASAC3	204.56	149.58	139.25	201.55	315.45
ASAC4	241.25	202.58	183.47	277.17	325.07
ASAC5	240.79	178.25	177.25	240.03	319.56
ASAC6	242.05	177.64	181.91	243.81	318.47
ASAC7	240.69	175.26	175.25	242.69	317.52

As can be seen in Tables 5 and 6, the adsorbent materials proposed in this current work presented very good adsorption capacities when compared with other adsorbents reported in the literature. It is also highlighted that avocado ACs also presented higher adsorption capacities when compared with other adsorbents reported in the literature. However, these results are very important because they highlight the excellent performance of avocado ACs on the removal of several

Table 6 Maximum sorption capacities of different adsorbents used for removal of various pharmaceuticals and phenolic compounds

Adsorbent	Phenolic compounds	Q (mg g^{-1})	References
Hyacinth AC	2-Nitrophenol	47.62	Isichei and Okieimen (2014)
Mesoporous carbon	Resorcinol	37	Shou et al. (2016)
Mesoporous silica	Resorcinol	39.2	Guo et al. (2013)
Coal AC	3-Aminophenol	110	Petrova et al. (2011)
Mesoporous carbons	Resorcinol	40.6	Ren et al. (2016)
AC waste rubber	*p*-Cresol	250	Gupta al. (2014)
Eggshells carbons	Phenol	192	Giraldo and Moreno-Piraján (2014)
Activated carbon	2-Chlorophenol	549.5	Strachowski and Bystrzejewski (2016)
Aminated AC	Phenol	227.27	Yang et al. (2014)
Granular AC	Catechol	100	Suresh et al. (2011)
Granular AC	Resorcinol	113	Suresh et al. (2011)
Sludge AC	Resorcinol	406.9	Dos Reis et al. (2017)
Sludge AC	3-Aminophenol	454.5	Dos Reis et al. (2017)
Sludge AC	Hydroquinone	117.1	Dos Reis et al. (2017)
Sludge AC			Dos Reis et al. (2017)
	Pharmaceuticals		
Sludge AC	Diclofenac	156.7	Dos Reis et al. (2016b)
Sludge AC	Nimesulide	66.4	Dos Reis et al. (2016b)
Cotton waste AC	Tetracycline	109	Boudrahema et al. (2017)
Cotton waste AC	Paracetamol	105	Boudrahema et al. (2017)
Pineapple leaves AC	Caffeine	155.5	Beltrame et al. (2018)
Olive stone AC	Diclofenac	3.104	Larous and Meniai (2016)
Cocoa shell AC	Nimesulide	74.81	Saucier et al. (2015)
Human hair AC	Tetracycline	128.52	Ahmed et al. (2017)
Cocoa shell AC	Diclofenac	63.47	Saucier et al. (2015)

phenolic compounds and pharmaceutics toward other adsorbents described in Tables 5 and 6.

Conclusion

In this study, avocado seed was successfully used as raw material for producing activated carbons by conventional pyrolysis. In order to determine the best condition to produce the activated carbons, a DOE was employed by varying the temperature (500–700 °C) and time of pyrolysis (30–60 min).

The two evaluated factors (temperature and time of pyrolysis) strongly influenced the S_{BET} and pore volume values; both factors had a negative effect which means that increasing the values of factors leads to decreases in S_{BET} and pore volume values. The produced activated carbon exhibited high specific surface areas in the range of 1122–1584 m^2 g^{-1}. Surface characterisation revealed that ASACs have hydrophilic surfaces and have predominantly acidic groups on their surfaces.

The prepared ASACs were employed in the adsorption of 25 emerging organic compounds such as 10 pharmaceuticals and 15 phenolic compounds which presented high uptake values for all emerging pollutants. It was observed that the activated carbon prepared at higher temperature of pyrolysis (700 °C), which generated less total functional groups and presented higher HI, was the activated carbon with higher sorption capacity for uptaking emerging organic contaminants.

Based on results of this work, it is possible to conclude that avocado seed can be employed as a raw material to produce high surface area and very efficient activated carbons in relation to treatment of polluted waters with emerging organic pollutants.

Acknowledgments We are grateful to Chemaxon for giving us an academic research licence for the Marvin Sketch software, version 17.24.0 (http://www.chemaxon.com) 2017 used for emerging organic contaminant physical–chemical properties.

Funding information The authors gratefully thank the National Council for Scientific and Technological Development (CNPq, Brazil) and the

Coordination of Improvement of Higher Education personnel (CAPES, Brazil) for financial support of this work.

References

Ahmed MJ, Islam MA, Asif M, Hameed BH (2017) Human hair-derived high surface area porous carbon material for the adsorption isotherm and kinetics of tetracycline antibiotics. Bioresour Technol 243:778–784. https://doi.org/10.1016/j.biortech.2017.06.174

Ahmed MB, Zhou JL, Ngo HH, Guo W, Chen M (2016) Progress in the preparation and application of modified biochar for improved contaminant removal from water and wastewater. Bioresour Technol 214:836–851. https://doi.org/10.1016/j.biortech.2016.05.057

Ba-Abbad MM, Takriff MS, Kadhum AAH, Mohamad AB, Benamor A, Mohammad AW (2017) Solar photocatalytic degradation of 2-chlorophenol with ZnO nanoparticles: optimisation with D-optimal design and study of intermediate mechanisms. Environ Sci Pollut Res 24(3):2804–2819. https://doi.org/10.1007/s11356-016-8033-y

Barbosa-Jr F, Krug FJ, Lima EC (1999) On-line coupling of electrochemical preconcentration in tungsten coil electrothermal atomic absorption spectrometry for determination of lead in natural waters. Spectrochim Acta B 54(8):1155–1166. https://doi.org/10.1016/S0584-8547(99)00055-5

Barbosa-Jr F, Lima EC, Krug FJ (2000) Determination of arsenic in sediment and soil slurries by electrothermal atomic absorption spectrometry using W-Rh permanent modifier. Analyst 125(11):2079–2083. https://doi.org/10.1039/b005783p

Beltrame KK, Cazetta AL, de Souza PSC, Spessato L, Silva TL, Almeida VC (2018) Adsorption of caffeine on mesoporous activated carbon fibers prepared from pineapple plant leaves. Ecotoxicol Environ Saf 147(2018):64–71. https://doi.org/10.1016/j.ecoenv.2017.08.034

Besha AT, Gebreyohannes AY, Tufa RA, Bekele DN, Curcio E, Giorno L (2017) Removal of emerging micropollutants by activated sludge process and membrane bioreactors and the effects of micropollutants on membrane fouling: a review. J Environ Chem Eng 5(3):2395–2414. https://doi.org/10.1016/j.jece.2017.04.027

Bhatnagar A, Anastopoulos I (2017) Adsorptive removal of bisphenol A (BPA) from aqueous solution: a review. Chemosphere 168:885–902. https://doi.org/10.1016/j.chemosphere.2016.10.121

Botomé ML, Poletto P, Junges J, Perondi D, Dettmer A, Godinho M (2017) Preparation and characterization of a metal-rich activated carbon from CCA-treated wood for CO_2 capture. Chem Eng J 321:614–621. https://doi.org/10.1016/j.cej.2017.04.004

Boudrahema N, Delpeux-Ouldriane S, Khenniche L, Boudrahema F, Aissani-Benissada F, Gineys M (2017) Single and mixture adsorption of clofibric acid, tetracycline and paracetamol onto activated carbon developed from cotton cloth residue. Process Saf Environ Prot 111:544–559. https://doi.org/10.1016/j.psep.2017.08.025

Bruns RE, Scarmino IS, de Barros-Neto B (2006) Statistical design—Chemometrics, First edn. Elsevier, Amsterdam

Calvete T, Lima EC, Cardoso NF, Dias SLP, Ribeiro ES (2010) Removal of brilliant green dye from aqueous solutions using home made activated carbons. CLEAN – Soil, Air, Water 38(5-6):521–532. https://doi.org/10.1002/clen.201000027

Carmalin AS, Lima EC, Allaudeen N, Rajan S (2016) Application of graphene based materials for adsorption of pharmaceutical traces from water and wastewater—a review. Desalin Water Treat 57: 27573–27586

dos Reis GS, Adebayo MA, Sampaio CH, Lima EC, Thue PS, de Brum IAS, Dias SLP, Pavan FA (2017) Removal of phenolic compounds from aqueous solutions using sludge-based activated carbons prepared by conventional heating and microwave-assisted pyrolysis. Water Air Soil Pollut 228(33):1–17

dos Reis GS, Mahbub MKB, Wilhelm M, Lima EC, Sampaio CH, Saucier C, Dias SLP (2016a) Activated carbon from sewage sludge for removal of sodium diclofenac and nimesulide from aqueous solutions. Korean J Chem Eng 33(11):3149–3161. https://doi.org/10.1007/s11814-016-0194-3

dos Reis GS, Sampaio CH, Lima EC, Wilhelm M (2016b) Preparation of novel adsorbents based on combinations of polysiloxanes and sewage sludge to remove pharmaceuticals from aqueous solutions. Colloids Surf A Physicochem Eng Asp 497:304–315. https://doi.org/10.1016/j.colsurfa.2016.03.021

dos Reis GS, Wilhelm M, Silva TCA, Rezwan K, Sampaio CH, Lima EC, Souza SMAGU (2016c) The use of design of experiments for the evaluation of the production of surface-rich activated carbon from sewage sludge via microwave and conventional pyrolysis. Appl Therm Eng 93:590–597. https://doi.org/10.1016/j.applthermaleng.2015.09.035

Ennaciri K, Bacaoui A, Sergent M, Yaacoubi A (2014) Application of fractional factorial and Doehlert designs for optimizing the preparation of activated carbons from Argan shells. Chemometr Intell Lab 139:48–57. https://doi.org/10.1016/j.chemolab.2014.09.006

Fatta-Kassinos D, Michael C (2013) Wastewater reuse applications and contaminants of emerging concern. Environ Sci Pollut Res 20(6): 3493–3495. https://doi.org/10.1007/s11356-013-1699-5

Geissena V, Mol H, Klumpp E, Umlauf G, Nadal M, van der Ploeg M, van de Zee SEATM, Ritsema CJ (2015) Emerging pollutants in the environment: a challenge for water resource management. Inter Soil Water Conser Res 3(1):57–65. https://doi.org/10.1016/j.iswcr.2015.03.002

Ghattas AK, Fischer F, Wick A, Ternes TA (2017) Anaerobic biodegradation of (emerging) organic contaminants in the aquatic environment. Water Res 116:268–295. https://doi.org/10.1016/j.watres.2017.02.001

Gil A, Garcia AM, Fernandez M, Vicente MA, Gonzalez-Rodriguez B, Rives V, Korili AS (2017) Effect of dopants on the structure of titanium oxide used as a photocatalyst for the removal of emergent contaminants. J Ind Eng Chem 53:183–191. https://doi.org/10.1016/j.jiec.2017.04.024

Giraldo L, Moreno-Piraján JC (2014) Study of adsorption of phenol on activated carbons obtained from eggshells. J Anal Appl Pyrol 106: 41–47. https://doi.org/10.1016/j.jaap.2013.12.007

Goertzen SL, Theriault KD, Oickle AM, Tarasuk AC, Andreas HA (2010) Standardization of the Boehm titration. Part I. CO_2 expulsion and endpoint determination. Carbon 48(4):1252–1261. https://doi.org/10.1016/j.carbon.2009.11.050

Guo R, Guo J, Yu F, Gang DD (2013) Synthesis and surface functional group modifications of ordered mesoporous carbons for resorcinol removal. Microporous Mesoporous Mater 175(2013):141–146. https://doi.org/10.1016/j.micromeso.2013.03.028

Gupta VK, Nayak A, Agarwal S, Tyagi I (2014) Potential of activated carbon from waste rubber tire for the adsorption of phenolics: effect of pre-treatment conditions. J Colloid Interface Sci 417:420–430. https://doi.org/10.1016/j.jcis.2013.11.067

Isichei TO, Okieimen FE (2014) Adsorption of 2-nitrophenol onto water hyacinth activated carbon-kinetics and equilibrium studies. Environ Pollution 3:99–111

Jiang J-Q, Zhou Z, Sharma VK (2013) Occurrence, transportation, monitoring and treatment of emerging micro-pollutants in waste water—a review from global. Microchem J 110:292–300. https://doi.org/10.1016/j.microc.2013.04.014

Kishimoto N, Kobayashi M (2016) Effects of three additives on the removal of perfluorooctane sulfonate (PFOS) by coagulation using ferric chloride or aluminum sulfate. Water Sci Technol 73(12): 2971–2977. https://doi.org/10.2166/wst.2016.161

Larous S, Meniai A-H (2016) Adsorption of diclofenac from aqueous solution using activated carbon prepared from olive stones. Int J Hydrog Energy 41(24):10380–10390. https://doi.org/10.1016/j.ijhydene.2016.01.096

Leite AJB, Sophia AC, Thue PS, dos Reis GS, Dias SLP, Lima EC, Vaghetti JCP, Pavan FA, de Alencar WS (2017) Activated carbon from avocado seeds for the removal of phenolic compounds from aqueous solutions. Desalin Water Treat 71:168–181. https://doi.org/10.5004/dwt.2017.20540

Lemraski EG, Sharafinia S, Alimohammadi M (2017) New activated carbon from Persian mesquite grain as an excellent adsorbent. Phys Chem Res 5:81–98

Lima EC, Adebayo MA, Machado FM (2015) Chapter 4—experimental adsorption in carbon nanomaterials as adsorbents for environmental and biological applications, Bergmann CP, Machado FM editors, Springer pp.71-84. DOI https://doi.org/10.1007/978-3-319-18875-1_4

Lima EC, Barbosa-Jr F, Krug FJ (2000) The use of tungsten–rhodium permanent chemical modifier for cadmium determination in decomposed samples of biological materials and sediments by electrothermal atomic absorption spectrometry. Anal Chim Acta 409(1-2):267–274. https://doi.org/10.1016/S0003-2670(99)00861-2

Lima EC, Barbosa-Jr F, Krug FJ (2001) Lead determination in biological material slurries by ETAAS using W-Rh permanent modifier. Fres J Anal Chem 369(6):496–501. https://doi.org/10.1007/s002160000667

Lin L, Jiang W, Xu P (2017c) Comparative study on pharmaceuticals adsorption in reclaimed water desalination concentrate using biochar: impact of salts and organic matter. Sci Total Environ 601–602:857–864

Lin L, Wang H, Jiang W, Mkaouar RA, Xu P (2017a) Comparison study on photocatalytic oxidation of pharmaceuticals by TiO_2-Fe and TiO_2-reduced graphene oxide nanocomposites immobilized on optical fibers. J Hazard Mat 333:162–168. https://doi.org/10.1016/j.jhazmat.2017.02.044

Lin L, Wang H, Xu P (2017b) Immobilized TiO2-reduced graphene oxide nanocomposites on optical fibers as high performance photocatalysts for degradation of pharmaceuticals. Chem Eng J 310:389–398. https://doi.org/10.1016/j.cej.2016.04.024

Matamoros V, Salvado V (2013) Evaluation of a coagulation/flocculation-lamellar clarifier and filtration-UV-chlorination reactor for removing emerging contaminants at full-scale wastewater treatment plants in Spain. J Environ Manag 117:96–102. https://doi.org/10.1016/j.jenvman.2012.12.021

Montgomery DC (2017) Design and analysis of experiments, 9th edn. John Wiley & Sons, New York

Petrova B, Tsyntsarski B, Budinovaa T, Petrova N, Velasco LF, Ania CO (2011) Activated carbon from coal tar pitch and furfural for the removal of p-nitrophenol and m-aminophenol. Chem Eng J 172(1):102–108. https://doi.org/10.1016/j.cej.2011.05.075

Prenzel T, Döge K, Motta RPO, Wilhelm M, Rezwan K (2014) Controlled hierarchical porosity of hybrid ceramics by leaching water soluble templates and pyrolysis. J Eur Ceram Soc 34(6):1501–1509. https://doi.org/10.1016/j.jeurceramsoc.2013.11.033

Prola LDT, Acayanka E, Lima EC, Umpierres CS, Vaghetti JCP, Santos WO, Laminsi S, Njifon PT (2013a) Comparison of Jatropha curcas shells in natural form and treated by non-thermal plasma as biosorbents for removal of Reactive Red 120 textile dye from aqueous solution. Ind Crop Prod 46:328–340. https://doi.org/10.1016/j.indcrop.2013.02.018

Prola LDT, Machado FM, Bergmann CP, de Souza FE, Gally CR, Lima EC, Adebayo MA, Dias SLP, Calvete T (2013b) Adsorption of Direct Blue 53 dye from aqueous solutions by multi-walled carbon nanotubes and activated carbon. J Environ Manag 130:166–175. https://doi.org/10.1016/j.jenvman.2013.09.003

Pubchem 2017: https://pubchem.ncbi.nlm.nih.gov/ site visited on September 27th, 2017

Puchana-Rosero MJ, Lima EC, Ortiz-Monsalve S, Mella B, da Costa D, Poll E, Gutterres M (2017) Fungal biomass as biosorbent for the removal of Acid Blue 161 dye in aqueous solution. Environ Sci Pollut Res 24(4):4200–4209. https://doi.org/10.1007/s11356-016-8153-4

Puchana-Rosero MJ, Adebayo MA, Lima EC, Machado FM, Thue PS, Vaghetti JCP, Umpierres CS, Gutterres M (2016) Microwave-assisted activated carbon obtained from the sludge of tannery-treatment effluent plant for removal of leather dyes. Colloids Surf A: Physicochem Eng Aspects 504:105–115. https://doi.org/10.1016/j.colsurfa.2016.05.059

Ren H, Shou W, Ren C, Gang DD (2016) Preparation and post-treatments of ordered mesoporous carbons (OMC) for resorcinol removal. Int J Environ Sci Technol 13(6):1505–1514. https://doi.org/10.1007/s13762-016-0990-7

Ribas MC, Adebayo MA, Prola LDT, Lima EC, Cataluna R, Feris LA, Machado FM, Pavan FA, Calvete T (2014) Comparison of a home-made cocoa shell activated carbon with commercial activated carbon for the removal of reactive violet 5 dye from aqueous solutions. Chem Eng J 248:315–326. https://doi.org/10.1016/j.cej.2014.03.054

Rossner A, Snyder SA, Knappe DRU (2009) Removal of emerging contaminants of concern by alternative adsorbents. Water Res 43(15):3787–3796. https://doi.org/10.1016/j.watres.2009.06.009

Rovani S, Rodrigues AG, Medeiros LF, Cataluña R, Lima EC, Fernandes AN (2016) Synthesis and characterisation of activated carbon from agroindustrial waste—preliminary study of 17β-estradiol removal from aqueous solution. J Environ Chem Eng 4(2):2128–2137. https://doi.org/10.1016/j.jece.2016.03.030

Saucier C, Adebayo MA, Lima EC, Cataluna R, Thue PS, Prola LDT, Puchana-Rosero MJ, Machado FM, Pavan FA, Dotto GL (2015) Microwave-assisted activated carbon from cocoa shell as adsorbent for removal of sodium diclofenac and nimesulide from aqueous effluents. J Hazard Mater 289:18–27. https://doi.org/10.1016/j.jhazmat.2015.02.026

Saucier C, Karthickeyan P, Ranjithkumar V, Lima EC, dos Reis GS, de Brum IAS (2017) Efficient removal of amoxicillin and paracetamol from aqueous solutions using magnetic activated carbon. Environ Sci Pollut Res 24(6):5918–5932. https://doi.org/10.1007/s11356-016-8304-7

Shou W, Chao B, Ahmad ZU, Gang DD (2016) Ordered mesoporous carbon preparation by the in situ radical polymerization of acrylamide and its application for resorcinol removal. J Appl Polym Sci 133(19). https://doi.org/10.1002/APP.43426

Strachowski P, Bystrzejewski M (2016) Comparative studies of sorption of phenolic compounds onto carbon-encapsulated iron nanoparticles, carbon nanotubes and activated carbon. J Mol Liq 213:351–359

Suresh S, Srivastava VC, Mishra IM (2011) Study of catechol and resorcinol adsorption mechanism through granular activated carbon: characterization, pH and kinetic study. Sep Sci Technol 46(11):1750–1766. https://doi.org/10.1080/01496395.2011.570284

Takdastan A, Mahvi AH, Lima EC, Shirmardi M, Babaei AA, Goudarzi G, Neisi A, Farsani MH, Vosoughi M (2016) Preparation, characterization, and application of activated carbon from low-cost material for the adsorption of tetracycline antibiotic from aqueous solutions. Water Sci Technol 74(10):2349–2363. https://doi.org/10.2166/wst.2016.402

Thommes M, Kaneko K, Neimark AV, Olivier JP, Rodriguez-Reinoso F, Rouquerol J, Sing KSW (2015) Physisorption of gases, with special reference to the evaluation of surface area and pore size distribution (IUPAC Technical Report). Pure Appl Chem 87:1051–1069

Thue PS, Adebayo MA, Lima EC, Sieliechi JM, Machado FM, Dotto GL, Vaghetti JCP, Dias SLP (2016) Preparation, characterization and application of microwave-assisted activated carbons from wood chips for removal of phenol from aqueous solution. J Mol Liq 223:1067–1080. https://doi.org/10.1016/j.molliq.2016.09.032

Thue PS, dos Reis GS, Lima EC, Sieliechi JM, Dotto GL, Wamba AGN, Dias SLP, Pavan FA (2017) Activated carbon obtained from sapelli

wood sawdust by microwave heating for o-cresol adsorption. Res Chem Intermed 43(2):1063–1087. https://doi.org/10.1007/s11164-016-2683-8

Umpierres CS, Prola LDT, Adebayo MA, Lima EC, dos Reis GS, Kunzler DDF, Dotto GL, Arenas LT, Benvenutti EV (2017) Mesoporous Nb_2O_5/SiO_2 material obtained by sol–gel method and applied as adsorbent of crystal violet dye. Environ Technol 38(5): 566–578. https://doi.org/10.1080/09593330.2016.1202329

Wang M, Li G, Huang LH, Xue J, Liu Q, Bao N, Huang J (2017) Study of ciprofloxacin adsorption and regeneration of activated carbon prepared from Enteromorpha prolifera impregnated with H3PO4 and sodium benzenesulfonate. Ecotox Environ Safe 139:36–42. https://doi.org/10.1016/j.ecoenv.2017.01.006

Yang G, Chen H, Qin H, Feng Y (2014) Amination of activated carbon for enhancing phenol adsorption: effect of nitrogen-containing functional groups. Appl Surf Sci 293:299–305. https://doi.org/10.1016/j.apsusc.2013.12.155

Yang J, Jin YX, Yu XP, Yue QF (2017) High surface area ordered mesoporous carbons from waste polyester: effective adsorbent for organic pollutants from aqueous solution. J Sol-Gel Sc Technol 83(2):413–421. https://doi.org/10.1007/s10971-017-4419-7

Zhang BP, Han XL, Gu PJ, Fang SQ, Bai J (2017a) Response surface methodology approach for optimization of ciprofloxacin adsorption using activated carbon derived from the residue of desilicated rice husk. J Mol Liq 238:316–325. https://doi.org/10.1016/j.molliq.2017.04.022

Zhang YJ, Zhu H, Szewzyk U, Lubbecke S, Geissen SU (2017b) Removal of emerging organic contaminants with a pilot-scale biofilter packed with natural manganese oxides. Chem Eng J 317: 454–460. https://doi.org/10.1016/j.cej.2017.02.095

Zhuo N, Lan Y, Yang W, Yang Z, Li X, Zhou X, Liu Y, Shen J, Zhang X (2017) Adsorption of three selected pharmaceuticals and personal care products (PPCPs) onto MIL-101(Cr)/natural polymer composite beads. Sep Purif Technol 177:272–280. https://doi.org/10.1016/j.seppur.2016.12.041

Contents lists available at ScienceDirect

Journal of Environmental Chemical Engineering

journal homepage: www.elsevier.com/locate/jece

Hybrid adsorbents of tannin and APTES (3-aminopropyltriethoxysilane) and their application for the highly efficient removal of acid red 1 dye from aqueous solutions

Anderson J.B. Leite[a], Eder C. Lima[a], Glaydson S. dos Reis[a,b,*], Pascal S. Thue[a], Caroline Saucier[a], Fabiano S. Rodembusch[a], Silvio L.P. Dias[a], Cibele S. Umpierres[a], Guillherme L. Dotto[c]

[a] Institute of Chemistry, Federal University of Rio Grande do Sul (UFRGS), Av. Bento Gonçalves 9500, Postal Box 15003, ZIP 91501-970, Porto Alegre, RS, Brazil
[b] Department of Metallurgy, Federal University of Rio Grande do Sul (UFRGS), Av. Bento Gonçalves 9500, Porto Alegre, RS, Brazil
[c] Chemical Engineering Department, Federal University of Santa Maria (UFSM), Santa Maria, RS, Brazil

ARTICLE INFO

Keywords:
Tannins
Hybrids
Tannin adsorbent
Kinetic and isotherm models

ABSTRACT

Hybrid adsorbents were prepared by reacting tannin with different amounts of 3-aminopropyltriethoxysilane (APTES). The materials were characterized by SEM, TEM, FTIR, CHN, N_2 adsorption/desorption isotherms and vapor sorption (water and n-heptane adsorptions–for determination of the hydrophobicity-hydrophilicity ratio). The modified materials were utilized as adsorbents for the removal of Acid Red 1 (AR-1) dye from aqueous solutions. The N_2 isotherm results showed low porosities of the modified materials, however they presented high efficient adsorption of AR-1 dye. To find a proof of hybridization between tannin and APTES, the materials were characterized by Diffuse Reflectance Ultraviolet-Visible Absorption (DRUV) spectroscopy. The results indicate that the electronic structure of the final materials was changed, and was related to a hybrid formation between tannin and APTES.

For the adsorption experiments, the best experimental conditions were reached at pH 2.0, contact time of 8 h and at 50 °C. The equilibrium and kinetics adsorption data were well represented by the Liu isotherm and the General order kinetic models, respectively. The maximum adsorption capacity of 418.3 mg g^{-1} was obtained at 50 °C for a tannin-APTES material at ratio 1:1 (Tan-Ap-1.0). Based on experimental data it was found that electrostatic interactions and hydrogen bonds between adsorbent and AR-1 dye played the most important role in the adsorption process.

Effect of temperature and thermodynamic studies revealed that the adsorption processes of AR-1 onto tannin materials are dependent on temperature and are exothermic and spontaneous. With regards to the applicability of the adsorbents for treating simulated effluents, they showed an excellent outcome confirming their high-efficiency for dye adsorption.

1. Introduction

Dyes have polluted waterways from rapidly growing industrial activities. Dyes are overused in several industrial processes such as paper, food, plastic, and textiles to enhance the aesthetic values of their products [1]. Without proper treatment, the discharge of effluents containing dyes might cause several problems to the environment [1–3]. The presence of dyes in water bodies can cause devastating harm to aquatic life by hindering chemical oxygen demand and photosynthetic processes and dyes may be toxic or carcinogenic [1–3]. In addition, many dyes are difficult to degrade, as they are generally stable to light, oxidizing agents and they are also resistant to aerobic digestion [1–3].

Several methods of wastewater treatment (biological processes and advanced oxidation processes) have been used for the removal of dyes, however due to their complex molecular structures, many dyes are recalcitrant and are not easily decomposed [4–7]. Therefore, most of these methods show low effectiveness for removing dyes, and have high costs and/or undesirable environmental impacts. In this context, in the last few decades, many studies have reported the use of adsorption methods for the efficient removal of dyes from wastewaters [8–13].

The adsorption method is a common one, and represents a cost-effective approach for solving many problems pertaining to the

* Corresponding author at: Institute of Chemistry, Federal University of Rio Grande do Sul (UFRGS), Av. Bento Gonçalves 9500, Postal Box 15003, ZIP 91501-970, Porto Alegre, RS, Brazil.
E-mail addresses: glaydsonambiental@gmail.com, glaydson.simoes@ufrgs.br (G.S. dos Reis).

http://dx.doi.org/10.1016/j.jece.2017.08.022
Received 10 May 2017; Received in revised form 14 August 2017; Accepted 17 August 2017
Available online 24 August 2017

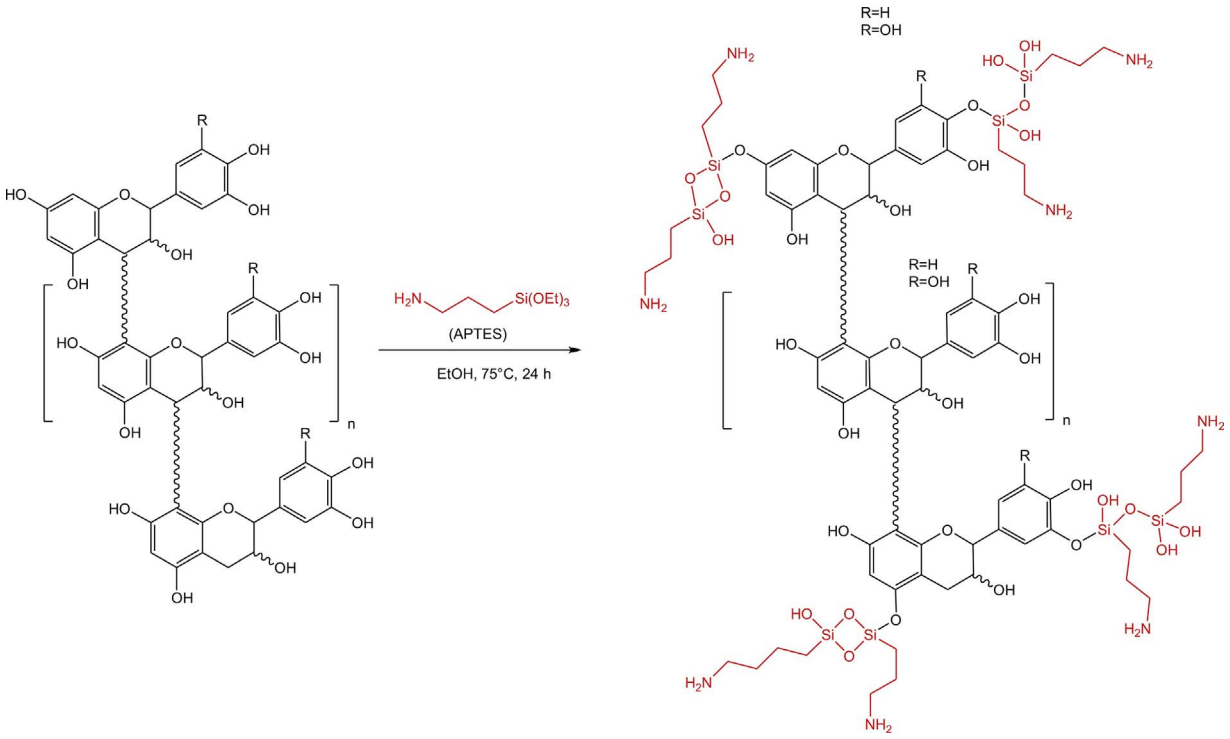

Fig. 1. Proposal of the chemical bond between the tannin and the silica derivative APTES. In this scheme a simplified model was used to represent the complex tannin structure, with random covalent bond between APTES and the tannin portion.

treatment of wastewaters [14]. One advantage of the adsorption methods is that the adsorbents can be regenerated and reutilized which makes the process cheaper [14].

A myriad of adsorbents exist and among the available adsorbents, activated carbons are prevalent, because of their excellent adsorptive characteristics [13,14]. However, in order to prepare activated carbon, it is necessary to perform several steps such as chemical or physical activation using different atmospheres, leaching and washing, which generates a high energy expenditure, resulting in a more expensive process [13,14].

In the last few years, adsorbents based on waste biomass have emerged as low, cost-effective materials for wastewater treatment [7,10,12,15]. The use of biomaterials with no pyrolysis makes the adsorption process very affordable and more environmentally friendly [15]. Among the considerable variety of biomaterials, this paper is focused on the preparation and use of adsorbents of tannin and APTES for the removal of Acid Red 1 dye (AR-1) from aqueous solution.

Tannins are one type of a natural biopolymer composed of polyphenols that form cross-linked precipitable complexes with proteins, and are one of the most abundant classes of compounds on earth behind cellulose, hemicellulose, and lignin [15]. The most common tannin feedstocks are black acacia, mimosa bark, quebracho wood, pine bark and Gambier shoot and leaf [15].

However, tannins are highly hydrophilic and water-soluble materials, which restricts their application to water purification, therefore tannins need to pass through immobilization before being used as adsorbents [15]. To make the tannin immobilized, which means suitable for water purification, it is necessary to perform some kind of surface or structure modifications. Tannins are very easily modified in many ways due to the existence of free hydroxyl groups (-OH) on their surfaces, which can be utilized as points of attachment with functional agents [15].

Up to the best knowledge of the authors, no work has been reported concerning the preparation of hybrid materials combining tannin and APTES and using them as highly efficient adsorbents for removing AR-1 dye. In this way, we present here a novel adsorbent from tannin and *3*-aminopropyltriethoxysilane (APTES). The materials were characterized by several analytical techniques and also were successfully applied as highly efficient adsorbents for AR-1 dye removal from aqueous solutions.

2. Materials and methods

2.1. Chemicals, reagents and solutions

Deionised water was used for the preparation of all solutions. Acid Red 1 (AR-1) (see Supplementary Fig. 1- $C_{18}H_{13}N_3Na_2O_8S_2$, 509.415 g mol^{-1}), was procured from Vetec (São Paulo, SP Brazil) and used without further purification. All solutions were prepared at pH of 2.0. A stock solution, 5000 mg L^{-1}, of AR-1 was prepared, and various diluted solutions for isothermal and experimental kinetic work were prepared from serial dilution of the stock solution. The pH of the adsorbate solutions were adjusted using the Digimed DM-22 pHmeter (Diadema, SP, Brazil) with a 0.10 mol L^{-1} NaOH and/or HCl.

Ethanol was procured from Merck (Rio de Janeiro, Brazil) while 3-aminopropyltriethoxysilane (APTES, 98%) and NH_4OH (28–30% v/v) were furnished by Sigma-Aldrich (São Paulo, Brazil).

Weibull AQ is a light-brown product that is rich in tannin (95–98%) and was obtained from Tanac S.A (Monte Negro, RS, Brazil) in a powder form (particle powder bellow 300 mesh).

2.2. Preparation of hybrid adsorbents

Hybrid adsorbents of tannin and APTES (Tan-Ap-x.x) were prepared by using a basic catalyst (NH_4OH (28–30% v/v)) for the hydrolysis of APTES at pH 10–11 Typically, 5 g of dried tannin was dispersed in 50 mL of ethanol and ammonia solution (100–250 μL). Then, 2.5 g of 3-triethoxysilylpropylamine (APTES, 98%) was added. The mixture was stirred (300 rpm) under reflux for 24 h at 75 °C until the final materials were formed. This procedure allows producing hybrids of tannin and silicate material through a one-step method. The addition of ammonia solution to the mixture leads to the rapid hydrolysis and polymerization

of APTES mixed with tannin (see Fig. 1). Subsequently, the product was dried at 70 °C for 16 h, in a muffle furnace. The material produced in this step is Tan-Ap-0.5. In a similar way, the Tan-Ap-1.0 and Tan-Ap-2.0 samples were prepared, using 5 g of tannin and 5 g of APTES, and 5 g of tannin and 10.0 g of APTES, respectively.

In order to better visualize the interaction between the organic and inorganic moieties, Fig. 1 presents a schema of the chemical bond between the tannin and APTES as a representative interaction between the inorganic part and the organosilicon derivatives presented in this work.

2.3. Characterization of adsorbent materials

The specific surface areas of modified and unmodified tannins were determined by the adsorption of N_2 at 77 K, using a TriStar II 3020 Micromeritics Instrument. The pore-size distribution (PSD) was calculated by the Barrett–Joyner–Halenda (BJH) method. Before measurements, samples were outgassed for 16 h at 120 °C.

Elemental analysis was performed using an elemental analyzer (Perkin Elmer M CHNS/O model 2400). Shortly, 0.05 g oven dried samples were used to determine total carbon, hydrogen and nitrogen. Oxygen (O) mass fraction was determined by subtracting the ash, C, N, and H mass fraction from the total mass of the sample.

The functional groups present on surfaces of the samples was studied using a Fourier Transform Infra-Red (FTIR) spectrometer (Bruker, model alpha) in the range 4000–400 cm^{-1}, using pellets with 0.01 g of samples mixed with 0.1 g of KBr.

The surface morphologies were imaged by using a Scanning Electron Microscope (SEM) Instrument (JEOL microscope, model JSM 6060) connected to a secondary electron detector and Energy Dispersive X-ray Spectroscopy (EDS) for elemental mapping.

For hydrophobic-hydrophilic ratio experiments, 0.3 g of modified and unmodified tannins were oven-dried in 10 mL beakers at 70 °C for 24 h. The samples were cooled in a desiccator before determining their accurate weight. Then the beakers were exposed in a saturated atmosphere with solvent vapor (n-heptane or water) in Erlenmeyer flasks plugged with a ground glass joint, using 60 mL of solvent. The samples were placed in such a way that the 10 mL-beakers were not in contact with the solvent and wall of the Erlenmeyer flask as described elsewhere [16,17]. The experiment was carried out inside of a temperature-regulated chamber at 25 °C. After 24 h, the samples were removed from the Erlenmeyer flasks, dried carefully from the outside with laboratory tissues and weighed again. The vapor amount adsorbed on the samples was obtained by the difference between the final and initial weight of the solid sample and expressed in mg g^{-1}. The hydrophobic-hydrophilic ratio was calculated by the ratio of the amount adsorbed of n-heptane vapor (mg g^{-1}) divided by the amount adsorbed of water-vapor (mg g^{-1}) [16,17].

Diffuse reflectance ultraviolet-visible (DRUV) was obtained on a Shimadzu UV-2450 spectrophotometer using an ISR-2200 Integrating Sphere Attachment at 25 °C in a spectral range of 200–800 nm. The baseline was obtained using $BaSO_4$ (Wako Pure Chemical Industries, Ltd.). In these experiments, the samples were treated as powder. Physical mixtures of equal amounts of APTES and Tannin than those used to prepare the hybrid materials (w/w) was also investigated for comparison.

2.4. Batch adsorption studies

Aliquots of 20.00 mL of 100.00–2500.0 mg L^{-1} (initial pH ranging from 2.0 to 8.0) of AR-1 were added to 50.0 mL Falcon flat tubes containing 30 mg of adsorbent materials. The flasks were capped, and placed horizontally in a shaker with a rigorous controlled temperature system (precision of 0.1 °C) furnished by Oxylab (RS, Brazil), and the system was agitated between 5 min to 24 h. Afterwards, to separate the adsorbents from the aqueous solutions, the flasks were centrifuged using a Fanem centrifuge, and aliquots of 1–5 mL the supernatant were properly diluted to 10.0–100.0 mL in calibrated flasks using a suitable blank solution (pH ranging from 2.0 to 8.0).

The residual solutions of AR-1 after adsorption were quantified using UV–vis spectrophotometer (T90+ UV–vis spectrophotometer, PG Instruments, London, United Kingdom) at a maximum wavelength of 531.5 nm.

The amount of AR-1 adsorbed by the tannin adsorbents and the percentage of removal were calculated using Eqs. (1) and (2), respectively:

$$q = \frac{(C_o - C_f)}{m}.V \tag{1}$$

$$\%Removal = 100.\frac{(C_o - C_f)}{C_o} \tag{2}$$

Where q is the amount of AR-1 uptake by the absorbent (mg g^{-1}), C_o is the initial AR-1 concentration put in contact with the adsorbent (mg L^{-1}), C_f is the AR-1 concentration (mg L^{-1}) after the batch adsorption experiment, V is the volume of AR-1 solutions (L) put in contact with the adsorbent, and m is the mass (g) of adsorbents.

The experiments of desorption were carried out according to the procedure: a 200.0 mg L^{-1} of AR-1 dye was shaken with 30.0 mg of each adsorbent for 1 h. Then, the loaded adsorbents were filtered in 0.7 μm Millipore® glass-fiber filters and they were firstly washed with water for removing non-adsorbed dye. Then, the dye adsorbed on the adsorbents were agitated with 20.0 mL of: ethanol; acetone; NaOH aqueous solutions (0.25- 2.0 mol L^{-1}); and mixture of 1 V acetone + 1 V NaOH (0.25-2.0 mol L^{-1}) for 15–60 min. The desorbed dye was separated and estimated as described above.

2.5. Quality assurance and statistical evaluation of models

All of the experiments were carried out in triplicate to ensure reproducibility, reliability and accuracy of data. The relative standard deviations of all measurements were < 5%. Blanks were run in parallel and corrected when necessary [18].

The solutions of AR-1 were stored in glass bottles, which were cleaned by immersing in 1.4 mol L^{-1} HNO_3 for 24 h [19], rinsing with deionized water, drying and keeping them in cabinets.

Standard AR-1 solutions (between 2.00–20.0 mg L^{-1}), in parallel with a blank (pH 2.0 aqueous solution), were used for linear analytical calibration. The calibration curve was performed on the UV-Win software of the T90+ PG Instruments spectrophotometer. All of the analytical measurements were repeated thrice, and the precisions of the standards were better than 3.2% (n = 3). The detection limit of the dye was 0.11 mg L^{-1} with a signal/noise ratio of 3 [20]. The standard AR-1 solution (10.0 mg L^{-1}) was used as quality control after every five measurements to ensure accuracy of the solutions [21].

Nonlinear methods with successive interactions were calculated by Simplex method and also by the Levenberg–Marquardt algorithm based on the non-linear fitting facilities of the Microcal Origin 2015 software, and they were used to fit the kinetic and equilibrium data. A determination coefficient (R^2), an adjusted determination coefficient (R^2_{adj}) and the standard deviation of the residue (*SD*) were employed to analyze the suitability of the models [22].

Residual standard deviation measures the difference between the theoretical and experimental amounts of AR-1 removed from solutions. The R^2, R^2_{adj} and *SD* are given in Eqs (3), (4) and (5), respectively [22].

$$R^2 = \left(\frac{\Sigma_i^n (q_{i,exp} - \bar{q}_{i,exp})^2 - \Sigma_i^n (q_{i,exp} - q_{i,model})^2}{\Sigma_i^n (q_{i,exp} - \bar{q}_{i,exp})^2}\right) \tag{3}$$

$$R^2_{adj} = 1-(1-R^2).\left(\frac{n-1}{n-p-1}\right) \tag{4}$$

$$SD = \sqrt{\left(\frac{1}{n-p}\right)\cdot\sum_{i}^{n}(qi,\ exp - qi,\ model)^2} \quad (5)$$

In these equations, $q_{i,model}$ represents the individual theoretical q value predicted by the model; $q_{i,exp}$ represents each individual experimental q value; $\overline{q}_{exp}$is the average of the experimental q values; n represents the number of experiments; p represents the number of parameters in the model [22].

2.6. Kinetic models

Pseudo-first order, pseudo second-order, general order kinetic and intra-particle diffusion models were used to analyze the kinetic data [22]. The mathematical representations of respective models are shown in Eqs. (6)–(9).

$$q_t = q_e\cdot[1-exp(-k_1\cdot t)] \quad (6)$$

$$q_t = \frac{q_e^2 k_2 t}{[k_2(q_e)\cdot t + 1]} \quad (7)$$

$$q_t = q_e - \frac{q_e}{[k_N(q_e)^{n-1}\cdot t\cdot(n-1)+1]^{1/1-n}} \quad (8)$$

$$q_t = k_{id}\sqrt{t} + C \quad (9)$$

2.7. Equilibrium models

Eqs. (10)–(12) represent respectively the Langmuir, Freundlich and Liu isotherm models [22]. These models were used for analysis of the equilibrium data.

$$q_e = \frac{Q_{max}\cdot K_L\cdot C_e}{1 + K_L\cdot C_e} \quad (10)$$

$$q_e = K_F\cdot C_e^{1/n_F} \quad (11)$$

$$q_e = \frac{Q_{max}\cdot(K_g\cdot C_e)^{n_L}}{1 + (K_g\cdot C_e)^{n_L}} \quad (12)$$

Where C_e is the supernatant concentration at the equilibrium (mg L^{-1}); K_L is the Langmuir equilibrium constant (L mg^{-1}); Q_{max} is the maximum adsorption capacity (mg g^{-1}); K_F is the Freundlich equilibrium constant [mg g^{-1} (mg $L^{-1})^{-1/n}$]; n_F is the Freundlich exponent (dimensionless); K_g is the Liu equilibrium constant (L mg^{-1}) and n_L is the dimensionless exponent of the Liu equation.

2.8. Simulated effluents

The synthetic effluents were prepared by mixing several dyes with other organic compounds and some inorganic salts, which are commonly presented in real industrial effluents [23]. Two different effluents were made with different concentrations, which are presented as the effluents shown in Table 1. The effluents were prepared at pH 2.0. The aim of using simulated effluents is to test the performance of adsorbents for the treatment of industrial effluents from dyeing houses.

3. Results and discussion

3.1. Textural characteristics

Textural parameters of raw and modified tannins are listed in Table 2. Tannin adsorbents presented low specific surface areas despite the APTES ratio used for the tannin material preparation (see Table 2). Raw tannin showed the lowest S_{BET}, equal to 1.86 $m^2\ g^{-1}$, and total pore volume of 0.0042 $cm^3\ g^{-1}$. The small porosity data is in agreement with those data observed in literature [17]. After modification with APTES, the porosities of tannin materials had a very small increase, however the values kept very low (see Table 2).

Porosity is not the only parameter that determines whether a material could be successfully employed for scavenging pollutants from aqueous solutions and effluents. The morphologies and functionalities of their surfaces also might play an important role on such application.

Supplementary Fig. 2 shows SEM micrographs of tannin adsorbents before (A) and after modification by APTES (B, C and D). Remarkable differences in the morphologies of the materials were observed, mainly among the structure of pure tannin and tannin-APTES hybrid materials. It can be seen that the sample of pure tannin shows a fibrous and uncompact surface. After the modification step, adding APTES under different ratios, the surface became compact [24,25]. Supplementary Fig. 2 reveals that the pure tannin was fully modified after combination with APTES, which might indicate that the silicate material formed during the sol-gel method should have encapsulated the tannin material, as represented in Fig. 1.

TEM micrographs of the unmodified and modified materials are displayed in Supplementary Fig. 3. As was noted in the SEM images, remarkable differences in the morphologies of the unmodified and modified materials were also confirmed by the TEM images. The pristine form of tannin (see Supplementary Fig. 3A) is revealed by a round structure, while the hybrid materials possess aggregate structures, suggesting that indeed the tannin was encapsulated by the silicate material.

3.2. Elemental analysis

Elemental analysis (CHNS) was used to analyze the major elemental concentrations (in percentage atomic concentration) of the raw material and the modified tannin-APTES. The percentages of carbon, nitrogen, sulphur and hydrogen were determined. As expected pure tannin showed the highest carbon and lowest nitrogen contents, these results are expected because as APTES is added, the content of silicon and nitrogen increases, while the carbon content decreases (see

Table 1
Chemical composition of the synthetic effluents.

Dyes	λ_{max} (nm)	Concentration (mg L^{-1})	
		Effluent A	Effluent B
Acid Red 1	531.5	40.00	80.00
Procion Blue MX-R	594.0	10.00	20.00
Reactive Black 5	597.5	10.00	20.00
Cibacron Brilliant Yellow 3G-P	402.0	10.00	20.00
Reactive Orange 16	493.0	10.00	20.00
Other compounds			
NaCl		20.00	40.00
Na_2CO_3		20.00	40.00
CH_3COONa		20.00	40.00
Na_3PO_4		20.00	40.00
KNO_3		20.00	40.00
Humic Acid		10.00	20.00
Sodium Dodecyl Sulfate		10.00	20.00
Na_2SO_4		10.00	20.00
NH_4Cl		10.00	20.00
pH[a]		2.0	2.0

[a] pH of solution was adjusted with 0.1 mol L^{-1} NaOH and/or HCl.

Table 2
Textural properties of modified tannin adsorbents.

Sample	BET surface area ($m^2\ g^{-1}$)	Total pore volume ($cm^3\ g^{-1}$)	Pore Diameter (A)
Tan.Ap-0.5	9.53 ± 2.1	0.0288 ± 0.0012	108 ± 11
Tan.Ap-1.0	7.89 ± 2.3	0.0273 ± 0.0013	100 ± 10
Tan.Ap-2.0	8.67 ± 2.2	0.0302 ± 0.0010	114 ± 12

Table 3
Elemental analysis and hydrophobicity index (HI).

Amostras	C (%)	H (%)	N (%)	S (%)	Silane group inserted (mmol g^{-1}) [a]	HI [b]
tannin	49.98	5.842	0.4400	0.1299	–	0.1818
Tan.Ap-0.5	45.79	6.007	2.838	0.1110	1.71	0.4844
Tan.Ap-1.0	41.44	6.128	4.164	0.1033	2.66	0.6704
Tan.Ap-2.0	39.61	6.567	5.301	0.1158	3.47	0.5809

[a] For the silane group insertion, it was considered that SiC_3H_8N was inserted in the tannin matrix. Calculations were based on N content increased.

[b] HI- amount adsorbed of vapor of n-heptane (mg g^{-1}) divided by amount adsorbed of vapor of water (mg g^{-1}).

Table 3). As seen in the table, the carbon content of the samples decreased from 49.98% to 39.61% and nitrogen increased from 0.4400% to 5.301%, these results might cause great influences on the surface functionalities of the materials, which might reflect on their abilities for up taking the AR-1 dye in aqueous solutions. Based on the percentage of increase of N in the adsorbents Tan.Ap-0.5, Tan.Ap-1.0 and Tan.Ap-2.0, the amount of silane group inserted in the tannin matrix was calculated, and these values were 1.71, 2.66 and 3.47 mmol g^{-1} respectively. In these calculations, it was considered that the SiC_3H_8N group was inserted into the matrix of tannin, as depicted on Fig. 1.

3.3. FTIR

The FTIR analysis gives valuable information about the presence of chemical functional groups on the surface of any material. Fig. 2 shows functional groups present on the surface of the tannin adsorbent materials.

Fig. 2 provides the spectra of pure tannin (Fig. 2A) and modified tannin such as Tan-Ap-0.5 (Fig. 2B), Tan-Ap-1.0 (Fig. 2C), and Tan-Ap-2.0 (Fig. 2D). It seems that the pure tannin presents more bands in the regions from 400 to 1800 cm^{-1} compared with other modified materials (see Fig. 2). The main groups found in pure tannin are: the broad peak at 3395 cm^{-1}, due to stretching vibrations of O—H groups of phenolic compounds [12,14,26]; the band at 2924 cm^{-1} that can be assigned to C—H stretching vibrations; the band at 1616 cm^{-1}, which can be assigned to carboxyl group (HO—C═O) [10,12,26]; C—O stretching vibration at 1028 cm^{-1}; the vibration at 1198 cm^{-1} could be assigned to C—O—C stretching of ethers present in the tannin [10,14]; the bands at 1505, 1451 could be assigned to asymmetric carboxylate stretch and aromatic ring mode; the band at 1340 [10,26], could be assigned to CH_2 bending [12,14,26], and the band at and 1235 cm^{-1} could be assigned to C—O stretch of phenol [10,26]. And the band at 837 cm^{-1} could be assigned to out of plane C—H bends [10,12,26].

The Tan-Ap-0.5, Tan-Ap-1.0 and Tan-Ap-2.0 samples present basically the same FTIR bands with some shifts. For O—H, stretching the bands of Tan-Ap-0.5, Tan-Ap-1.0 and Tan-Ap-2.0 are 3410, 3419 and 3414 cm^{-1}, respectively [12,14,26]. Comparing with the O—H band of original tannin that was 3395 cm^{-1}, it could be concluded that a band shift of 15, 24, and 19 cm^{-1}, respectively for Tan-Ap-0.5, Tan-Ap-1.0 and Tan-Ap-2.0 was observed. This result indicates that O—H band of phenol should be forming a chemical bond with APTES as depicted on Fig. 1. The bands at 1617, 1620 and 1617 cm^{-1} can be assigned to the carbonyl group (C═O) of carboxylic acid [10,12,26]. When compared with the pure tannin, this band was 1616 cm^{-1}. Considering the resolution of the spectra of 4 cm^{-1}, any band shift lower than 10–12 cm^{-1} (3 times the resolution of the spectra) could not be considered a remarkable shift of chemical bond [10,12,26]. The small

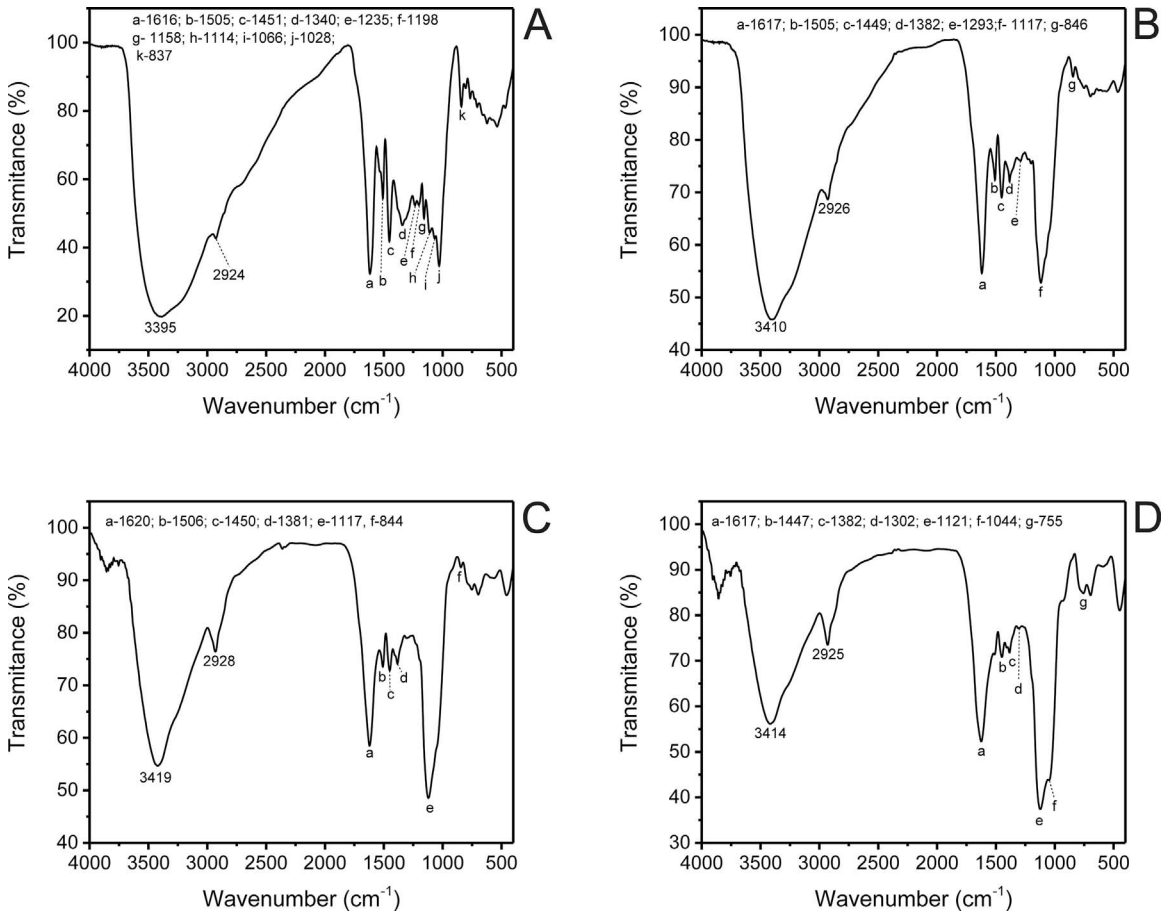

Fig. 2. FTIR of A: tannin; B: Tan-Ap-0.5; C: Tan-Ap-1.0; D: Tan-Ap-2.0.

bands at 1505 and 1449, 1506 and 1450, and 1447 cm^{-1} could be assigned to ring modes of aromatics of the Tan-Ap-0.5, Tan-Ap-1.0 and Tan-Ap-2.0 samples, respectively [10,12,26]; the bands at 1382, 1381 and 1382 cm^{-1}, could be assigned to bending of C—H, bonds of the Tan-Ap-0.5, Tan-Ap-1.0 and Tan-Ap-2.0 samples, respectively [10,12,26]. The bands at 1117, 1117 and 1044, could be assigned to asymmetric C—O—C ether and O—C—C of aromatic ester; C—O of phenol of the tannins present in the Tan-Ap-0.5, Tan-Ap-1.0 and Tan-Ap-2.0 could also be assigned to Si-O-Si groups present in the chemically modified materials [3]. It should be stressed that the band at 1235 cm^{-1} of the tannin that could be assigned to C—O stretch of phenol had disappeared of the spectra of Tan-Ap-0.5, Tan-Ap-1.0 and Tan-Ap-2.0, indicating that the formation of the chemical bond of APTES with the tannin should take place, as depicted on Fig. 1. Finally, the bands at 846, 844 and 755 cm^{-1}, are assigned to out of plane C—H bends [10,12,26], of Tan-Ap-0.5, Tan-Ap-1.0 and Tan-Ap-2.0, respectively.

3.4. Hydrophobicity-hydrophilicity ratio

The hydrophobicity-hydrophilicity ratio (HI) is defined as the amount of adsorbed vapor of n-heptane (mg g^{-1}) divided by the amount adsorbed of vapor of water (mg g^{-1}) [15]. The HI values of the tannin materials are presented in Table 3. The results demonstrate that all samples present HI ratios lower than 1, which means that the tannin materials have high affinity for water, and therefore are hydrophilic materials. These results can be attributed to the presence of a huge amount of hydroxyl (—OH) groups, which can easily be bonded to H_2O molecules [15,16]. The hydrophilicity of tannin materials might facilitate their better dispersion in aqueous media, which can indicate the possibility of enhancing the ability of the tannin materials for scavenging AR-1 dye by the adsorption process.

It was also observed that pure tannin presents lower HI values, and as APTES was incorporated in the material, the HI value was increased for Tan-Ap-0.5 and Tan-Ap-1.0. However, for Tan-Ap-2.0 the value of HI was slightly decreased in relation to Tan-Ap-1.0. The incorporation of APTES on the material increased the amount of n-propyl group of the APTES, which is aliphatic and presents higher hydrophobicity than the tannin material. However, all values of HI of all the material listed on Table 3, still remain below 1.00

3.5. Photophysical characterization in the solid state

The diffuse reflectance UV–vis spectroscopy (DRUV) was applied in order to evaluate the electronic properties of the obtained materials in comparison with the tannin and APTES precursors, as well as their physical mixtures. Fig. 3 depicts the DRUV spectra of the final materials (left) and their physical mixtures (right), where changes could be observed. Both spectra indicate increase on the absorption intensity in the visible region due to the tannin contribution, mainly located at higher wavelengths. In this region, the silyl derivative APTES presents an almost absent absorption. A higher amount of the APTES on the hybrid leads to a lower absorption intensity at around 300 nm. On the other hand, the lower amount of APTES allow a higher intensity in this region of the spectrum, similar to that observed for pure tannin. It is well-know that the absorption region around 300 nm is related to π-π* electronic transition, which are typical for phenolic compounds present in the tannin structure [27,28]. Thus, the preliminary results indicate the formation of a hybrid material, as already reported in the literature to materials prepared using silica and tannin [25]. In this case, the silyl derivative probably bound to the phenolic structure of the tannin, specifically to the phenolic hydroxyl, as proposed in Scheme 1. In addition, it can be observed that the higher tannin:APTES ratio (2.0:1.0) seems does not affect at all the electronic properties of the final hybrid material in comparison with the ratio 1.0:1.0. These hybrid materials, as well as the pure tannin presented almost constant absorption intensities below 300 nm. On the other hand, in the prepared physical mixtures, the absorption intensities in the visible region increases increasing the tannin amount, as expected. Furthermore, all studied physical mixtures presented similar absorption intensities below 300 nm. By analyzing this Fig. 3, is possible to check that the hybrid materials are different from the simple physical mixture of tannin and APTES, concluding that a covalent chemical bond between the tanning and APTES occurred, as depicted on Fig. 1.

3.6. Effect of the acidity of the AR-1 solution

The suitable pH of a dye for being adsorbed depends on its interaction with the adsorbent. Therefore, the pH of the solution is one of the influential factors affecting the adsorption of a dye on an adsorbent [3,10–14,23]. For this study, pH values in the range of 2 and 8 were investigated for the removal of AR-1 from aqueous solutions (250 mg L^{-1}) using Tan-AP adsorbents (see Fig. 4). Analysing this figure, it is seen that the maximum percentage of removal occurred at pH 2.0 for all the adsorbents. Using the Tan-Ap-0.5, the percentage of removal of AR-1 dye decreased from 91.5% (pH 2) to 28.5 (pH 8); for Tan-Ap-1.0 the percentage of dye removal decreased from 91.1% (pH 2) to 25.6% (pH 8); and finally, for Tan-Ap-2.0, the percentage of AR-1 dye removal decreased from 68.5% to 16.5%. This behaviour of the effect of initial pH of the dye solution is compatible with a mechanism of electrostatic attraction of negatively charged dye (see Supplementary Fig. 1) even at pH 2.0, because the pK_a values of the sulfonic acids present in the structure of the dye are −2.25 and −2.99, and the positively protonated amino group of APTES at pH 2.0, as already reported in the literature [29]. Further kinetic, equilibrium and thermodynamic data will confirm this mechanism of adsorption.

Another important observation in these data, is that the sorption capacity of Tan-Ap-2.0 is lower than Tan-Ap-0.5 and Tan-Ap-1.0, however in all tested adsorbents, the maximum removal occurred when the initial pH of adsorbate solution was kept at 2.0, showing that the mechanism of adsorption should follow an electrostatic mechanism [29].

3.7. Kinetic studies

The kinetic curves and fitting parameters are displayed in Supplementary Fig. 4 (Tan-Ap-0.5), Supplementary Fig. 5 (Tan-Ap-1.0) and Supplementary Fig. 6 (Tan-Ap-2.0) and Table 4.

The suitability of the models was analysed using the values of adjusted determination coefficient (R^2_{Adj}) standard deviation of residues (*SD*) [3,22,26,30]. Lower SD and higher R^2_{Adj} values mean smaller differences between theoretical and experimental q values. Therefore, between the studied models, the general-order kinetic model presented the lowest *SD* (varying from 0.2946 to 0.9547) and highest R^2_{Adj} values were 0.9999 for all tannin-APTES adsorbents (see Table 4). In this context, it is noted that the q_e values of the general order kinetic model are closer to the experimental q_e values when compared to other kinetic adsorption models. These results indicate that the general order kinetic model best explains the adsorption process of AR-1 dye using tannin-APTES adsorbents.

Considering that the general order kinetic equation presents different values for n (order of adsorption rate) when the concentration of the AR-1 dye is changed, it is difficult to compare the kinetic parameters of the model. In this regard, $t_{1/2}$ and $t_{0.95}$ were used to compare the kinetics of AR-1 dye removal onto the adsorbents, where $t_{1/2,}$ was defined as the time to achieve half of saturation (q_e) in the kinetic results, $t_{0.95}$ was the time to achieve 95% of the saturation (q_e) [31].

It should be highlighted that the kinetics of adsorption of AR-1 dye on Tan-Ap-0.5, Tan-Ap-1.0 and Tan-Ap-2.0 was moderate when compared with removal of other adsorbates in activated carbons [31,32]. The calculated $t_{1/2}$ values from the general order kinetic model were 0.9237 and 0.8975 h for Tan-Ap-0.5, which corresponds to an average

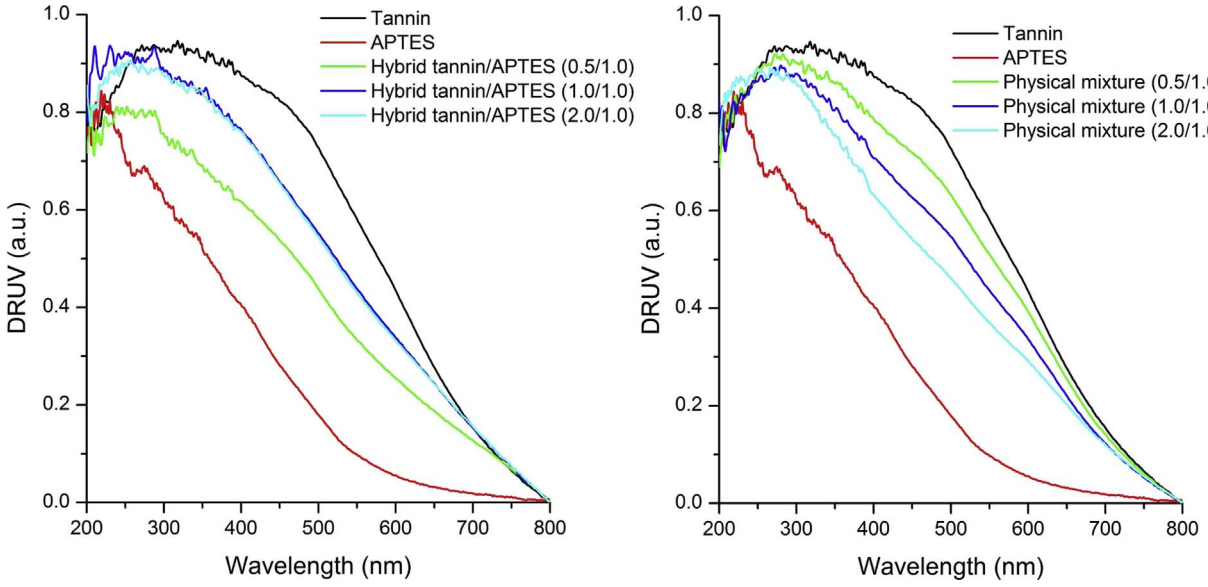

Fig. 3. Diffuse reflectance UV–vis (DRUV) absorption of (left) hybrid materials prepared from APTES and tannin and (right) physical mixture of both at same tannin/APTES proportion (w/w).

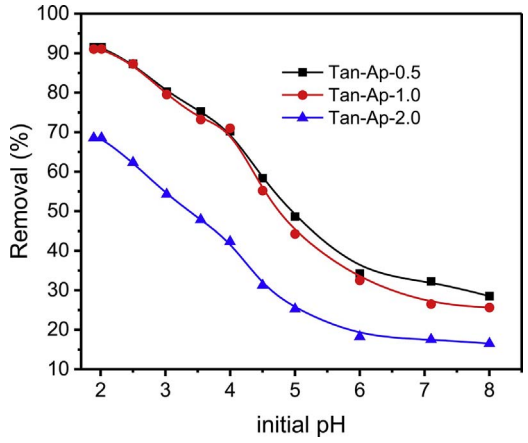

Fig. 4. Effect of initial pH of AR-1 solution on its percentage of removal. Temperature 25 °C, mass of adsorbent 30.0 mg, time of contact 24 h.

of 54.6 min; 1.414 and 1.326 h for Tan-Ap-1.0 which corresponds to an average of 81.8 min; and 1.231 and 1.147 h for Tan-Ap-2.0, which corresponds to an average of 71.4 min. Recently published $t_{1/2}$ values have been reported as lower than 8.2 min [31] for adsorption of phenol onto wood chips activated carbons, also $t_{1/2}$ values lower than 6 and 1.8 min for adsorption of amoxicillin and paracetamol, respectively, using magnetic activated carbons [32], confirming that the kinetics of adsorption of AR-1 dye onto the adsorbents was moderate, when compared with other systems adsorbates/adsorbents.

Another valuable information obtained in Table 4 is the $t_{0.95}$, which gives an idea of the minimum time of contact between the adsorbate and adsorbent to attain equilibrium, making an average value of the two values reported on Table 4, the $t_{0.95}$ values for adsorption of AR-1 dye onto Tan-Ap-0.5, Tan-Ap-1.0 and Tan-Ap-2.0, were respectively, 9.63, 13.45 and 14.45 h. In the subsequent experiments, the time of equilibrium established for the adsorption equilibrium was fixed at 12, 16 and 18 h, for the adsorption of AR-1 dye, onto Tan-Ap-0.5, Tan-Ap-1.0 and Tan-Ap-2.0, respectively. This increase in the time of contact is to guarantee that in any concentration of the adsorbate, the time of contact will be enough to attain the equilibrium [32,33].

3.8. Equilibrium studies

The isotherms of adsorption of AR-1 on Tan-Ap-0.5, Tan-Ap-1.0 and Tan-Ap-2.0 adsorbents were performed using the following experimental conditions: pH 2.0, mass adsorbent dosage of 1.5 g/L, temperature was varied from 25 °C to 50 °C, and the time of equilibrium established for the adsorption equilibrium was fixed at 12, 16 and 18 h, for the adsorption of AR-1 dye, onto Tan-Ap-0.5, Tan-Ap-1.0 and Tan-Ap-2.0, respectively.

The isotherm curves are shown in Supplementary Fig. 7 (Tan-Ap-0.5), Supplementary Fig. 8 (Tan-Ap-1.0) and Supplementary Fig. 9 (Tan-Ap-2.0) with their fitting parameters in Table 5. On the basis of R^2_{Adj} and SD values (see Table 5), the Liu model is the best isotherm model for adsorption of AR-1 onto the three adsorbents. The Liu model presented the highest R^2_{Adj} and lowest values for *SD*, which means that the values of q calculated by the isotherm model were similar to the q measured experimentally [3,10,11,22].

Comparing the three tannin-Aptes adsorbents it was found that Tan-Ap-2.0 was the adsorbent with generally the lowest sorption capacity at all of the six temperatures studied. On the other hand, for Tan-Ap-0.5 and Tan-Ap-1.0, the behaviour was anomalous. For the 25°–35 °C interval the Tan-Ap-0.5 presented a slightly higher maximum sorption capacity (0.98%–7.00%) than Tan-Ap-1.0. Otherwise for the interval of 40°–50 °C occurred the opposite, the Q_{max} values of Tan-Ap-0.5 were 2.35%–19.29% lower when compared with Tan-Ap-1.0 for adsorption of AR-1 dye.

So far, there have been a few adsorbents reported for the adsorption of AR-1 dye. The maximum adsorption capacities AR-1 dye onto different kinds of adsorbents are listed in Table 6. As shown in Table 6, the three adsorbents studied present very good Q_{max} values compared with several of those presented in Table 6 [34–40].

Considering that the authors have optimized the best conditions for obtaining a maximum value of Q_{max}, the adsorbent Tan-Ap-0.5, Tan-Ap-1.0, and Tan-Ap-2.0 could be ranked as 3°, 2° and 5°, respectively, in relation to the value of the Q_{max} of the 14 adsorbents presented in Table 6. Therefore, these tannin-APTES adsorbents could be classified as very good adsorbents for the removal of AR-1 dye from aqueous solutions.

Table 4
Kinetic fitting parameters for adsorption of AR-1 onto Tan-Ap-0.5, Tan-Ap-1.0 and Tan-Ap-2.0 adsorbents. All values are expressed with four significant digits. Conditions initial pH of adsorbate 2.0, initial concentrations of 250.0 and 500.0 mg L^{-1}, adsorbent mass of 30 mg.

	Tan-Ap-0.5		Tan-Ap-1.0		Tan-Ap-2.0	
C_0 (mg L^{-1})	250.0	500.0	250.0	500.0	250.0	500.0
Pseudo-first order						
k_f (min^{-1})	0.7558	0.7750	0.5003	0.5311	0.5817	0.6204
q_e (mg g^{-1})	142.2	180.5	141.5	175.6	101.2	113.0
R^2 adjusted	0.9914	0.9921	0.9946	0.9941	0.9916	0.9913
SD (mg g^{-1})	4.939	5.995	4.059	5.233	3.560	4.011
$t_{1/2}$ (h)	0.9171	0.8944	1.385	1.305	1.192	1.117
Pseudo-second order						
k_s (g mg^{-1} min^{-1})	0.006551	0.005303	0.004046	0.003512	0.006807	0.006577
q_e (mg g^{-1})	155.5	197.1	158.6	195.9	112.3	124.9
R^2 adjusted	0.9989	0.9989	0.9991	0.9991	0.9995	0.9995
SD (mg g^{-1})	1.784	2.198	1.626	2.040	0.8526	0.9730
$t_{1/2}$ (h)	0.9816	0.9569	1.559	1.453	1.309	1.218
General-order						
k_N [h^{-1} (g $mg^{-1})^{n-1}$]	0.03402	0.03465	0.03011	0.02724	0.02283	0.02341
q_e (mg g^{-1})	149.6	189.1	149.8	185.6	108.4	120.6
n	1.666	1.636	1.600	1.607	1.741	1.734
R^2 adjusted	0.9997	0.9999	0.9999	0.9999	0.9999	0.9999
SD (mg g^{-1})	0.9547	0.3530	0.2946	0.3518	0.4359	0.4358
$t_{1/2}$ (h)	0.9237	0.8975	1.414	1.326	1.231	1.147
$t_{0.95}$ (h)	9.996	9.265	13.80	13.09	15.05	13.85

3.9. Thermodynamic study, desorption and mechanism of adsorption

Thermodynamic studies for the adsorption of AR-1 onto tannin adsorbents were carried out in the temperature range of 25–50 °C (298 to 323 K). Calculated thermodynamic parameters for the adsorption of AR-1 onto tannin adsorbents are shown in Table 7, and these calculations were made according with the literature [3,10–14,22,26,30–32]. The R^2_{adj} values of the plots are > 0.99, which indicates the reliability of the values of ΔH° and ΔS° calculated.

Under the temperature range studied, the calculated Gibbs's free energy, (ΔG°), and standard entropy (ΔS°) presented negative and positive values, respectively, which confirms that the sorption process is spontaneous and favourable, and a decrease in the organization of the system was obtained, this should be due to release of water molecules before the AR-1 dye adsorbed on the surface of the adsorbent [41,42].

The ΔG° is an important parameter for explaining the thermodynamic process of adsorption with regards to the spontaneity of the adsorption process; a higher negative value of ΔG° indicates a more energetically favourable adsorption. The adsorptive process will occur favourably and spontaneously at a given temperature if ΔG° exhibits a negative value [22,29,31,32,41].

The positive value of the standard entropy, ΔS°, suggests an increase of the randomness of the adsorption process at the solid/solution interface during the uptake of AR-1 dye molecules onto tannin adsorbent surfaces and reflects the affinity of the tannin adsorbents for adsorbing AR-1 dye [22,29,41].

Changes in enthalpy (ΔH°) for all adsorbents were negative, which indicates the exothermic nature of the adsorption process [29]. The magnitude of enthalpy of AR-1 dye onto Tan-Ap-0.5, Tan-Ap-1.0 and Tan-Ap-2.0 corresponds to a physical adsorption process [42], since íts values is < 40 kJ mol^{-1} [43].

As was seen thus far, the tannin materials presented poor porosities which in a certain way could enable the application of these materials in the adsorption process. However, based on surface characterization, and adsorption data it was determined that the electrostatic attraction and hydrogen bonds have played an important role in the adsorption process through interactions between tannin materials and AR-1 dye. This statement is supported also by thermodynamics with the magnitude of ΔH° [43].

In order to check the reuse of the hybrid adsorbents for the adsorption of AR-1 dye, desorption experiments were carried-out. Several eluents such as, ethanol; acetone; NaOH aqueous solutions (0.25–2.0 mol L^{-1}); and mixture of 1 V acetone + 1 V NaOH (0.25–2.0 mol L^{-1}) were tested for regeneration of the loaded adsorbent (see Table 8). For all tested adsorbents, the mixture of acetone + aqueous solutions of NaOH (0.75–2.0 mol L^{-1}) were efficient to desorb the dye uptaken by the adsorbents, on the other hand, the recoveries of the adsorbent using aqueous NaOH of different concentrations as regenerating solutions occurred from about 1% to 65% after 1 h of agitation. The organic solvents such as ethanol, acetone alone was also not so efficient for the dye desorption from the hybrid adsorbents (recoveries < 70%). The best elution efficiency was obtained with the mixture 1V of acetone + 1V of 0.75–2.0 mol L^{-1} NaOH. This result confirms the FTIR results and the pH studies described above. The AR-1 dye at pH 2.0 is attracted electrostatically by the hybrid adsorbents. This interaction was corrupted with the NaOH solution. However, besides this electrostatic interaction, there are also some interactions between the aromatic groups present on the adsorbents with the aromatic rings of the dye. For breaking this interaction, it was required acetone to improve the elution efficiency (which attained up to 97.85% with the mixture acetone + 2.0 mol L^{-1} NaOH). In addition, the hybrid adsorbent eluted with the mixture acetone + 0.75–2.0 mol L^{-1} were reutilized for the adsorption of the AR-1 dye, attaining a sorption efficiency of about 75% in the second cycle, 65% in the third cycle of adsorption/desorption when compared with the first cycle of adsorption/desorption. Therefore, the use of hybrid tannin-APTES adsorbent for dye adsorption could be economically viable since it allows its regeneration.

The mechanism of adsorption should follow the steps (see Fig. 5): step 1 under acid conditions (pH = 2.0), the amino group of the silicate are protonated, becoming positively charged [10,29]; in step 2 the positively charged adsorbent material attracts, electrostatically, the negatively charged AR-1 dye (sulfonic groups of AR-1 dye present pK_a values of −2.25 and −2.99), see Supplementary Fig. 1). This type of interaction was thoroughly presented for adsorption of different anionic dyes using different adsorbents [10–14,23,30,31]. Besides of electrostatic attraction, also hydrogen bond could be formed with the keto-amide, azo groups of the dye with the hydroxyl groups of the tannin. This second interaction also could take place and contribute to overall adsorption of AR-1 adsorption onto Tannin-APTES adsorbents.

Table 5
Langmuir, Freundlich and Liu isotherm parameters for the adsorption of AR-1 onto Tannin-APTES adsorbents.

	Tan-Ap-0.5					
	25 °C	30 °C	35 °C	40 °C	45 °C	50 °C
Langmuir						
Q_{max} (mg g^{-1})	202.1	224.7	248.9	280.2	298.5	283.4
K_L (L mg^{-1})	0.3002	0.3482	0.2384	0.2486	0.2154	0.3845
R^2_{adj}	0.9682	0.9727	0.9881	0.9999	0.9866	0.9402
SD (mg g^{-1})	11.64	12.23	7.618	0.7913	10.75	21.01
Freudlich						
K_F (mg g^{-1} (mg L^{-1})$^{-1/nF}$)	102.7	112.2	144.4	146.4	148.7	148.4
n_F	10.14	9.587	12.60	10.38	9.792	10.17
R^2_{adj}	0.9421	0.9225	0.9670	0.8641	0.9249	0.9796
SD (mg g^{-1})	15.70	20.61	12.69	32.83	25.40	12.26
Liu						
Q_{max} (mg g^{-1})	216.6	236.5	258.4	282.3	308.8	337.6
K_g (L mg^{-1})	0.3944	0.3399	0.2922	0.2497	0.2140	0.1859
n_L	0.4607	0.5737	0.6071	0.9732	0.6743	0.3587
R^2_{adj}	0.9999	0.9999	0.99997	0.9999	0.9999	0.9999
SD (mg g^{-1})	0.5775	0.2431	0.3843	0.3727	0.5613	0.3708
	Tan-Ap-1.0					
	25 °C	30 °C	35 °C	40 °C	45 °C	50 °C
Langmuir						
Q_{max} (mg g^{-1})	193.5	219.1	205.7	283.6	342.2	354.5
K_L (L mg^{-1})	0.4345	0.3313	0.4361	0.2548	0.2268	0.2778
R^2_{adj}	0.9496	0.9894	0.9413	0.9946	0.9959	0.9428
SD (mg g^{-1})	12.62	7.016	14.35	6.5690	7.014	24.95
Freudlich						
K_F (mg g^{-1} (mg L^{-1})$^{-1/nF}$)	112.6	123.4	118.8	144.7	161.6	188.4
n_F	12.37	11.80	11.90	9.902	9.021	10.41
R^2_{adj}	0.9721	0.9213	0.9820	0.8937	0.9060	0.9819
SD (mg g^{-1})	9.384	18.39	7.9475	29.16	33.73	14.04
Liu						
Q_{max} (mg g^{-1})	214.5	225.3	241.5	289.1	348.5	418.3
K_g (L mg^{-1})	0.3881	0.3338	0.2888	0.2484	0.2136	0.1867
n_L	0.4149	0.6864	0.3494	0.7887	0.7847	0.3674
R^2_{adj}	1.000	0.9999	0.9999	0.9999	0.9999	0.9999
SD (mg g^{-1})	0.4041	0.2682	0.3939	0.4446	0.3549	0.3360
	Tan-Ap-2.0					
	25 °C	30 °C	35 °C	40 °C	45 °C	50 °C
Langmuir						
Q_{max} (mg g^{-1})	126.3	175.1	188.4	207.7	222.8	243.4
K_L (L mg^{-1})	0.3049	0.4475	0.3032	0.2645	0.2083	0.2042
R^2_{adj}	0.9614	0.9851	0.9988	0.9965	0.9875	0.9703
SD (mg g^{-1})	6.645	6.878	1.965	3.712	7.301	12.48
Freudlich						
K_F (mg g^{-1} (mg L^{-1})$^{-1/nF}$)	82.88	90.22	105.0	116.5	120.2	123.3
n_F	15.91	10.07	11.92	11.89	11.09	10.04
R^2_{adj}	0.9970	0.9106	0.8685	0.8709	0.9395	0.9696
SD (mg g^{-1})	1.867	16.86	20.78	22.44	16.05	12.61
Liu						
Q_{max} (mg g^{-1})	161.2	181.85	187.5	206.1	230.7	266.2
K_g (L mg^{-1})	0.4211	0.3548	0.3017	0.2556	0.2151	0.1797
n_L	0.2256	0.6422	1.138	1.214	0.6651	0.4886
R^2_{adj}	0.9999	0.9999	0.9999	0.9990	0.9999	0.9999
SD (mg g^{-1})	0.4008	0.4560	0.4050	1.957	0.5640	0.2187

3.10. Treatment of synthetic dye effluents

In order to figure out if the tannin-APTES adsorbents could be successfully employed for treatment of synthetic wastewater containing dyes, in this work two synthetic dye-housing effluents containing various dyes and inorganic and organic compounds were prepared (see Table 1).

The UV–vis spectra of the untreated and treated effluents with tannin-APTES adsorbents were recorded from 190 to 800 nm (see Fig. 6). Efficiency of treatment of the effluents was made by monitoring the areas under the absorption bands from 190 to 800 nm. This approach gives the percentage of removal of all the components present in the synthetic effluents. For effluent A, the percentages of removal were 97.1%, 98.0% and 93.2% for Tan-Ap-0.5, Tan-Ap-1.0 and Tan-Ap-2.0,

Table 6
Maximum sorption capacities of different adsorbents used for removal of Acid Red 1 dye.

Adsorbent	Q_{max} (mg g^{-1})	Ref.
Industrial municipal sludge	56.1	[34]
Coal fly ash	92.59	[35]
Magnetic metal-organic framework	142.9	[36]
Magnetic Fe_3O_4/MgAl-LDH composite	92.0	[36]
Aluminium Sulphate	32.26	[37]
Ferric Chloride	250.0	[37]
Ferrous Sulphate	6.630	[37]
kaolin modified with 1-hexyl, 3-decahexyl imidazolium ionic liquid	842.7	[38]
Mg-Al-layered double hydroxide	108.0	[39]
Commercial activated carbon	129	[40]
Carbon nanospheres	158	[40]
Tan-Ap-0.5	337.6	This work
Tan-Ap-1.5	418.3	This work
Tan-Ap-2.0	226.2	This work

Table 8
Desorption of dye-loaded Tan-Ap-0.5, Tan-Ap-1.0 and Tan-Ap-2.0. Conditions: initial AR-1 concentration, 200 mg L^{-1}; mass of adsorbent, 30.0 mg; pH 2.0; time of contact, 12 h.

Composition of eluent	Tan-Ap-0.5	Tan-Ap-1.0	Tan-Ap-2.0
0.25 mol L^{-1} NaOH	2.35	1.25	2.45
0.50 mol L^{-1} NaOH	14.50	15.65	13.25
0.75 mol L^{-1} NaOH	35.65	36.54	35.68
1.0 mol L^{-1} NaOH	45.65	42.25	44.25
1.5 mol L^{-1} NaOH	55.23	51.25	56.78
2.0 mol L^{-1} NaOH	62.30	64.25	65.24
ethanol	47.80	50.21	48.54
acetone	68.25	69.54	67.58
1 V acetone + 1 V NaOH (0.25 mol L^{-1})	75.25	76.54	75.28
1 V acetone + 1 V NaOH (0.50 mol L^{-1})	88.65	89.54	90.14
1 V acetone + 1 V NaOH (0.75 mol L^{-1})	96.25	95.25	96.54
1 V acetone + 1 V NaOH (1.0 mol L^{-1})	96.35	96.74	96.78
1 V acetone + 1 V NaOH (1.5 mol L^{-1})	96.24	96.47	96.54
1 V acetone + 1 V NaOH (2.0 mol L^{-1})	97.85	96.75	96.24

respectively. For effluent B, the percentages of removal were 96.3%, 97.3% and 90.9%. Considering that the effluents A and B, are complex and contain large amounts of dyes, organic matter, surfactants, and inorganic ions, it can be stated that Tan-Ap-0.5 and Tan-Ap-1.0 can be applied in real wastewater treatment. On the other hand, Tan-Ap-2.0 presented lower performance when compared with the other adsorbents. This achievement is compatible with the Q_{max} reported in Table 5.

4. Conclusion

In this work, hybrid materials were prepared by mixing tannin with APTES and the resulting modified materials were characterized and applied to remove AR-1 dye from aqueous solutions by adsorption. The characterization data such indicate the formation of a type I hybrid material, through covalent bond probably between the silyl derivative and the hydroxyl groups present in the phenolic structures of the tannin. The modified tannins exhibit high adsorption properties compared with unmodified tannin.

The best experimental conditions were reached at pH 2.0, time of 8 h and at 50 °C. The equilibrium and kinetics adsorption data were well fit by the Liu and general-order models, respectively. The maximum adsorption capacity of 418.3 mg g^{-1} was obtained at 50 °C for a tannin-APTES material at ratio 1:1 (Tan-Ap-1.0). Based on experimental data it was found that electrostatic interactions and hydrogen bonds between the hybrid adsorbents and AR-1 dye have played an important role in its adsorption process.

Effect of temperature was studied and showed that the Q_{max} increases with an increase in the temperature. The estimated thermodynamic parameters established the suitability of the AR-1 dye adsorption process and the ΔG° values confirm the feasibility and spontaneity of the adsorption process. The modified materials were tested through the treatment of synthetic dye effluents and showed excellent outcome in the treatment of such effluents.

Acknowledgments

We would like to thank to CAPES and CNPq for financial support and fellowships. We also would like to thanks Dr. Aaron Young for revising the English of the manuscript. In addition, we would like to thanks to Tanac, for giving us the Weibull AQ® is a light-brown product that is rich in tannin. Finally, we also thank Chemaxon for giving an academic research license for the Marvin Sketch software, Version 17.11.0, (http://www.chemaxon.com), 2017 used for organic compounds physical-chemical properties.

Appendix A. Supplementary data

Supplementary data associated with this article can be found, in the online version, at http://dx.doi.org/10.1016/j.jece.2017.08.022.

Table 7
Thermodynamic parameters of the adsorption of Acid Red 1 on Tannin-APTES adsorbents.

Temperature (K)	298	303	308	313	318	323
Tan-Ap-0.5						
K_g (L mol^{-1})	200.900	173.100	148.900	127.200	109.000	94.720
ΔG° (kJ mol^{-1})	−30.25	−30.39	−30.50	−30.59	−30.67	−30.77
ΔH° (kJ mol^{-1})	−24.25	–	–	–	–	–
ΔS° (J K^{-1} mol^{-1})	20.2	–	–	–	–	–
R^2_{adj}	0.9993	–	–	–	–	–
Tan-Ap-1.0						
K_g (L mol^{-1})	197.700	170.100	147.100	126.600	108.800	95.130
ΔG° (kJ mol^{-1})	−30.21	−30.34	−30.47	−30.37	−30.66	−30.78
ΔH° (kJ mol^{-1})	−23.54	–	–	–	–	–
ΔS° (J K^{-1} mol^{-1})	22.40	–	–	–	–	–
R^2_{adj}	0.9996	–	–	–	–	–
Tan-Ap-2.0						
K_g (L mol^{-1})	214.500	180.700	153.700	130.200	109.600	91.530
ΔG° (kJ mol^{-1})	−30.41	−30.49	−30.58	−30.65	−30.68	−30.68
ΔH° (kJ mol^{-1})	−27.08	–	–	–	–	–
ΔS° (J K^{-1} mol^{-1})	11.30	–	–	–	–	–
R^2_{adj}	0.9982	–	–	–	–	–

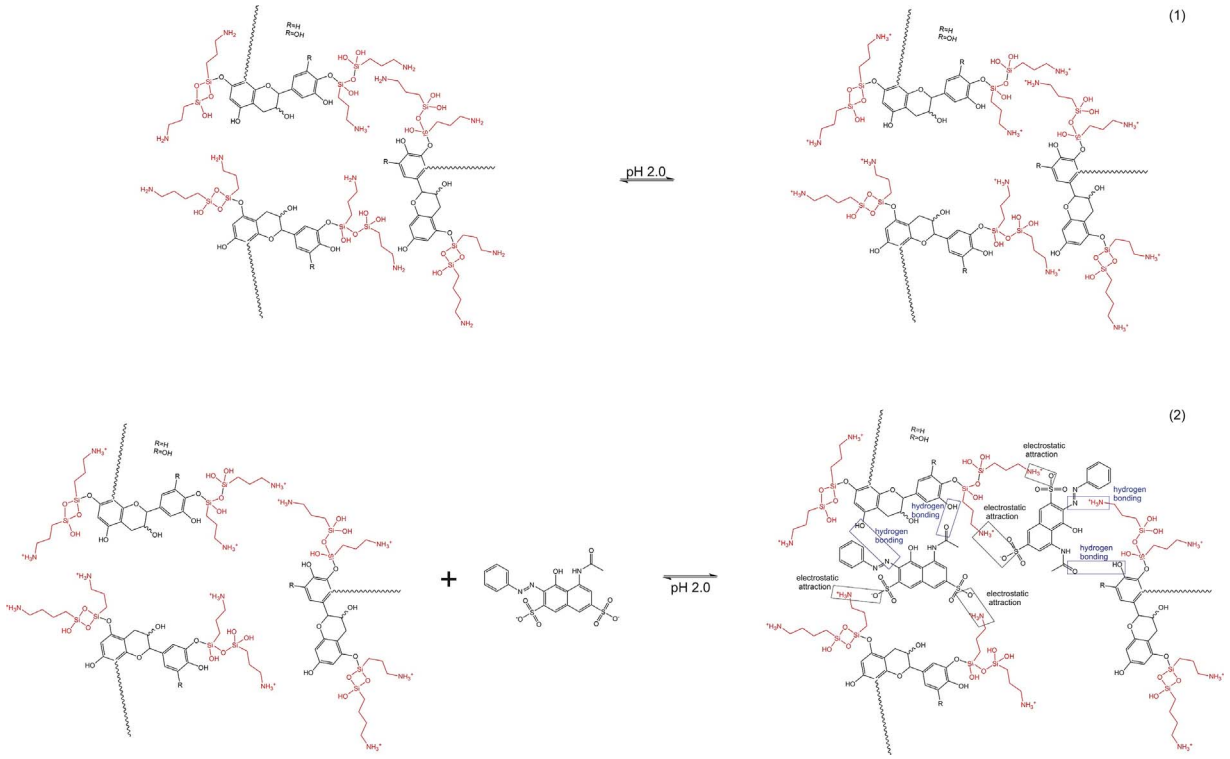

Fig. 5. Mechanism of adsorption of AR-1 dye onto tannin-APTES hybrids. Calculator Plugins of the software MarvinSketch Version 17.11.0, ChemAxon (http://www.chemaxon.com), 2017, were used for structure property prediction and calculation of the more probable chemical structure of the AR-1 dye and tannin-APTES hybrid at pH 2.0.

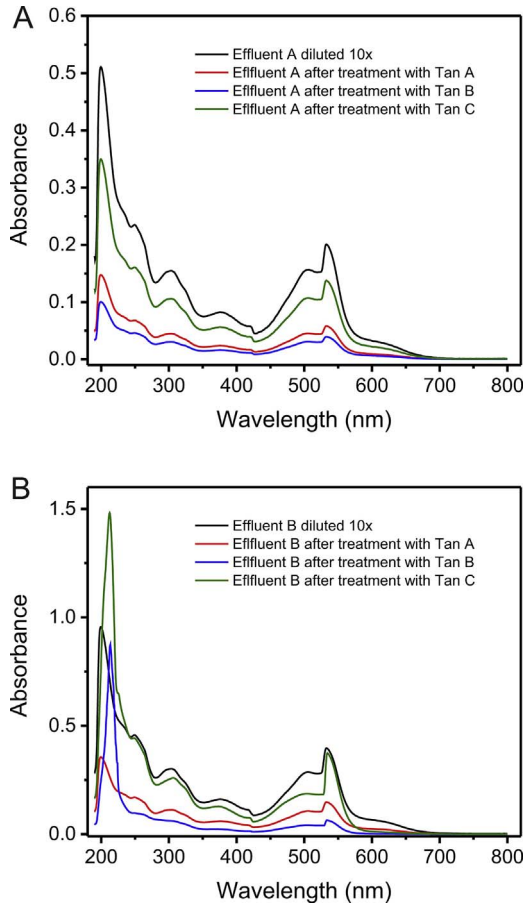

Fig. 6. Simulated effluents. A- effluent A; B- effluent B. For chemical composition of effluents, see Table 1.

References

[1] A. Khatri, M.H. Peerzada, M. Mohsin, M. White, A review on developments in dyeing cotton fabrics with reactive dyes for reducing effluent pollution, J. Clean. Prod. 87 (2015) 50–57.

[2] T. Ngulube, J.R. Gumbo, V. Masindi, A. Maity, An update on synthetic dyes adsorption onto clay based minerals: a state-of-art review, J. Environ. Manage. 191 (2017) 35–57.

[3] CS, L.D.T. Umpierres, M.A. Prola, E.C. Adebayo, G.S. Lima, D.D.F. dos Reis, Kunzler, L.T. Dotto, E.V. Arenas, Mesoporous Nb_2O_5/SiO_2 material obtained by sol–gel method and applied as adsorbent of crystal violet dye, Environ. Technol. 38 (2017) 566–578.

[4] M.B. Kurade, T.R. Waghmode, S.M. Patil, B.H. Jeon, S.P. Govindwar, Monitoring the gradual biodegradation of dyes in a simulated textile effluent and development of a novel triple layered fixed bed reactor using a bacterium-yeast consortium, Chem. Eng. J. 307 (2017) 1026–1036.

[5] N. Liu, X. Xie, B. Yang, Q. Zhang, C. Yu, X. Zheng, L. Xu, R. Li, J. Liu, Performance and microbial community structures of hydrolysis acidification process treating azo and anthraquinone dyes in different stages, Environ. Sci. Pollut. Res. 24 (2017) 252–263.

[6] L. Bu, Z. Shi, S. Zhou, Enhanced degradation of Orange G by permanganate with the employment of iron anode, Environ. Sci. Pollut. Res. 24 (2017) 388–394.

[7] A. Rajeswari, S. Vismaiya, A. Pius, Preparation, characterization of nano ZnO-blended cellulose acetate-polyurethane membrane for photocatalytic degradation of dyes from water, Chem. Eng. J. 313 (2017) 928–937.

[8] D.S.P. Franco, E.H. Tanabe, D.A. Bertuol, G.S. dos Reis, E.C. Lima, G.L. Dotto, Alternative treatments to improve the potential of rice husk as adsorbent for methylene blue, 2016 Water Sci. Technol. 75 (2017) 296–305.

[9] M.V. Niri, M. Shirmardi, A. Asadi, H. Golestani, A. Naeimabadi, M.J. Mohammadi, M.H. Farsani, Reactive Red 120 dye removal from aqueous solution by adsorption on nano-alumina, J. Water Chem. Technol. 36 (2014) 125–133.

[10] L.D.T. Prola, E. Acayanka, E.C. Lima, C.S. Umpierres, J.C.P. Vaghetti, W.O. Santos, S. Laminsi, P.T. Njifon, Comparison of *Jatropha curcas* shells in natural form and treated by non-thermal plasma as biosorbents for removal of Reactive Red 120 textile dye from aqueous solution, Ind. Crop. Prod. 46 (2013) 328–340.

[11] L.D.T. Prola, F.M. Machado, C.P. Bergmann, F.E. de Souza, C.R. Gally, E.C. Lima, M.A. Adebayo, S.L.P. Dias, T. Calvete, Adsorption of Direct Blue 53 dye from aqueous solutions by multi-walled carbon nanotubes and activated carbon, J. Environ. Manage. 130 (2013) 166–175.

[12] M.S. Bretanha, G.L. Dotto, J.C.P. Vaghetti, S.L.P. Dias, E.C. Lima, F.A. Pavan, *Giombo persimmon* seed (GPS) an alternative adsorbent for the removal toluidine blue dye from aqueous solutions, Desalin. Water Treat. 57 (2016) 28474–28485.

[13] A.J.B. Leite, A.C. Sophia, P.S. Thue, G.S. dos Reis, S.L.P. Dias, E.C. Lima, J.C.P. Vaghetti, F.A. Pavan, W.S. de Alencar, Activated carbon from avocado seeds for the removal of phenolic compounds from aqueous solutions, Desalin. Water

Treat. 71 (2017) 168–181.
[14] G.S. dos Reis, M. Wilhelm, T.C.A. Wilhelm, K. Rezwan, C.H. Sampaio, E.C. Lima, S.M.A.G.U. Souza, The use of design of experiments for the evaluation of the production of surface–rich activated carbon from sewage sludge via microwave and conventional pyrolysis, Appl. Therm. Eng. 93 (2016) 590–597.
[15] H.A.M. Bacelo, S.C.R. Santos, C.M.S. Botelho, Tannin-based biosorbents for environmental applications – a review, Chem. Eng. J. 303 (2016) 575–587.
[16] G.S. dos Reis, C.H. Sampaio, E.C. Lima, M. Wilhelm, Preparation of novel adsorbents based on combinations of polysiloxanes and sewage sludge to remove pharmaceuticals from aqueous solutions, Colloids Surf. A 497 (2016) 304–315.
[17] G.S. dos Reis, M. Adebayo, S.T. Pascal, C.H. Sampaio, E.C. Lima, S.L.P. Dias, I.A.S. De Brum, F. Pavan, Removal of phenolic compounds from aqueous solutions using sludge-Based activated carbons prepared by conventional heating and microwave-assisted pyrolysis, Water Air Soil Pollut. 228 (33) (2017) 1–17.
[18] F. Barbosa-Jr, E.C. Lima, F.J. Krug, Determination of arsenic in sediment and soil slurries by electrothermal atomic absorption spectrometry using W-Rh permanent modifier, Analyst 125 (2000) 2079–2083.
[19] E.C. Lima, F. Barbosa Jr, F.J. Krug, The use of tungsten–rhodium permanent chemical modifier for cadmium determination in decomposed samples of biological materials and sediments by electrothermal atomic absorption spectrometry, Anal. Chim. Acta 409 (2000) 267–274.
[20] E.C. Lima, F. Barbosa-Jr, F.J. Krug, Lead determination in biological material slurries by ETAAS using W-Rh permanent modifier, Fres. J. Anal. Chem. 369 (2001) 496–501.
[21] F. Barbosa Jr., F.J. Krug, E.C. Lima, On-line coupling of electrochemical preconcentration in tungsten coil electrothermal atomic absorption spectrometry for determination of lead in natural waters, Spectrochim. Acta B 54 (1999) 1155–1166.
[22] E.C. Lima, M.A. Adebayo, F.M. Machado, Kinetic and equilibrium models of adsorption, in: C.P. Bergmann, F.M. Machado (Eds.), Carbon Nanomaterials as Adsorbents for Environmental and Biological Applications, Springer, 2015, pp. 33–69.
[23] M.J. Puchana-Rosero, E.C. Lima, S. Ortiz-Monsalve, B. Mella, D. da Costa, E. Poll, M. Gutterres, Fungal biomass as biosorbent for the removal of Acid Blue 161 dye in aqueous solution, Environ. Sci. Pollut. Res. 24 (2017) 4200–4209.
[24] L.A. Rodrigues, K.K. Sakane, E.A.N. Simonetti, G.P. Thim, Cr total removal in aqueous solution by PHENOTAN AP based tannin gel (TFC), J. Environ. Chem. Eng. 3 (2015) 725–733.
[25] C. dos Santos, Á. Vargas, N. Fronza, J.H.Z. dos Santos, Structural, textural and morphological characteristics of tannins from *Acacia mearnsii* encapsulated using sol-gel methods: applications as antimicrobial agents, Colloids Surf. B 151 (2017) 26–33.
[26] P.S. Thue, E.C. Lima, J.M. Sieliechi, C. Saucier, S.L.P. Dias, J.C.P. Vaghetti, F.S. Rodembusch, F.A. Pavan, Effects of first–row transition metals and impregnation ratios on the physicochemical properties of microwave-assisted activated carbons from wood biomass, J. Colloid Interface Sci. 486 (2017) 163–175.
[27] M. Kardel, F. Taube, H. Schulz, W. Schütze, M. Gierus, Different approaches to evaluate tannin content and structure of selected plant extracts – Review and new aspects, J. Appl. Bot. Food Qual. 86 (2013) 154–166.
[28] M. Friedman, H.S. Jürgens, Effect of pH on the stability of plant phenolic compounds, J. Agric. Food Chem. 48 (2000) 2101–2110.
[29] B. Royer, N.F. Cardoso, E.C. Lima, V.S.O. Ruiz, T.R. Macedo, C. Airoldi, Organofunctionalized kenyaite for dye removal from aqueous solution, J. Colloid Interface Sci. 336 (2009) 398–405.
[30] C. Saucier, M.A. Adebayo, E.C. Lima, R. Cataluna, P.S. Thue, L.D.T. Prola, M.J. Puchana-Rosero, F.M. Machado, F.A. Pavan, G.L. Dotto, Microwave-assisted activated carbon from cocoa shell as adsorbent for removal of sodium diclofenac and nimesulide from aqueous effluents, J. Hazard. Mater. 289 (2015) 18–27.
[31] P.S. Thue, M.A. Adebayo, E.C. Lima, J.M. Sieliechi, F.M. Machado, G.L. Dotto, J.C.P. Vaghetti, S.L.P. Dias, Preparation, characterization and application of microwave-assisted activated carbons from wood chips for removal of phenol from aqueous solution, J. Mol. Liq. 223 (2016) 1067–1080.
[32] C. Saucier, P. Karthickeyan, V. Ranjithkumar, E.C. Lima, G.S. dos Reis, I.A.S. de Brum, Efficient removal of amoxicillin and paracetamol from aqueous solutions using magnetic activated carbon, Environ. Sci. Pollut. Res. 24 (2017) 5918–5932.
[33] G.S. dos Reis, M.K.B. Mahbub, M. Wilhelm, C.H. Sampaio, E.C. Lima, C. Saucier, S.L.P. Dias, Activated carbon from sewage sludge for removal of sodium diclofenac and nimesulide from aqueous solutions, Korean J. Chem. Eng. 33 (2016) 3149–3161.
[34] M. Seredych, T.J. Bandosz, Removal of cationic and ionic dyes on industrial- municipal sludge based composite adsorbents, Ind. Eng. Chem. Res. 46 (2007) 1786–1793.
[35] T.C. Hsu, Adsorption of an acid dye onto coal fly ash, Fuel 87 (2008) 3040–3045.
[36] T. Wang, P. Zhao, N. Lu, H. Chen, C. Zhang, X. Hou, Facile fabrication of Fe_3O_4/MIL-101(Cr) for effective removal of acid red 1 and orange G from aqueous solution, Chem. Eng. J. 295 (2016) 403–413.
[37] N. Munilakshmi, M. Srimuralia, J. Karthikeyan, Adsorptive removal of acid red 1, from aqueous solutions by preformed flocs, Int. J. Current Eng. Technol. 3 (2013) 1456–1462.
[38] I.A. Lawal, B. Moodley, Column kinetic and isotherm studies of PAH (phenanthrene) and dye (acid red) on kaolin modified with 1-hexyl, 3-decahexyl imidazolium ionic liquid, J. Environ. Chem. Eng. 4 (2016) 2774–2784.
[39] R.R. Shan, L.G. Yan, Y.M. Yang, K. Yang, S.J. Yu, H.G. Yu, B.C. Zhu, B. Du, Highly efficient removal of three red dyes by adsorption onto Mg–Al-layered double hydroxide, J. Ind. Eng. Chem. 21 (2015) 561–568.
[40] F.C. Huang, C.K. Lee, Y.L. Han, W.C. Chao, H.P. Chao, Preparation of activated carbon using micro-nano carbon spheres through chemical activation, J. Taiwan Inst. Chem. Eng. 45 (2014) 2805–2812.
[41] C.N. Arenas, A. Vasco, M. Betancur, J.D. Martínez, Removal of indigo carmine (IC) from aqueous solution by adsorption through abrasive spherical materials made of rice husk ash (RHA), Process Saf. Environ. 106 (2017) 224–238.
[42] G.Z. Kyzas, N.K. Lazaridis, D.N. Bikiaris, Optimization of chitosan and (-cyclodextrin molecularly imprinted polymer synthesis for dye adsorption, Carbohyd. Polym. 91 (2013) 198–208.
[43] C.L. Sun, C.S. Wang, Estimation on the intramolecular hydrogen-bonding energies in proteins and peptides by the analytic potential energy function, J. Mol. Struct. 956 (2010) 38–43.